Intelligent Systems Approach for Automated Identification of Individual Control Behavior of a Human Operator

Kirill B. Zaychik and Frank M. Cardullo
State University of New York, Binghamton, New York

NASA STI Program . . . in Profile

Since its founding, NASA has been dedicated to the advancement of aeronautics and space science. The NASA scientific and technical information (STI) program plays a key part in helping NASA maintain this important role.

The NASA STI program operates under the auspices of the Agency Chief Information Officer. It collects, organizes, provides for archiving, and disseminates NASA's STI. The NASA STI program provides access to the NASA Aeronautics and Space Database and its public interface, the NASA Technical Report Server, thus providing one of the largest collections of aeronautical and space science STI in the world. Results are published in both non-NASA channels and by NASA in the NASA STI Report Series, which includes the following report types:

- TECHNICAL PUBLICATION. Reports of completed research or a major significant phase of research that present the results of NASA programs and include extensive data or theoretical analysis. Includes compilations of significant scientific and technical data and information deemed to be of continuing reference value. NASA counterpart of peer-reviewed formal professional papers, but having less stringent limitations on manuscript length and extent of graphic presentations.

- TECHNICAL MEMORANDUM. Scientific and technical findings that are preliminary or of specialized interest, e.g., quick release reports, working papers, and bibliographies that contain minimal annotation. Does not contain extensive analysis.

- CONTRACTOR REPORT. Scientific and technical findings by NASA-sponsored contractors and grantees.

- CONFERENCE PUBLICATION. Collected papers from scientific and technical conferences, symposia, seminars, or other meetings sponsored or co-sponsored by NASA.

- SPECIAL PUBLICATION. Scientific, technical, or historical information from NASA programs, projects, and missions, often concerned with subjects having substantial public interest.

- TECHNICAL TRANSLATION. English-language translations of foreign scientific and technical material pertinent to NASA's mission.

Specialized services also include creating custom thesauri, building customized databases, and organizing and publishing research results.

For more information about the NASA STI program, see the following:

- Access the NASA STI program home page at *http://www.sti.nasa.gov*

- E-mail your question via the Internet to help@sti.nasa.gov

- Fax your question to the NASA STI Help Desk at 443-757-5803

- Phone the NASA STI Help Desk at 443-757-5802

- Write to:
  NASA STI Help Desk
  NASA Center for AeroSpace Information
  7115 Standard Drive
  Hanover, MD 21076-1320

NASA/CR–2012-217555

Intelligent Systems Approach for Automated Identification of Individual Control Behavior of a Human Operator

Kirill B. Zaychik and Frank M. Cardullo
State University of New York, Binghamton, New York

March 2012

Acknowledgments

I would first like to extend my gratitude to Professor Frank Cardullo for his support and guidance on this research.

I also extend appreciation to Lon Kelly of the NASA contractor UNISYS for his technical support. Lon provided key assistance in implementing the large civil transport aircraft software package at the Man-Machine Systems Laboratory at SUNY Binghamton and educating me in good programming practice.

I would also like to express my appreciation to my colleague Gary George for providing experimental data essential to my research.

I also extend appreciation to Bob Mess in the Man-Machine Laboratory at SUNY Binghamton for his help and assistance in ensuring proper functioning of all computer equipment.

Abstract

Acceptable results have been obtained using conventional techniques to model the generic human operator's control behavior. However, little research has been done in an attempt to identify an individual based on his/her control behavior. The main hypothesis investigated in this study is that different operators exhibit different control behavior when performing a given control task. Furthermore, inter-person differences are manifested in the amplitude and frequency content of the non-linear component of the control behavior. Two enhancements to the existing models of the human operator, which allow personalization of the modeled control behavior, are presented in this manuscript.

One of the proposed enhancements accounts for the "testing" control signals, which are introduced by an operator for more accurate control of the system and/or to adjust his/her control strategy. Such enhancement uses the Artificial Neural Network (ANN), which can be fine-tuned to model the "testing" control behavior of a given individual. The other model enhancement took the form of an equiripple filter (EF), which conditions the power spectrum of the control signal before it is passed through the plant dynamics block. The filter design technique uses Parks-McClellan algorithm, which allows parameterization of the desired levels of power at certain frequencies. A novel automated parameter identification technique (APID) was developed to facilitate the identification process of the parameters of the selected models of the human operator. APID utilizes a Genetic Algorithm (GA) based optimization engine called the Bit-climbing Algorithm (BCA).

Proposed model enhancements were validated using the experimental data obtained at three different sources: the Manual Control Laboratory software experiments, Unmanned Aerial Vehicle simulation, and NASA Langley Research Center Visual Motion Simulator studies. Validation analysis involves comparison of the actual and simulated control activity signals. Validation criteria used in this study are based on comparing Power Spectral Densities of the control signals against that of the Precision model of the human operator.

This manuscript also addresses the issue of applying the proposed human operator model augmentation to evaluate the effectiveness of the motion feedback when simulating the actual pilot control behavior in a flight simulator. The proposed modeling methodology allows for quantitative assessments and prediction of the need for platform motion, while performing aircraft/pilot simulation studies.

Contents

List of Tables

List of Figures

x

Nomenclature

A	Amplitude
a_{00}, a_{01}	ANN bias nodes of the hidden and output layers respectively
a, b, c, d	ANN pre and post processing parameters
e	Tracking error signal
f	Activation function
K	Gain
K_e	Signal processing gain
K_n	Remnant gain
K_p	Precision model operator gain
K_r	TEC model gain
K_v	Vestibular system gain
K_1	Muscle spindles transfer function gain
K_2	Golgi tendons transfer function gain
k	Order of the plant dynamics
Q, R	Weighting coefficients of the Hosman descriptive model functional
q, r	Weighting coefficients of the OCM functional
T_i	Precision model operator lag time constant
T_L	Precision model operator lead time constant
T_N	Precision model neuromuscular time constant
T_n	Remnant band limiting filter transfer function time constant
T_1	Muscle spindles transfer function time constant
T_2	Golgi tendons transfer function time constant
u	Control input
u_{ij}	ANN internal signals: I – number of the layer; j – number of the node
w	Weighting coefficient
Y_c	Plant dynamics transfer function

Y_p	Operator/pilot model
x_i	i-th state variable (OCM)
ω_c	Crossover model crossover frequency
ω_n	Natural frequency of the control producing limb transfer function
ζ_n	Damping ratio of the control producing limb transfer function
τ_c	Crossover model delay time constant
τ_0	Cognitive processing time delay
δ	Control signal
Ψ_E	Azimuth error
Ψ_G	Gun turret azimuth
Ψ_T	Target azimuth
σ_x	Standard deviation of parameter x

Subscripts

Subscripts indicate to what the main symbol is related

$()_n$	Neuromuscular dynamics
$()_{ms}$	Motion system
$()_w$	Washout algorithm
$()_{C,att}$	Tracking error attitude
$()_{C,rate}$	Tracking error rate
$()_{SCC}$	Semicircular canals
$()_{otolith}$	Otoliths
$()_{visual}$	Visual system
$()_{tec}$	TEC
$()_{aircraft}$	Aircraft
$()_{wind}$	Wind disturbance

Acronym

AFRL   Air Force Research Laboratory

ANN   Artificial neural network

APID   Automated parameter identification technique

ASCII   American Standard Code for Information Interchange

BCA   Bit climbing algorithm

BFGS   Broyden-Fletcher-Goldfarb-Shanno algorithm

CRT   Cathode Ray Tube

DOF   Degree of freedom

EF   Equiripple filter

FIR   Finite impulse response

FIS   Fuzzy inference system

GA   Genetic algorithm

GUI   Graphic User Interface

ISV   Inter-subject variation

ITAR   International Traffic in Arms Regulations

LaRC   Langley Research Center

MMS   Man-machine system

OCM   Optimal control model

PID   Parameter identification

PSD   Power spectral density

RBPROP   Resilient back propagation algorithm

RMSE   Root mean square error

RPM   Revolutions per minute

SC   Soft computing

SGA   Simple genetic algorithm

STD   Standard deviation

STE   Synthetic Task Environment

TEC	Testing element of control
UAV	Unmanned Aerial Vehicle
USAF	United States Air Force
VMS	Visual Motion Simulator

1. Introduction

1.1. Modeling human operator

Understanding how a human controls a system and therefore, being able to predict operator behavior under varying conditions, are the primary motivations to develop human operator models. These models have many applications in a variety of areas. This manuscript contains the review of existing models of the human operator and also presents research into the development of model enhancements, which allow modeling control behavior of a given individual, rather than a generic human operator. This document also presents an intelligent systems based approach to automated parameter identification of parameters of selected human operator models.

The pioneer of operator modeling as we know and understand this term was Arnold Tustin [1]. In mid 40's he had performed a series of studies on modeling a gun turret operator. The gunner was to track a target by controlling the azimuth of the turret. If expressed in modern control theory terms, the gunner was performing a single degree of freedom control task. Figure 1.1 illustrates how Tustin [1] envisioned the operator plus plant system.
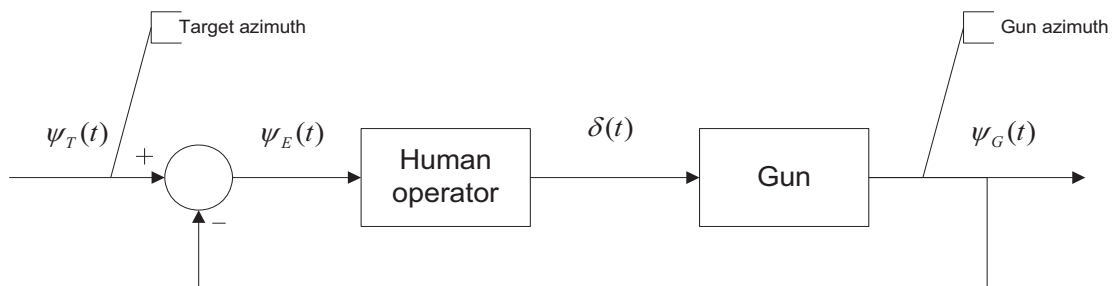
Figure 1.1. A block diagram representation of the task of controlling the gun turret

Over the years, the form of the man-machine system, with the human performing a manual control task has remained the same. What was subjected to change is the "Human operator" block. Tustin [1] hypothesized that the human can be described by a linear, constant coefficient

differential equation. By that time the theory of "linear-servomechanisms" was well developed, hence allowing it to be applied in the analysis of the manual control tasks.

McRuer [2] presented his vision of the human operator model, which is conventionally referred to as the Crossover Model. The essence of the model is that the human adapts his/her behavior to the plant dynamics. In his model, McRuer [2] introduces the remnant[*], which accounts for the non-linearities in the man-machine system.

The Optimal Control Model (OCM), developed by Kleinman, Baron, Levinson [3], describes the operator in the following manner:

> a well motivated, well-trained human operator behaves in a near optimal manner subject to his/her inherent limitations and constraints, and knowledge of the control task

At the heart of the OCM lies the Kalman predictor (filter), which estimates the values of the state variables given at each instant of time and the noisy measurements (observations) of linear combination of those variables.

Ronald Hess [4] has developed a model, which falls into a category of anthropomorphic or structural models, i.e. models which attempt to mimic the human psychomotor structure. The essential feature of the Hess structural model is that it has the so-called "proprioceptive" feedback, the path that provides the human with the sensational information. In addition to modeling the perceptual system, the model offers models of the visual, neuromuscular and central nervous systems.

Recently Cardullo, et al. [5] performed a study on improving and substantially expanding the Hess model. The essence of their approach was to include motion and force feedbacks into the model.

Chapter 2 describes in detail several conventional models of the human operator, such as the Crossover model, Hess structural model, Hosman descriptive model, and OCM. Some of the

---

[*] The term "remnant" is used to describe the noise injection by the human, and/or nonlinearities and errors in the system, given a linear representation of the human, and/or system dynamics. In most cases, remnant is modeled as a filtered white noise.

new approaches to modeling of the human operator, such as using fuzzy inference systems [6] and neuro-controllers [7] are presented as well.

1.2. Soft computing

Machine intelligence techniques, otherwise known as soft computing (SC) techniques, are becoming more and more popular in the research community. Such tools as Fuzzy Inference Systems (FIS), Artificial Neural Networks (ANN), Genetic Algorithms (GA), etc., are the constituent parts of the mathematical apparatus offered by the SC approach. Operator models developed with the utilization of these techniques may be classified as anthropomorphic, since all of the above mentioned SC techniques have their biological origins. Artificial neural networks, for instance, were designed with the real neuron structure in mind. The primary purpose of the fuzzy inference systems is to deal with imprecision and uncertainty in a manner as human being does it. Genetic algorithms function based on the concept of the "survival of the fittest". In addition to that, the SC methodology, if applied to the manual control problem, is capable of coping with highly non-linear plant dynamics or even in cases where the precise mathematical description of the controlled plant is impossible [4]. However, the more important feature of the SC techniques, which is more relevant to current research, is that FIS and ANN as well as their hybrids are data driven mathematical tools. In other words, models, which are designed based upon SC are 100% tuned, based on the existing data, and/or expert knowledge on the modeled phenomenon. For example, ANN is trained based on the available data, to pickup and adapt to any type of behavioral pattern. In case of FIS, if-then inference rules are defined based on either data or the expert knowledge.

Since the invention of SC in the mid 60's, there have been a number of attempts to develop a SC based model of a human operator. However, in those instances, the developed models were not the operator models, per se, but rather controllers.

- Fuzzy controller of the washing machine,
- Fuzzy controller of the subway train (Japan),
- Fuzzy controller of a helicopter (Japan)
- Fuzzy based controller of an automobile (Germany)

3

This list is just a few examples of the successful implementations of SC algorithms in the area of automatic control. The following paragraphs briefly describe one of the successful implementations of SC in the area of manual control of the vehicle.

In the early to mid 90's a group of scientists from Germany developed and successfully tested a soft computing based controller for the car. The controller was designed to operate as an autopilot and to control the lateral position of the car on the road. Figure 1.2 shows the closed control loop with a) the human and b) controller in the loop respectively. The primary objectives of the designed controller were to provide assistance in collision avoidance, lane switching and convoy driving.

The controller was designed in a form of a neural network. Obviously it is a data driven model, i.e. the neural net is tuning itself to mimic operator's behavior based on the existing pool of data on the response of the operator to varying driving conditions. The system dynamics of a car are highly nonlinear, especially with respect to velocity control. In this respect, the neural-net based controller exercises one of the major advantages of the neural network, i.e. it does not necessarily require the accurate knowledge of the controlled system (car), whereas the conventional controller design methods are restricted to the linear approximations of the controlled element.

Chapter 3 provides a more in-depth look at the structure and functionality of the ANN and its components.
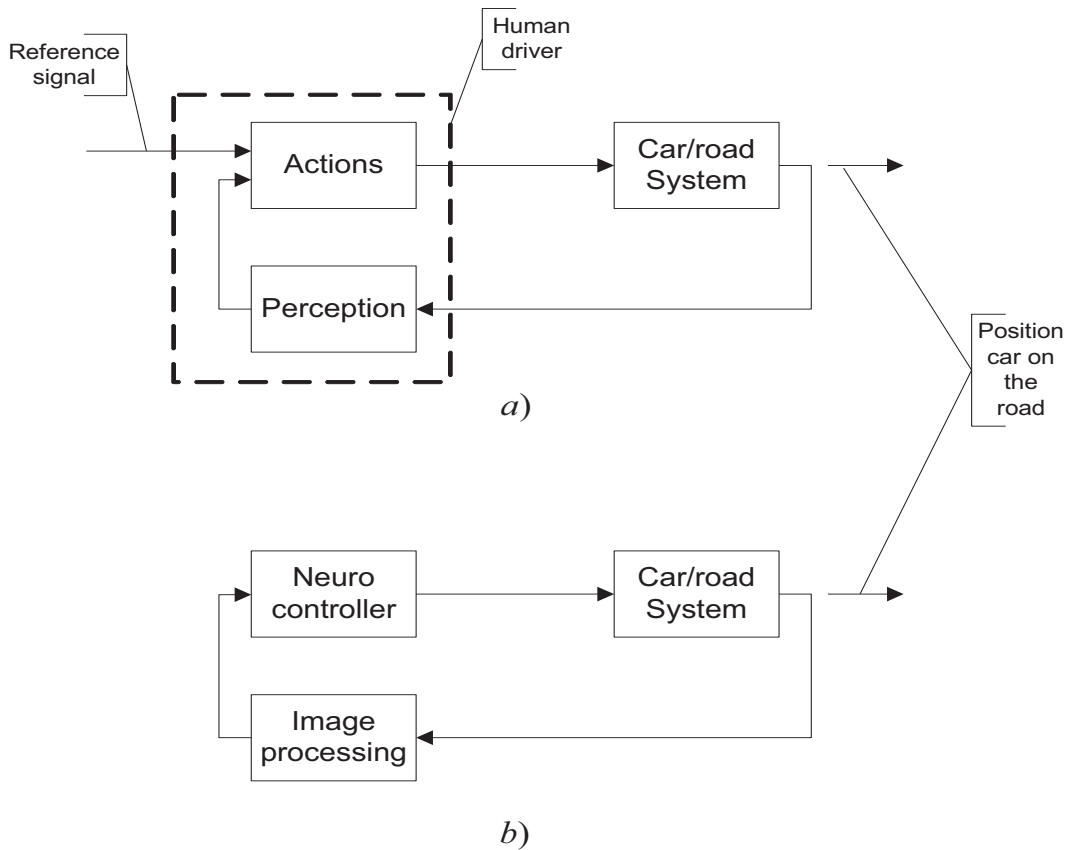
Figure 1.2. a) General Driver/Car closed control loop, b) the Neural Network/Car control system. Adopted from Neusser [7].

1.3. Scope of research

Conventional models of the human operator produce somewhat acceptable results modeling the control behavior of a generic operator. However, these models provide a limited ability to reproduce the non-linear components of the control behavior of an actual operator.

The issue of modeling a human operator was taken in this research one step further in an attempt to learn how to model individual behavior of different operators. Presented research applies SC techniques to better model the non-linear human behavior. The main hypothesis, which stimulated this research, can be described as: every individual may have his/her unique way of performing the same control task, e.g. a testing element of control behavior. Such behavioral "fingerprint" can be characterized by the power magnitude and frequency content of

the non-linear control behavior. By the testing element of control it is meant that as the human operator adapts to the system control dynamics, he/she applies different control inputs by observing/sensing the output. In other words, different operators may adapt to system dynamics by employing different learning/control strategies. Conventionally, non-linearities in the man-machine system are accounted for by introducing remnant, a band-limited white noise. Such an approach, however, has limited ability to discriminate among different operators. To overcome this difficulty, a complement of model enhancements have been developed, which are oriented toward modeling the testing (learning) element of control (TEC) portion of the overall non-linear control behavior. Chapter 5 provides in-depth description of the proposed model enhancements.

The proposed model enhancements comprise conventional signal processing elements as well as soft computing techniques, such as ANN. Since the development and tuning of the neural network is a data driven process, and the available data were quite limited, a novel automated parameter identification technique (APID) was developed to facilitate identification of individual-specific parameters of the human operator model and the enhancements. The backbone of the proposed APID is another SC technique known as a genetic algorithm (GA). More specifically, a bit-climbing version (BCA) of the GA is used. The essence of the APID is in using BCA to find an optimal combination of indentified parameters, which results in the closest approximation of the actual control behavior data. Chapter 6 contains detailed description of the BCA and it application. Results of application of the APID to the selected models of the human operator are presented in the chapter as well.

The potential spectrum of application of the computational tools to identify individual control behavior of different subjects is very broad. For example, availability of such tools allows for non-invasive identification of a particular operator for security reasons. Since the identification process involves parameter identification, it can be used to identify changes in the operator behavior due to numerous reasons, such as physical impairment, intoxication, motion sickness and so on. By comparing the actual control behavior of a pilot against that obtained during simulation it will be possible to perform a quantitative evaluation of the handling qualities of a particular simulator. Chapter 7 of this manuscript provides details on how the proposed APID can be applied to evaluate the effectiveness of the motion system feedback designed by Cardullo, et al. [5] to enhance the vestibular system feedback of the Hess structural model. Using

data obtained during experiments (Chapter 4) at the NASA Langley Research Center Visual Motion Simulator (VMS), it is shown, that the Hess Structural Model equipped with motion system feedback and TEC is capable of very close approximation of individual control behavior of various pilots. APID in this case allows quantitative assessment of the effectiveness of the motion system feedback. Moreover, it provides insight on what perception modalities dominate in human perception when performing a specific closed loop control task.

Chapter 8 of the manuscript draws a number of conclusions regarding the effectiveness of the implemented augmentations to the existing models of the human operator as well as discusses various directions for future research.

2. Literature review of conventional operator models.

2.1. Introduction

Understanding how a human controls a system or a plant and being able to predict operator behavior under varying conditions, are the primary driving forces in the area of operator modeling. This chapter concentrates on describing operator models that already have been developed in the flight controls and flight simulation communities.

The pioneer of operator modeling as we know and understand this term was Arnold Tustin [1]. In the mid 40's he performed a series of studies investigating the gun turret control task. The gunner was to track a target by controlling the azimuth of the turret. Using terms of classical control theory, the gunner was performing a single degree of freedom manual tracking control task. The overall structure of such a simple man-machine system can be illustrated by the following block-diagram.

Target azimuth

Gun azimuth

$\psi_T(t)$ $\psi_E(t)$ $\delta(t)$ $\psi_G(t)$

+   Human operator   Gun

−
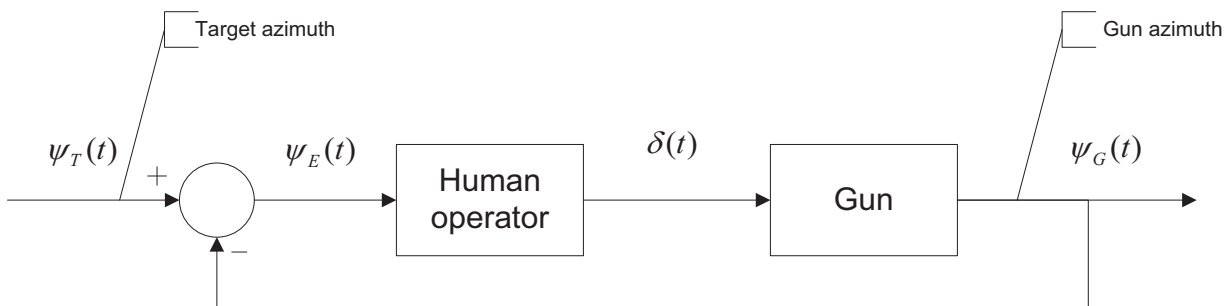
Figure 2.1. Man-machine system by Tustin [1]

Tustin [1] introduced several concepts of man-machine system modeling, which have been recognized and are still being used by the researchers in this field. Among such concepts are "quasi-linear system", "describing function", and "remnant". Tustin [1] found from the experimental data that the human operator can be modeled as a quasi-linear system, i.e. human operator output consists of the linear describing function portion and a non-linear remnant portion. The latter is represented by band-limited white noise.

8

As can be seen above, the architecture of the man-machine system, where human operator works in a closed loop with the dynamic system has preserved its original form almost unchanged. The "human operator" block, however, has been subject to some significant changes over the course of 60 some years. The following subsections describe several major mathematical models of the human operator that have been developed over this period of time.

2.2. Crossover model

Duane McRuer [2] in the early 70's summarized the knowledge and the experimental data available at that time in the area of manual control in the form of the model, which is referred to as crossover model.
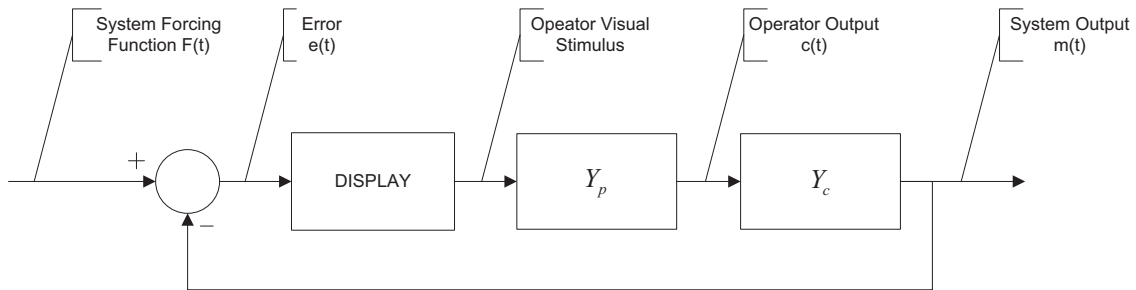
Figure 2.2. Basic Man Machine System by McRuer [2]

It has been empirically proven that the human operator adjusts his/her control behavior in such a manner so that the resulting "human+plant" open loop system dynamics is the same and can be described by the following simple transfer function.

$$Y_p Y_c = \frac{\omega_c e^{-\tau_e s}}{s},$$

(2.1)

Where ω_c and τ_c are the crossover frequency and the time delay respectively. In the frequency domain the crossover model is expressed in terms of criterion imposed on the crossover frequency and the phase margin. McRuer [2] determined that the human attempts to force the system to cross the $0dB$ line between 3 and 6 rad/sec with the phase margin between

25 and 45 degrees. Figure 2.3 illustrates how the crossover model works for different cases of plant dynamics.
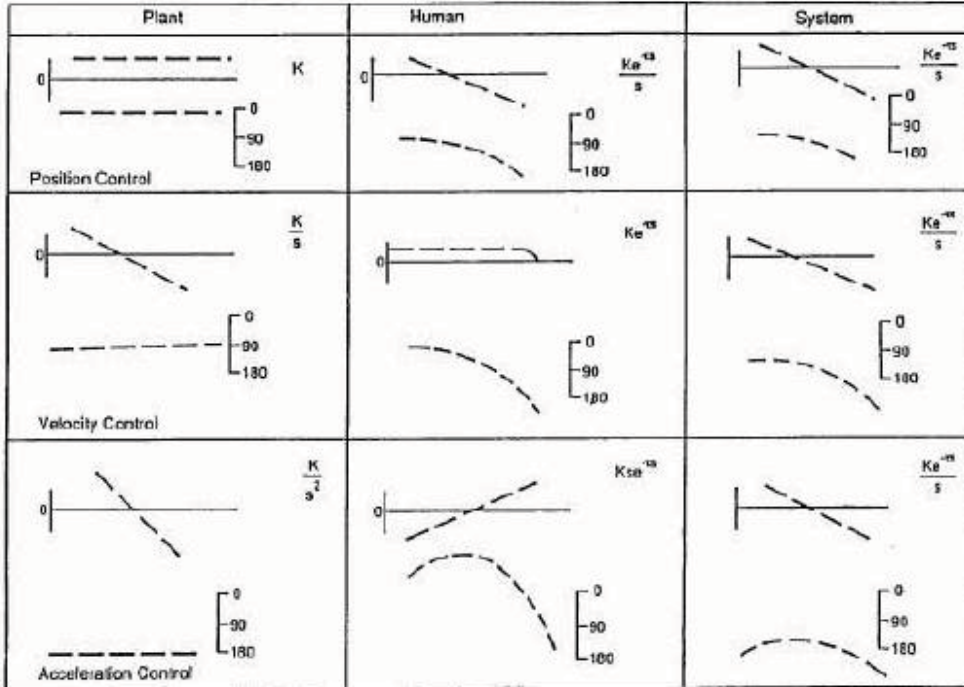
Figure 2.3. Crossover model frequency response for different plant dynamics (Flach, [9])

Based on the available experimental data for a variety of controlled elements, McRuer [8] derived that the linear component of the human control actions can be described by the following transfer function (Eq. 2.2).

$$Y_p(s) = \frac{K_p e^{-\tau_e s}(T_L s + 1)}{(T_I s + 1)(T_N s + 1)},$$
(2.2)
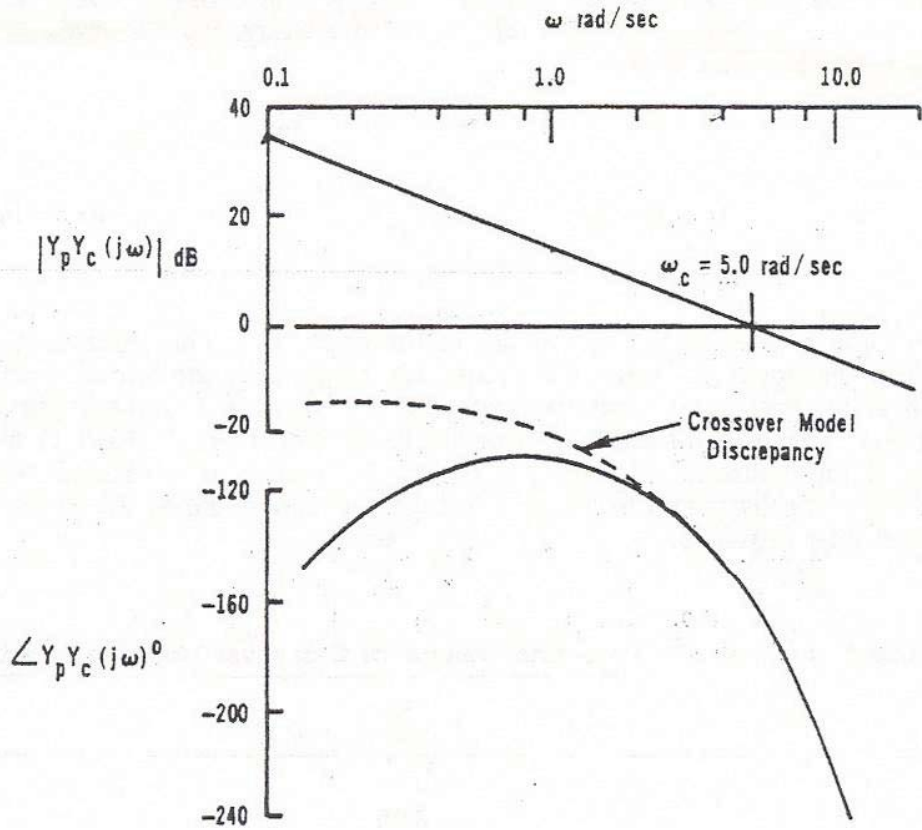
Figure 2.4. An example of the discrepancy between the actual data (solid) and the crossover model (dashed) in the area of lower frequencies (Hess, [4])

Where T_L is the lead time constant, T_I is the lag time constant, and finally T_N is the time constant of the neuromuscular portion of the transfer function. It is very important to note that the crossover model operates best only in the vicinity of the crossover frequency, i.e. where the "human+plant" dynamics is linear: the farther one gets away from that frequency, the more likely it is to observe the discrepancy between the actual and simulated data (Figure 2.4).

The logical extension of the crossover model was the "precision" model. The precision model makes the Y_p block of the model more complex in order to improve the performance in the crossover region as well as to eliminate the frequency discrepancy at the lower frequencies. Eq. 2.3 contains a mathematical expression of the precision model.

11

$$Y_p(s) = K_p e^{-\tau s} \left(\frac{T_L s + 1}{T_I s + 1} \right) \left(\frac{T_K s + 1}{T_K' s + 1} \right) \left(\frac{1}{(T_N s + 1)\left(\dfrac{s^2}{\omega_n^2} + 2\dfrac{\zeta_n}{\omega_n} s + 1 \right)} \right), \qquad (2.3)$$

The parameters T_L and T_I are used to describe the equalization capabilities of the human operator. The parameters T_K' and T_K are included to account for the phase discrepancy in the low frequency area, which is caused by the approximate nature of the crossover model. Precision model also contains a more complicated model of the neuromuscular dynamics: parameters T_N, ζ_n and ω_n are used to describe the dynamics of the control producing limb. It is very important to mention that the Precision model is almost solely used for matching experimental data pertaining to individual subjects, rather than for predictive purposes.

2.3. Optimal Control Model

The Optimal Control Model (OCM) was developed by Kleinman, et al. [3]. As opposed to the crossover model the OCM relies on the concepts of optimal control and estimation theory [3]:

> The basic assumption underlying our approach is that the well-motivated, well-trained human operator behaves in a linear optimal manner subject to his inherent limitation and constraints, and his control task

The essence of the OCM is in developing a describing function of the human operator rather than the transfer function describing only the linear component of the human operator behavior. In other words, Kleinman, et al. [3] succeeded in developing an algorithmic model of the human operator as opposed to structural models, pursued by Hess [4], Hosman [10], etc. The OCM in its core solves the stochastic linear quadratic Gaussian problem, i.e. finding parameters of the functional J (Eq. 2.4) that will drive it to its minimum.

$$J = E\left\{ \lim_{T \to \infty} \frac{1}{T} \int_0^T \left[q x_i^2(t) + r \dot{u}^2(t) \right] dt \right\}, \qquad (2.4)$$

12

The functional E represents the expected value of the expression in brackets. Coefficient q and r are the weighting coefficients, which determine the respective contributions of the state variables $x_i^2(t)$ and control output $\dot{u}^2(t)$ to the value of the integral.

The OCM (Figure 2.5) contains an optimal linear regulator in combination with the Kalman filter (optimal estimator). The Kalman filter produces optimal estimates of the values of the state variables, given the noisy measurements of the linear combinations of these state variables. There are two places where noise is injected into the model. These account for the non-linear distortions during observation of the controlled variable (observation noise) as well as the noise in executing the control movements (neuromuscular noise). The values of the noise variances are quite difficult to determine [3], since their values depend on various parameters, such as nature and type of display, physical environment as well as the individual characteristics of a human operator.

Figure 2.5. The Optimal Control Model of the human operator (Hess, [4])

One of the strongest benefits, however, of the OCM is that it is capable of modeling multichannel control of the plant by a human operator, something that a structural model will struggle with. The model is capable of dealing with multiple of state variables simultaneously thanks to the state space representation used by the model.

2.4. Hess Structural Model

Ron Hess [4] conceptualized his model while working in the area of aircraft handling qualities. The Hess structural model, falls into a category of anthropomorphic models of human operator. The name of the category speaks for itself: the Hess structural model is a physiologically inspired model. The structure of the model emulates the signal processing in the central nervous and neuromuscular systems, while the human is performing a manual control task. The Hess model shares this concept with its predecessor – the structural isomorphic model (Figure 2.6), proposed by McRuer [2]. The key idea of the Hess model is to simulate the feedback paths from various sensory modalities (Figure 2.7). The Hess structural model has a more simplified architecture, since some of the blocks in Figure 2.6 are difficult to identify.
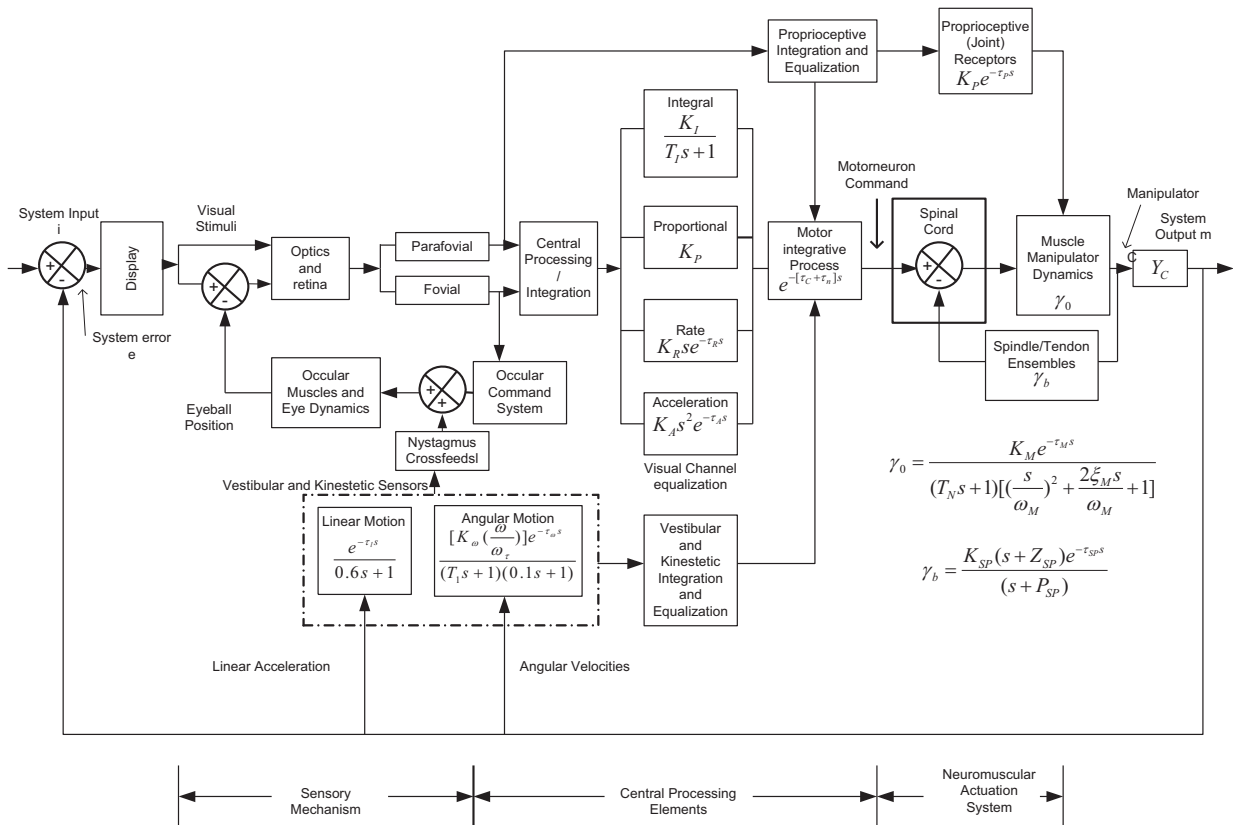
Figure 2.6. Isomorphic model of the human operator (McRuer, [11])

The human equalization then occurs through the feedback, which Hess [4] refers to as "proprioceptive" feedback. Moreover, the structural model was designed and its parameters are tuned to perform best in the vicinity of the crossover frequency.
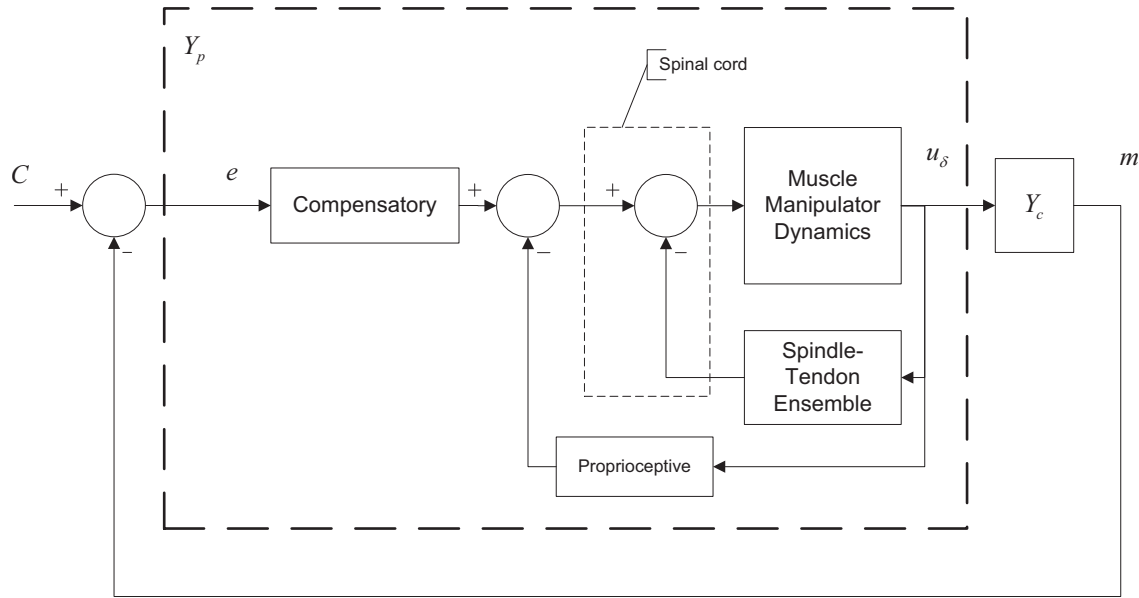
Figure 2.7. Major operator pathways for compensatory tracking (Hess, [4])
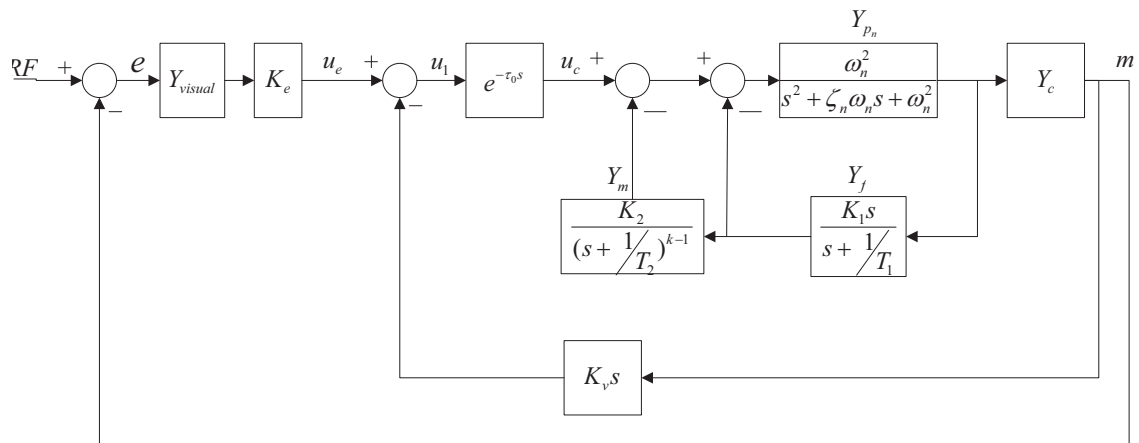
Figure 2.8. Structural model of the human operator (Hess, [4])

15

The following is a description of the functionality of the Hess model.

- The error signal is interpreted by the visual system and then presented to the human and multiplied by the gain K_e

- If the motion cues are available then the output signal, i.e. the rate of change of the output m is sensed by the vestibular system. Then it is multiplied by the gain K_v and subtracted from signal u_e. Please note that the version of the Hess model used during current research excludes the motion cues, i.e. K_v is equal to zero.

- The resulting signal u_1 is then passed through a delay, which is introduced there to account for the latency due to neuro-processing, motor nerve conduction, etc.

- Signal u_c forms the input to a closed loop system. In the open loop path there is a model Y_{p_n} of the limb driving the control inceptor.

- The proprioceptive feedback consists of two loops with the models of Golgi tendon organs and muscle spindles, which are illustrated by Y_m and Y_f blocks respectively. According to Hess [4], it is proprioceptive feedback that models the basic equalization capabilities of the human. The form of Y_m is determined by the form of Y_c, i.e. by the order k of the controlled plant.

If compared to the crossover model, the Hess structural model looks a lot more complex and overparameterized. However, it should not repulse anyone from using it; parameters of the model are generally chosen to satisfy criteria set forth by the crossover model. Table 2.1 contains nominal values of the parameters of the structural model with k being the order of the controlled plant.

Table 2.1. Hess structural model parameters (Hess, [4])

k	K_v	K_1	K_2	T_1(sec)	T_2(sec)	τ_0(sec)	ζ_n	ω_n $\left(rad/sec\right)$
0	0	1.0	2.0	5.0	a	0.15	0.707	10.0
1	0	1.0	2.0	5.0	b	0.15	0.707	10.0
2	0	1.0	10.0	2.5	a	0.15	0.707	10.0

a – selected to achieve K/s - like crossover characteristics

b – Parameter not applicable

K_e is chosen to provide desired crossover frequency

McRuer and Magdaleno [12] did a comprehensive study of the neuromuscular dynamics of the control limb of the human operator. They have derived the models of spindles, joint sensors, as well as the muscle/manipulator dynamics. These models could be incorporated into the structural model of the human operator in the format of the feedback (Figure 2.9). Hess, on the other hand, has limited "his" neuromuscular model to the second order transfer function with damping ratio ζ_n and natural frequency ω_n.

Figure showing block diagram with labels:

Retinal and Central Equalization

$K_e e^{-\tau_c s}$

Spinal Cord

Muscle/Manipulator Dynamics

$$\dfrac{-K_1 e^{-\tau_0 s}}{(1+T_N s)\left(1+\dfrac{2\zeta_a}{\omega_a}s+\dfrac{s^2}{\omega_a^2}\right)}$$

Display Input e

α_c

x

Manipulator Position c

Spindle Feedback

$$H_{sp}=\dfrac{K_{sp}(s+Z_{sp})e^{-\tau_{sp}s}}{(s+P_{sp})}$$

Effective Joint Sensor Feedback

$$H_J = K_J e^{-\tau_J s}$$

$K_{(-)}$ = gain.
$\tau_{(-)}$ = time delay.
T_N = muscle/manipulator lag time constant.
ζ_a, ω_a = muscle/manipulator damping ratio and undamped natural frequency.
Z_{SP}, P_{SP} = zero and pole of muscle spindle transfer function.

Figure 2.9. Components of the neuromuscular system (Magdaleno, [12])

The performance of the Hess structural model is generally quite satisfactory for most single degree of freedom compensatory manual control tasks. Figure 2.10 illustrates the frequency response function of the structural model as opposed to the precision model and experimental data. It can be seen, that the Hess model is free of the phase drop at the lower frequencies, which had been observed with the crossover/precision model.

18
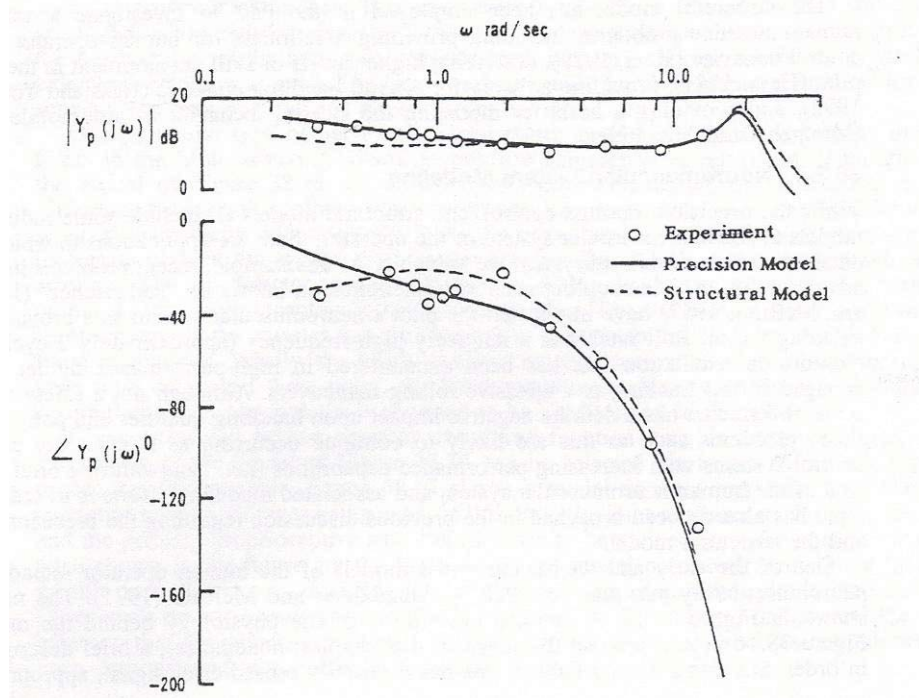
Figure 2.10. Sample comparison between Hess structural model, precision model and experimental data (Hess, [4])

2.5. Enhanced Hess structural model

The work on enhancing and expanding of the Hess structural model was conducted by Cardullo, et al. [5] in the framework of an investigation of influence of motion and force cueing on pilot performance. Therefore the sensory modality models of the vestibular and the haptic systems have incorporated into the overall structure of the Hess model. The vestibular system representation included models of both semicircular canals and otoliths, as well as the seat haptic receptors. These newly added modalities were implemented in a similar fashion to the proprioceptive feedback of the original Hess structural model.

The model of semicircular canals were modeled as given in Eq. 2.5:

$$\frac{\hat{\omega}}{\omega} = 5.73 \frac{80s}{(1+80s)(1+5.73s)}, \tag{2.5}$$

where ω is the angular velocity and $\hat{\omega}$ is the perceived angular velocity.

19

The model for the otoliths (Eq. 2.6) was:

$$\frac{F_p}{F} = \frac{(4 + 0.4s)}{(0.08s^2 + 5.016s + 1)},$$ (2.6)

Where F_p is the perceived specific force and F is the actual specific force resulting from the translational motion.

The haptic channel was modeled as:

$$\frac{F_{haptic}}{F} = \frac{(s + 0.01)}{(s + 0.1)},$$ (2.7)

Figure 2.11 illustrates the modified version of the Hess model. It can be seen that the new structural model also includes models of the motion system and that of the seat. The simulator motion system was modeled as a second order system (Eq. 2.8):

$$\frac{\omega_{ms}^2}{s^2 + 2\xi_{ms}\omega_{ms} + \omega_{ms}^2},$$ (2.8)

With $\omega_{ms} = 31.4 \frac{rad}{sec}$ and $\zeta_{ms} = 0.7$
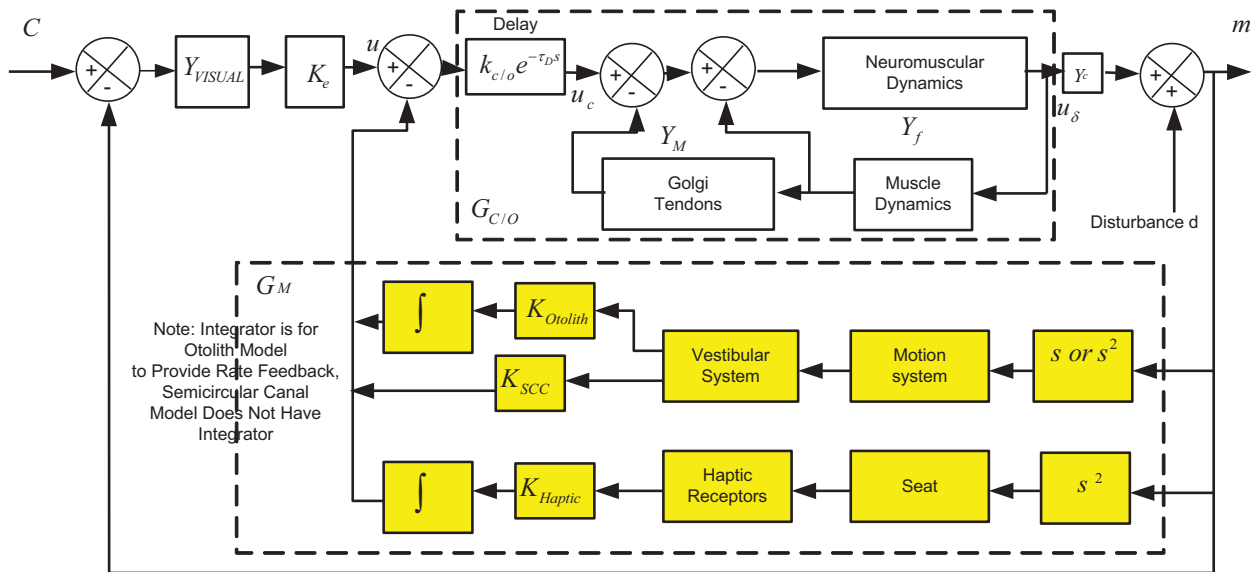
Figure 2.11. George – Cardullo-Hess Structural Pilot Model. Adopted from Cardullo, et al. [5]

20

The motion system dynamics also incorporates a washout algorithm, which was modeled by a high-pass filter of the following form (Eq. 2.9):

$$\frac{\omega_w^2}{s^2 + 2\zeta_w\omega_w + \omega_w^2},\tag{2.9}$$

With $\omega_w = 1.02\,rad/\sec$ and $\zeta_w = 1.0$

The Pacinian Corpuscles receptors were modeled as follows (Eq. 2.10):

$$\frac{F_S}{\Delta_d} = \frac{(s+0.01)}{(s+0.1)},\tag{2.10}$$

Where F_S is perceived haptic force on the buttocks and Δ_d is skin displacement.

The seat/human interaction model was given as (Eq. 2.11):

$$\frac{\Delta_d}{F} = \frac{9.8}{(s^2 + 0.12s + 453)},\tag{2.11}$$

Where F is the specific force applied to the seat cushion from the translational motion.

The parameters of all systems included in the enhanced Hess model are summarized in Table 2.2. Parameters of the expanded Hess structural model, which it inherited from the original version of the model were tuned manually so that the frequency response of the model complies with the requirements set by the crossover model in terms of the crossover frequency and the amount of phase margin in the system.

Table 2.2. Parameters of the expanded version of the Hess structural model

Hess structural model parameters										
Control Element Dynamics	K	K_e	$k_{C/O}$	K_1	K_2	$1/T_1$	$1/T_2$	τ_0	ζ_n	ω_n
$1/s$	1.0	1.0	20.0	3.0	2.0	0.01	-	0.1	0.707	10.0
$1/s^2$	1.0	1.0	20.0	3.0	2.0	0.01	0.1	0.1	0.707	10.0
Vestibular and Haptic rate feedback parameters										
Control Element Dynamics	K_{SCC}			$K_{Otolith}$			K_{Haptic}			
$1/s$	0.1			0.1			0.1			
$1/s^2$	0.1			0.1			0.1			

The overall performance of the model with added sensory modalities was considered to be satisfactory: the phase margin for added feedback sensory data was improved, which was supported by the experimental data [5]. Note that this model is used in Chapter 7 for analysis using data obtained at the NASA Visual Motion Simulator facility.

2.6. Hosman descriptive model

Hosman [10] has developed and validated the descriptive pilot model in 1996. The model is designed to simulate the pilot's behavior when performing a tracking task. A block diagram of the descriptive model is given in Figure 2.12.
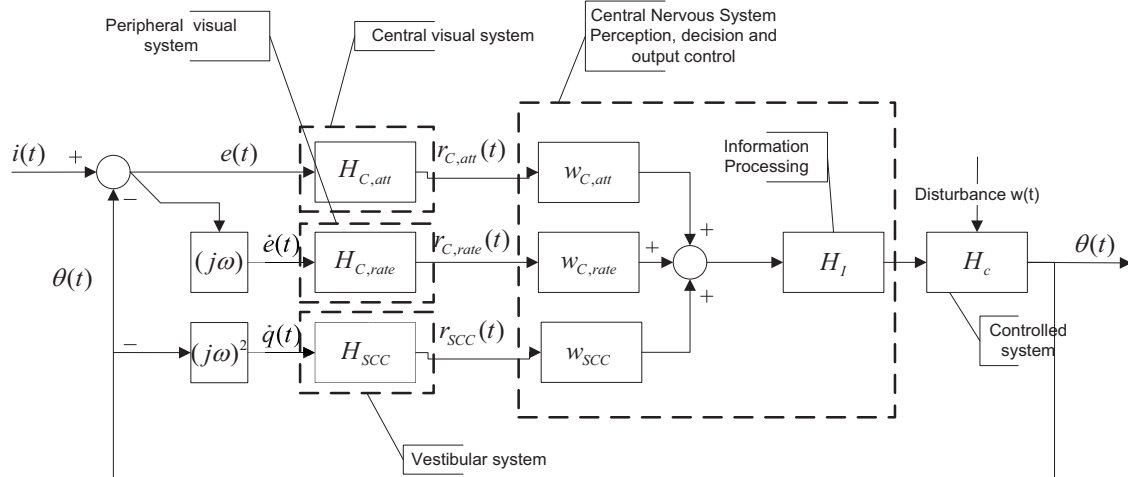
Figure 2.12. Block diagram of the descriptive pilot model (Hosman, [10])

The model is designed in such a way that the human perceives motion by means of two sensory modalities: vision and the vestibular system. Vision senses the attitude and angular rate, whereas vestibular system (semicircular canals SCC) is sensitive to angular accelerations. In the "central nervous system" subsystem the sensory information from three pathways are weighted and converged (summed up) into one single output. Each individual weighting coefficient W_i emphasizes the contribution of each sensory output.

The "information processing" block incorporates the time delay due to both the signal processing and neuromuscular-manipulator control.

The process of tuning/adjusting the pilot model revolves around minimizing the following cost function (Eq. 2.12):

$$J = \sum (e^2 + Q \cdot u^2 + R \cdot \dot{u}^2),$$ (2.12)

This cost function was designed to achieve the following:

- Good performance tracking

- Effective control effort

- Adequate bandwidth and stability of the control loop as expressed in the crossover frequency and in the phase margin.

23

For these reasons, the mean square of the control signal and its first derivative are added to the cost function. Q and R depend on the aircraft characteristics and on the task to be performed: either the maneuver or disturbance.

In his study [10], Hosman had demonstrated great potential of the model to provide good approximation of the actual data for various combinations of display both with and without motion. Figure 2.13 contains bode diagrams of the descriptive model, simplified precision model vs. actual data.
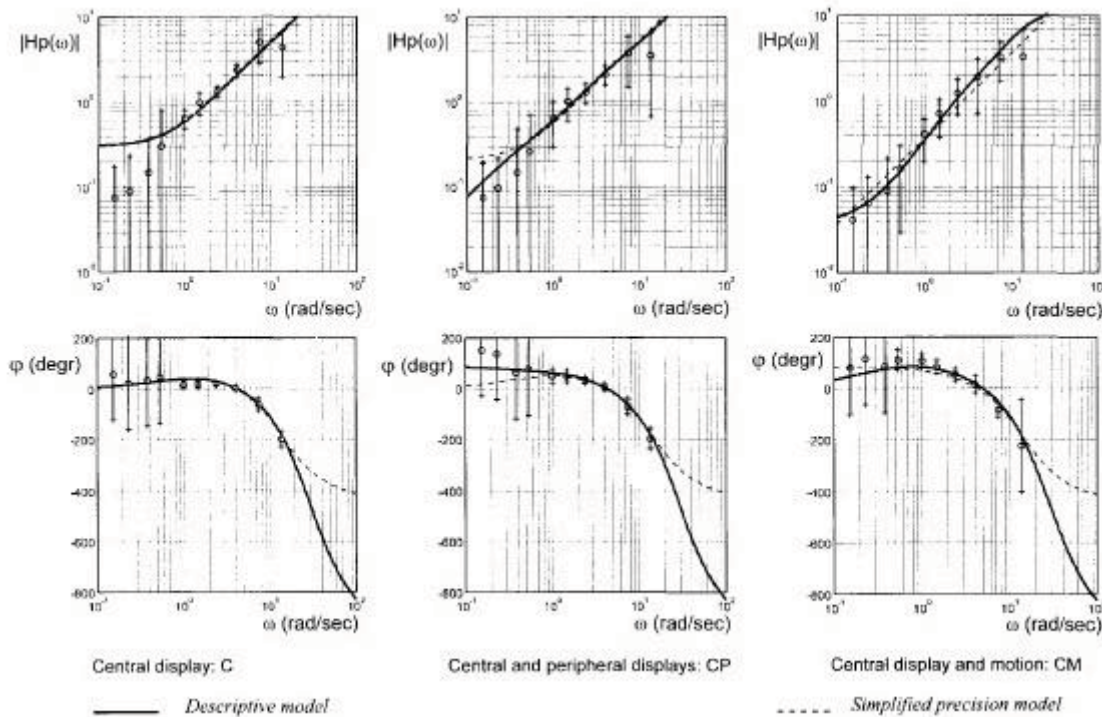
Figure 2.13. Bode plots of the descriptive model, simplified precision model and the actual frequency response (Hosman, [10])

It can be seen on these bode diagrams, that the descriptive model is in very good correlation with the experimental data. It also does not exhibit any deviation from the actual data in the lower frequencies range as opposed to the simplified precision model. As a final remark, it is important to mention that the descriptive model has a great potential to be able to capture individual differences in control behavior between various pilots. This can be accomplished by fine tuning the gain coefficients in the central nervous system block of the model.

2.7. Soft Computing based models

As a preliminary point, note that it was deemed to be unnecessary to get into a rigorous description of the fuzzy set theory in this section, therefore only a brief description will follow.

Fuzzy Set Theory (FST), a relatively young discipline of numerical computing, was founded by Lofti A. Zadeh [13]. Some decades later, Zadeh drew attention to the connections between FST and other relatively new numerical approaches, which led to an integrated concept of Soft Computing (SC). Zadeh [13]1 developed a theory of fuzzy sets, which as opposed to conventional theory allows for imprecise definitions, i.e. sets can be described using linguistic terms, such as small, medium, large, etc. The theory of Fuzzy Logic is based on inference algorithms, which relay elements of the input space to the elements of the output space by means of the linguistic rules. Such rules are often constructed based on the observation of the modeled process, assumptions and/or expert knowledge of the human operator involved in the process. The input and output spaces are, in turn, divided into sets, which are described by linguistic terms. The imprecision in definition of fuzzy sets is achieved with the concept of membership functions, which allow for a given element of the input/output space to be simultaneously a part of two (or more) different fuzzy sets. The key feature of fuzzy logic is that it attempts to model the inference processes of the human mind. The same concept, of biologically inspired algorithms, is shared by other essential contributors of SC, such as Artificial Neural Networks and Evolutionary Computing. Chapter 3 describes in detail the basics of these concepts, since they have become the main engine of the proposed parameter identification algorithm used in current research. In the subsequent paragraphs a brief description of the fuzzy based model of the human operator is given.

Since fuzzy theory provides a sufficient mathematical apparatus to model the inference processing phenomenon of the human mind, it was a natural decision to use it to model human operating in a closed loop with plant. The model developed by George [6], describing the behavior of a human operator performing one degree of freedom compensatory task, is a very good example of how the conventional manual control theory can be incorporated with the SC apparatus to form a hybrid model. In the compensatory task, the human operator tries to nullify the error, which is presented to him/her via a display, in the presence of random disturbances in the control process. The core of the model is the Fuzzy Inference System (FIS), which infers the

control output based on the amount of the tracking error. Figure 2.14 illustrates the fuzzy set definition for the human control and the displayed tracking error.
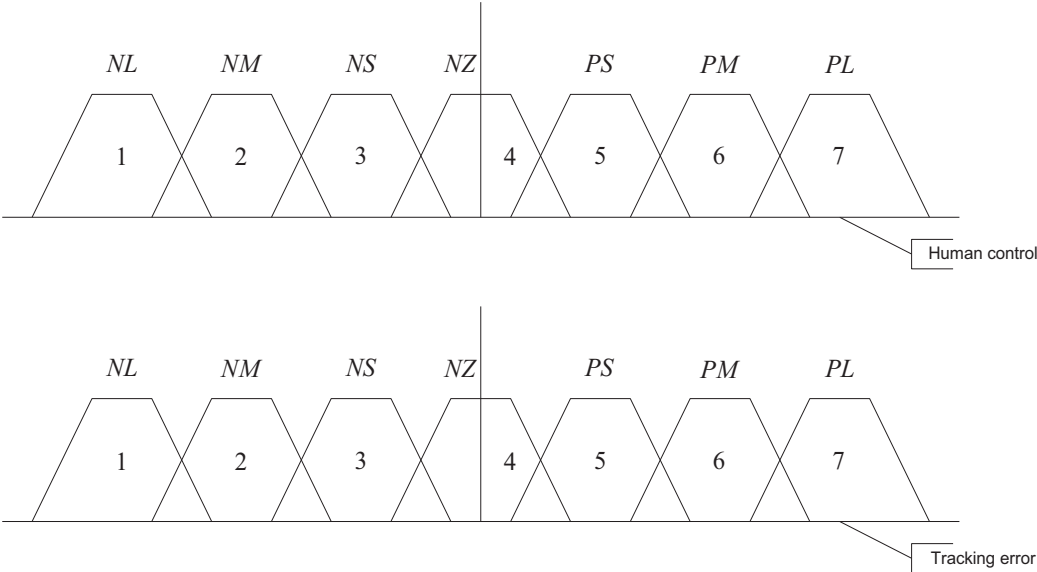
Figure 2.14. Fuzzy set definition. Adapted from George [6]

The linguistic terms used to describe the input space (tracking error) and the output space (control) are summarized in Table 2.3.

Table 2.3. Linguistic set definitions

Human Control Output	*Tracking Error*
NL - Negative Large	NL - Negative Large
NM - Negative Medium	NM - Negative Medium
NS - Negative Small	NS - Negative Small
NZ - Near Zero	NZ - Near Zero
PS - Positive Small	PS - Positive Small
PM - Positive Medium	PM - Positive Medium
PL - Positive Large	PL - Positive Large

The designed fuzzy inference system (FIS) based model contains the following production-rule system, which define the inference mechanism of the approach:

- If error is NL THEN human control is NL
- If error is NM THEN human control is NM
- If error is NS THEN human control is NS
- If error is NZ THEN human control is NZ
- If error is PS THEN human control is PS
- If error is PM THEN human control is PM
- If error is PL THEN human control is PL

The model was able to produce results rivaling the accuracy of the structural model of the human operator. Figure 2.15 contains power spectrum densities of the simulated and the actual control data.
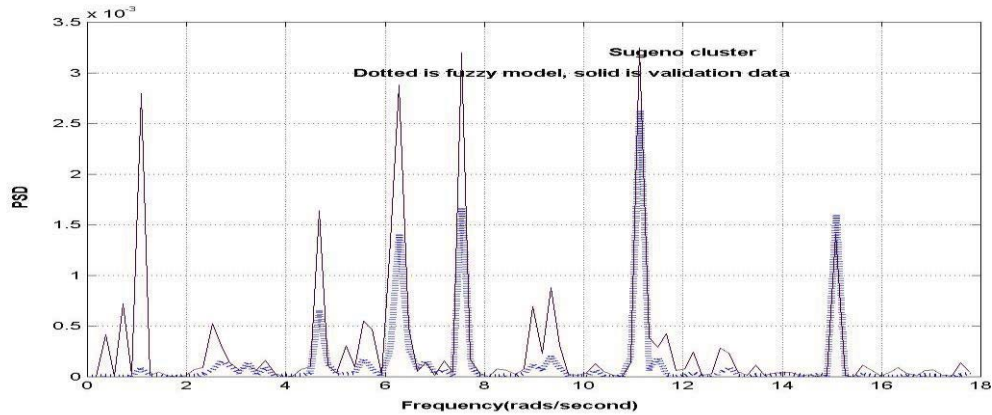
Figure 2.15. PSD of the fuzzy model (dotted) vs. PSD of the actual control data (solid) (George, [14])

It can be seen that the simulated control activity is in good correlation with the actual data. Some discrepancy is observed in the area of lower frequencies as well as power of some "bins" is underestimated. Overall performance of such simple FIS based model was deemed to be satisfactory.

The most recent research by George [14] has demonstrated that much better results are obtained if the Adaptive Neuron Fuzzy Inference System (ANFIS) is used. ANFIS is a hybrid product of the FIS and Artificial Neural Network (ANN).

2.8. Summary

This brief excursion into the history of the development of human operator models demonstrated a few things: despite the complexity of the available models, none of them are perfect: whether it is too complex and overparameterised, or it fails to correctly simulate the behavior of a pilot at certain frequencies. All conventional operator models have one thing in common – they are quite good in simulating behavior of a generic pilot, i.e. individual differences of pilots, their individual control strategies are usually averaged out to produce the average (generic) control behavior. The non-linear part of the control behavior, which is referred to as remnant, is usually modeled as a band-limited white noise. Very little research has been done in an attempt to model individual control strategy of different operators.

28

The other peculiarity that is shared by all human operator models mentioned in this overview is that there is no universal rule or methodology on how to choose parameters of these models. In most cases it is done manually in order to drive the given model to comply with either the crossover model standards or to match a given set of data.

This research is aimed to cover these flaws in operator modeling. Instead of looking at the problem from the standpoint of modeling a generic operator, it is proposed to take advantage of the individual differences between operators and develop a universal enhancement that will allow to model such differences, namely the control strategy (Chapter 5). This approach essentially models that portion of the remnant, which account for the control strategy of every individual operator. On the other hand, this research develops algorithm for automated tuning of the parameters of any given model of the human operator (Chapter 4). This study will test the proposed algorithms on three major human operator models: Hess structural model, Hosman descriptive model and OCM.

One thing is certain – the quest for the universal model is still on.

3. Overview of machine intelligence technique

3.1. Introduction

Chapter 2 presented a brief description of one of the essential aspects to the body of Soft Computing (SC) techniques, namely the fuzzy inference system. This chapter exposes the reader to other SC techniques, such as Artificial Neural Networks (ANN) and Genetic Algorithms (GA), which is one type of Evolutionary Computing. Research by George [14] has demonstrated that SC techniques can be successfully applied in the area of man-machine systems. This study heavily relies on SC. The proposed parameter identification technique, described in this manuscript, utilizes GA in its core. Moreover, modeling of individual control strategy is accomplished with help from ANN. More detailed discussions in terms of this application follow in Chapters 4 and 5.

Soft Computing can be characterized as a toolbox, which can be used when building intelligent systems, designed to model the human ability to reason, make decisions and adapt. The roots of soft computing lie with the concepts of Artificial Intelligence (AI), however it involves more advanced techniques rather than concentrating only on symbolic manipulation, inherent to conventional AI. An alternative term for SC is Computation Intelligence and some researchers use the generic term Machine Intelligence to encompass both SC and traditional AI. The main constituents of SC are neural networks, fuzzy inference systems and derivative-free optimization, such as genetic algorithms.

This study employs neural nets and genetic algorithms, therefore the subsequent sections of this chapter describe in detail the specifics of these computational paradigms.

3.2. Neural Nets

Artificial Neural Networks, or simply Neural Networks (NN), are one of the primary constituents of the SC domain of computational arsenal. The design of NN is mainly inspired by the natural cognitive processes occurring in most living organisms. One of the main features of the NN is its potential to process an enormous amount of data by engaging in parallel processing. The sheer amount of inter neuron connections ensure its stability and immunity to errors, which

can damage some of the connections. Another important feature of the NN is its capability to mimic the human's ability to learn as well as to cluster data.

It is also very important to mention that NN as well as other SC tools are capable of forming hybrids with other SC methods and paradigms, thus bringing us closer to modeling a larger range of natural processes.

The following paragraphs discuss the biologically inspired basis for building the ANN. Artificial Neural Networks were originally inspired by and built in an attempt to model natural processes of data collection, interpretation and processing occurring in nervous systems of living organisms. The main unit of operation of such systems is a neuron. In order to build a fully functioning model of the nervous system one needs to model the neuron first.

German scientist Heinrich Wilhelm Gottfried von Waldeyer-Hartz in 1891 introduced the term "neuron" to describe nerve cells, which are responsible for transporting signals in and out of brain. The neuron has a body with a nucleus. Numerous extensions project away from the body of the neuron. These extensions are crucial, since they conduct signals into and out of the neuron, thus communicating with other neurons. There are two types of extensions:

- Dendrites. Extensions of this type are characterized by smaller size and a large number of branches. The neuron uses dendrites to receive signals from other neurons.
- Axon. Axon is the single, thick extension of the neuron, which is responsible for transmitting the outbound signal to other neurons. Transmission occurs via axon terminals.
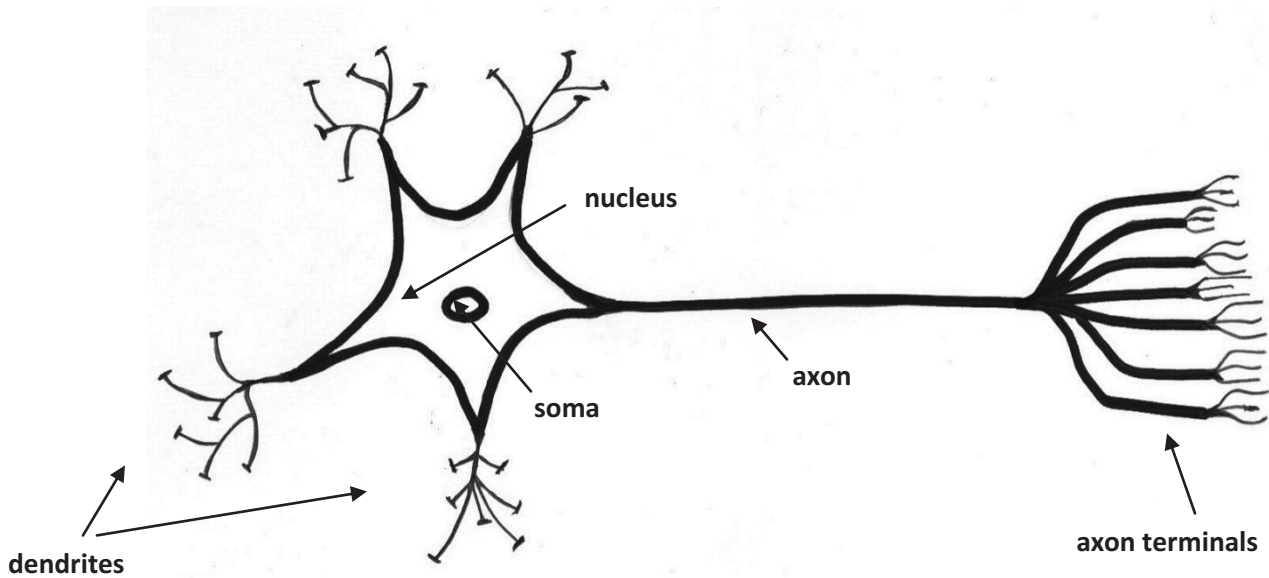
Figure 3.1. Schematic representation of a neuron

Transmitting signals between the axon terminals and/or dendrites/soma is a highly complicated electrochemical process. There are two types of dendrites: excitatory and inhibitory. If an excitatory dendrite is stimulated then it is more likely for the neuron to "fire", i.e. conduct the signal. If an inhibitory dendrite is stimulated, then it is more likely that neuron will be passive. The probability of different dendrites to be stimulated is proportional to the amount of a special chemical substance in the vicinity of a particular dendrite. It can be concluded from the above, that mathematically speaking, one can assign a "weighting" coefficient to every dendrite of a given neuron: the larger the coefficient the more likely it is to be stimulated. In the mathematical model of the neuron, all incoming signals will be multiplied by those weighting coefficients to ensure proper functioning of a neuron. Whether the dendrite is excitatory or inhibitory can be modeled by making the associated weighting coefficient positive (excitatory) or negative (inhibitory). The neuron firing mechanism depends upon the cumulative action of dendrites: if excitatory dendrites "outweigh" the inhibitory, the neuron will fire. Mathematically it can be expressed as if y_i, the sum of weighted signals coming from the stimulated dendrites (Eq. 3.1), exceeds some activation threshold, the neuron passes through, i.e. a signal (fires), to other neurons connected to it. The magnitude of the signal passed depends on the absolute value of y_i relative to the activation threshold value.

$$y_i = \sum_{j=1}^{N} w_{ij} a_j \tag{3.1}$$

There are several ways of implementing the activation function. One of the most common is the sigmoid activation function (3.2). Graphically such function is represented in Figure 3.2.

$$f(x) = \frac{1}{1 + e^{-\beta x}} \tag{3.2}$$

The parameter β is usually defined by the user. As it can be seen from Figure 3.2 this parameter determines the slope of the activation function. The higher the value of β, the more it is likely for the activation function to perform in a switch-like fashion. Conversely, the smaller the value of β, the lower the slope of the activation function becomes.
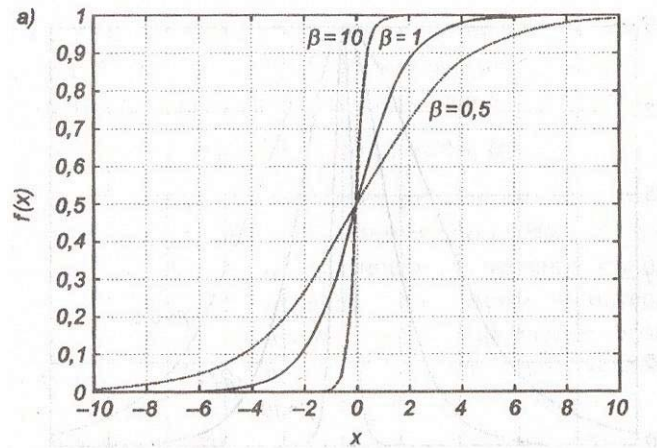
Figure 3.2. Sigmoid activation function (Osowski, [15])

Summarizing the above, the model of the neuron can be represented in a form of the signal flowchart as shown in Figure 3.3: the weighted signals from other neurons are first summarized, then are passed through the activation function; the output is then passed on to another layer of neurons or being interpreted as the final output of the neural network.
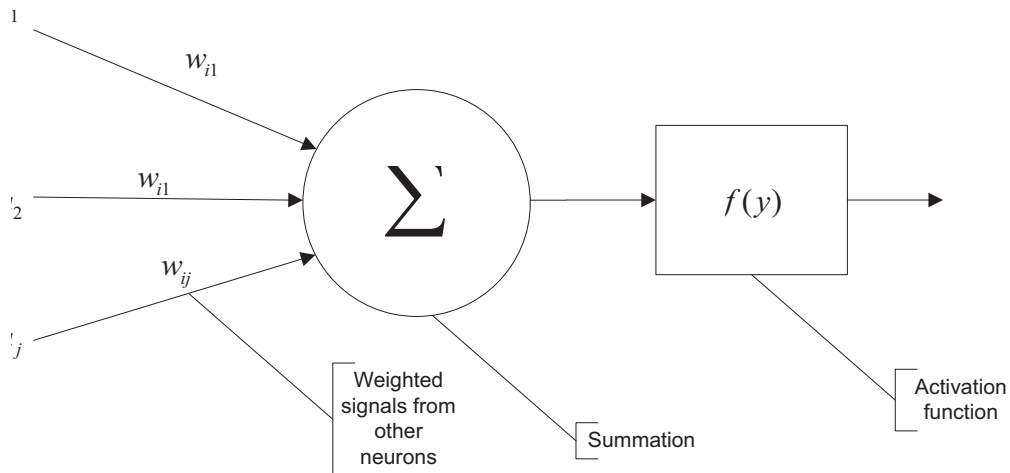
Figure 3.3. Schematics of a mathematical model of a neuron

An essential part of any ANN is its training. The most commonly used training mechanisms are based on minimization of some error function. Usually it would be the discrepancy between some actual and simulated data. The output of the ANN is represented as a function of all weighting coefficients used by the network. Training of the network is essentially optimizing those weighting coefficients to minimize the error function. Osovsky [15] summarizes a large variety of training algorithms. To name a few: Algorithm of variable metrics by Broyden-Fletcher-Goldfarb-Shanno (BFGS algorithm), Levenberg–Marquardt algorithm, Steepest decent algorithm, Resilient Back Propagation (RBPROP), etc. This manuscript does not contain descriptions of the training algorithms for the sake of brevity. For more detail refer to the original source [15]. It is shown in the following chapters; however, that training of the ANN in its conventional sense can be avoided completely. The weighting coefficients are optimized by the proposed parameter identification technique according to some fitness criteria imposed on the output signal of the system.

There are no rigorous recommendations as far as the number of neurons and/or layers of neurons to be used by ANN are concerned. Such decisions are to be made by the user. However, it is very important to be aware of the problem of overparameterizing the network, i.e. introducing a larger than necessary number of neurons/layers into the network. A large number of weighting coefficients will result in poor time-effectiveness of the training algorithm and may also lead to a problem of overtraining the network. Overtraining, also known as overfitting, can lead to results, which are significantly off the range of the training data, thus rendering the

network useless. Moody [16] provides guidelines on how to select the number of weighting coefficients in order to avoid potential overtraining.

For the current research ANN was chosen as the primary tool for modeling the portion of operator's remnant, which accounts for the operator's control strategy. One may argue that fuzzy inference systems are more appropriate to be used when modeling control strategy, since FIS are more inspired by the topology of the decision making process. The counter argument here is that process of decision making has a lower frequency when compared to control strategy decision made based on the reflexes. One of the data sets (Chapter 4) used in this study was obtained with the Manual Control Laboratory (MCL) software. The control task there can be characterized by the high frequency components present both in the reference input as well as the operator control activity. Therefore, it has been hypothesized that an operator bases his/her control strategy inputs using reflexes rather than some rigorous decision making algorithm. In addition to that, the high pace of the control task makes it difficult to extract the if-then rules, which establish the input/output relationship of the FIS. Chapter 5 describes details of the network implementation and incorporation into an existing structural model of a human operator.

3.3. Simple Genetic Algorithm

The family of derivative-free optimization algorithms, which are often referred to as Genetic Algorithms (GA), is a major contributor to the armament of the soft-computing techniques. The term *derivative free* is used here is to emphasize the fact that there are no derivatives taken during the algorithm's execution. However, genetic algorithms still use some evaluation criteria, on which basis they converge to an extremum in a fashion similar to that of the conventional optimization algorithm such as gradient descent.

GA were first researched by Holland [17] and later summarized by Goldberg [18] in a form of a theory of simple genetic algorithms (SGA). This section of the chapter will introduce the reader to the basic concepts of operation of SGA's since they have become the optimization engine for the automated parameter identification technique (APID) designed and used in this study.

The GA is the global search technique frequently used while solving optimization problems. GA's are largely inspired by evolutionary biology and encompass such concepts as

inheritance, mutation, selection and recombination. The concept of natural selection (also known as "survival of the fittest") ensures that only the most "fit" parameters are selected from each generation. The overall structure of a simple GA is shown in Figure 3.4. It will become evident from further discussion that the problem of automated parameter identification can be interpreted as a multi degree of freedom optimization problem, i.e. a large number of parameters have to be optimized simultaneously.

There are several reasons why GA's were used in this study. Among them is the fact that conventional optimization methods, such as golden search and exhaustive search are deemed to be less computationally efficient (number of iterations and mathematical manipulations it requires to converge) than a GA based optimization. The other vote for using GA's as opposed to conventional optimization methods is determined by avoiding the problem of prioritization of parameters when looking for an optimal solution. GA's optimize all parameters at once by means of representing parameters in the form of a string, or, speaking in terms of genetic programming, chromosome.
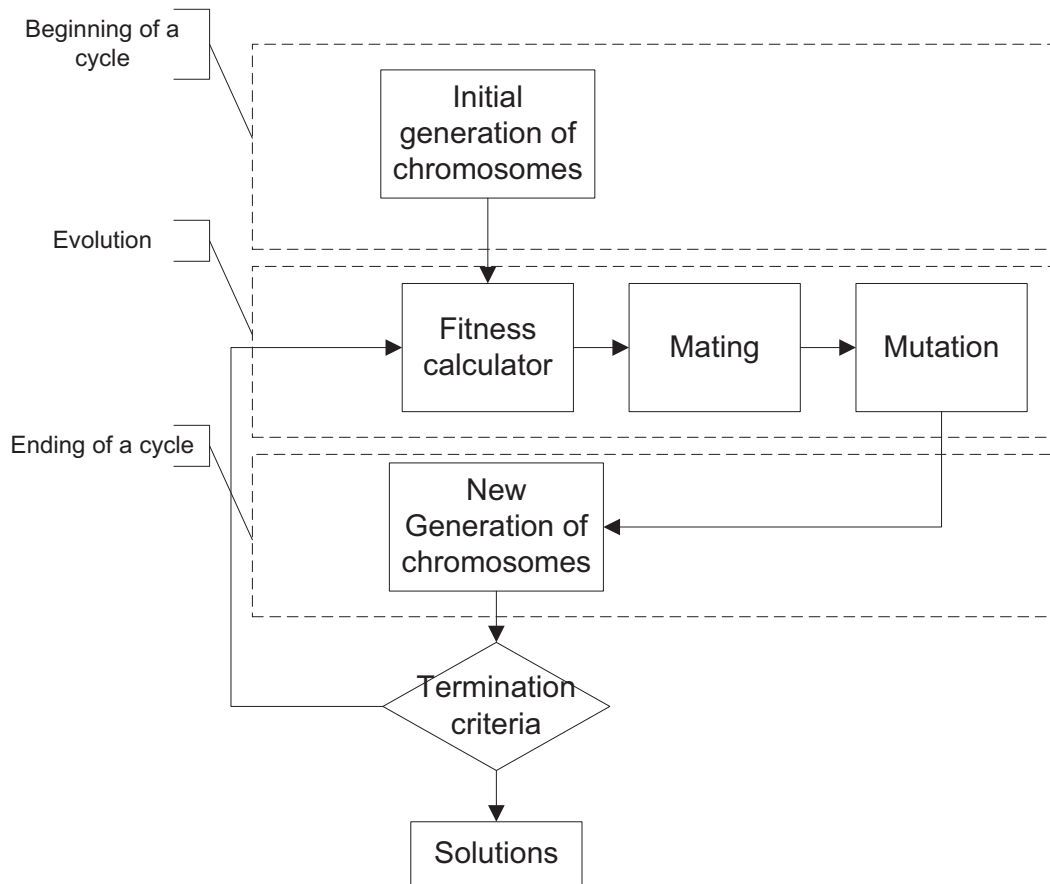
Figure 3.4. Simple GA structure flowchart

It can be seen that a GA is implemented as an iterative process. Every iteration, which is referred to as an epoch or cycle of evolution, begins with the generation of candidate solutions, i.e. a large number of chromosomes. Usually chromosomes of the first generation are generated arbitrarily or based on the "best guess" of the final solution. Generations of the chromosomes are updated at the end of the iteration. Each chromosome is a binary representation of the string of parameters, which are being optimized. Each parameter in a chromosome occupies a certain number of bits depending on the desired accuracy of estimation. Figure 3.5 graphically illustrates the structure of a sample chromosome.
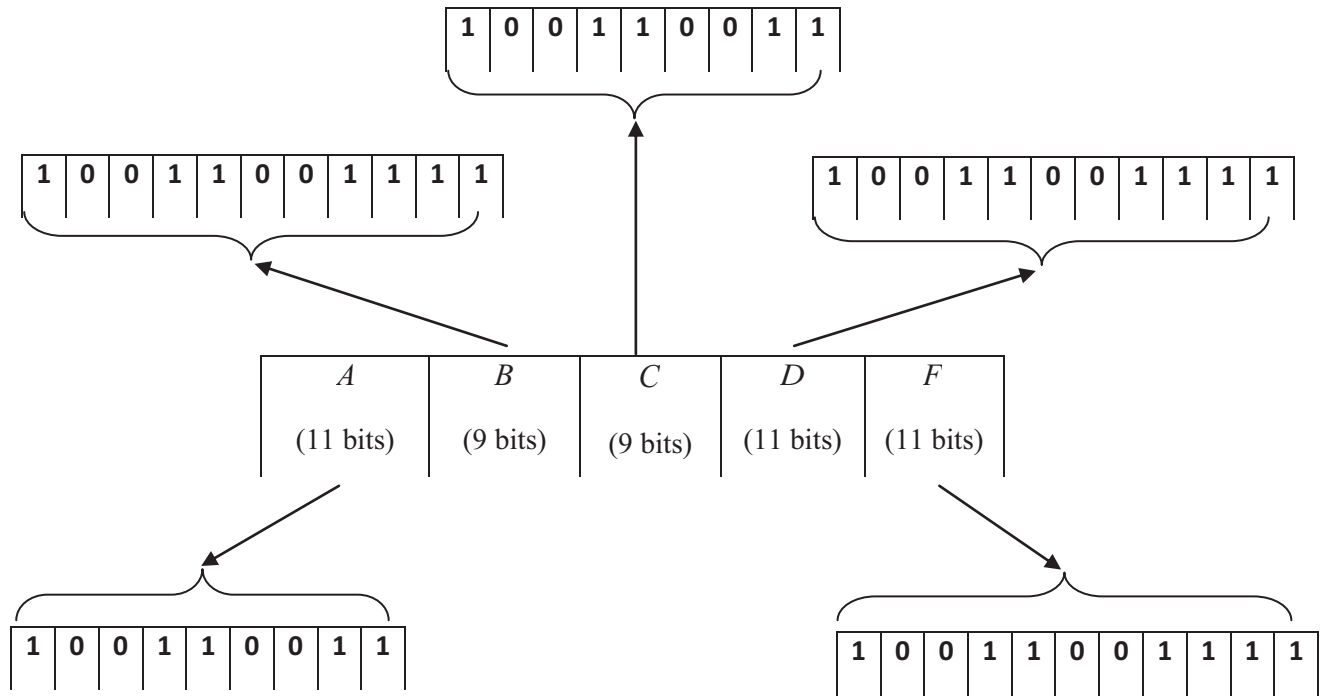
Figure 3.5. Example of a chromosome structure. A,B,C,D and F are parameter to be optimized

Within one epoch chromosomes evolve to a generation of new ones. This happens by means of mating, which is followed by mutation. Mating occurs in pairs, which are formed randomly. The process of mating is often implemented as a gene exchange at the crossover point. The crossover point for each substring is selected randomly for each round of mating. Figure 3.6 contains schematics of how the gene exchange occurs at the crossover point. Two mating chromosomes are divided into two parts: P_{1X} and P_{1Y} for the first mating chromosome, and P_{2X} and P_{2Y} for the other mating chromosome. The resulting offspring chromosome inherits one part from the first parent and the other part from the second parent.
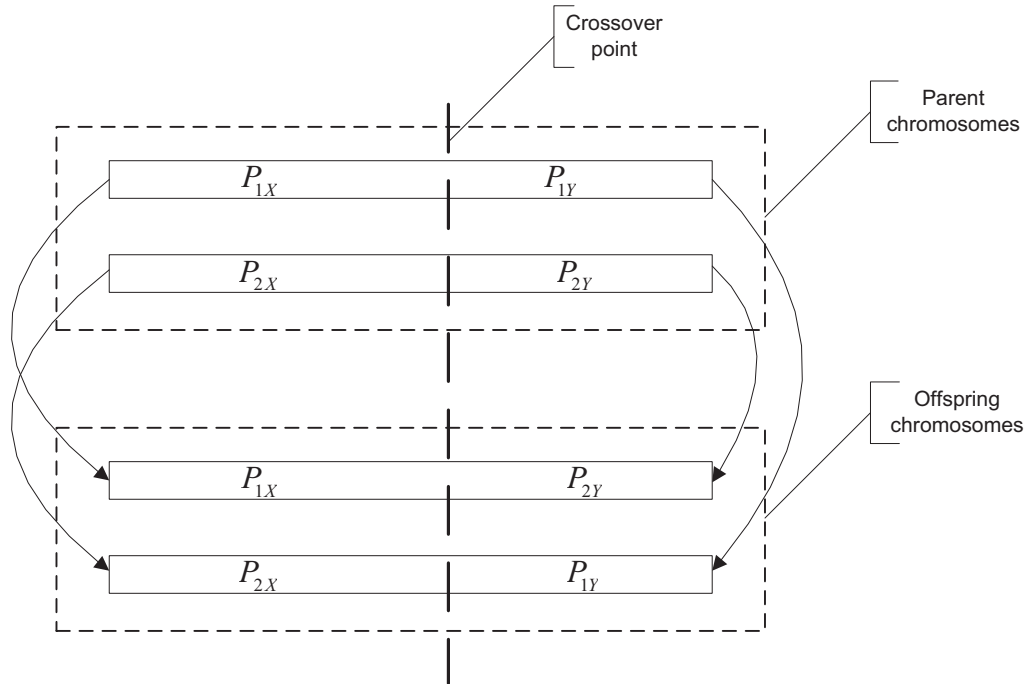
Figure 3.6. Mating algorithm

As the algorithm progresses through generations, solutions evolve toward a better solution. This is ensured by the concept of natural selection. The worthiness of every chromosome is evaluated by calculating its fitness. Several of the most fit chromosomes are selected and cloned to the next generation unchanged. The rest of the chromosomes are bound for mating.

Mutation is yet another biologically inspired process which is also implemented within the GA. Each gene of the offspring chromosome may change its value according to certain probability. This event occurs after the gene recombination described in the previous paragraph. The resulting chromosome forms a new member of the next generation.

Mutation completes the evolutionary process within a single epoch. The resulting generation of chromosomes is then used in the next iteration of the algorithm. Usually, the algorithm terminates when either a predetermined number of iterations has been reached, or a satisfactory fitness level has been reached. If the algorithm has terminated due to a maximum, user defined number of generations; a satisfactory solution may or may not have been reached.

Davis [19] has developed a variation of the hill climbing optimization algorithm, which is essentially a hybrid of a classical hill climbing technique and an SGA. The algorithm is referred

to as bit-climbing algorithm. It inherited binary notation from SGA. On the other hand it manipulates only a single chromosome. Moreover, steps like mating and mutation are omitted, since a new generation chromosome is produced by flipping every bit of a chromosome in a certain order. Chapter 6 concentrates on describing the proposed automated parameter identification technique, which uses the bit-climbing algorithm. Greater detail of the algorithm and its implementation are given there in. During preliminary research it was established that both algorithms (bit-climbing and SGA) yield result of the same accuracy. However, the decision on using the bit-climber algorithm in the final application was made based on the fact that it is computationally faster than the SGA.

4. Description of Experiments

4.1. Introduction

There are three sets of data used in this study. Each set was obtained via different sources: Manual Control Laboratory (MCL) Software, Predator Unmanned Aerial Vehicle (UAV) simulations by USAF, and NASA Langley Research Center (LaRC) Visual Motion Simulator (VMS) facility.

The first data set was obtained with the use of the Manual Control Laboratory (MCL) software package and involves a total of 19 subjects. The key feature of the MCL is that it simulates a very basic compensatory tracking task. The software allows modifying the controlled plant dynamics, reference signal, number of degrees of freedom etc. The test subject population in the MCL experiments were very diverse, i.e. it included both novice and experienced operators. The software package allowed recording the full state of the system in a format acceptable for future analysis in MATLAB.

The second data set was provided by the United States Air Force Research Laboratory (US AFRL) and involves data collected from the Predator UAV simulator. Experiments involved performing a mid-air maneuver of changing (reducing) the airspeed while maintaining the altitude and attitude of the aircraft. One of the main features of the task is that due to some peculiarities of the visual system of the simulator (Figure 4.6) it can be considered as a pursuit tracking task, rather than purely compensatory tracking. It will be shown that this results in a slight modification of the structural model of the human operator. The recorded data set included the full state of the aircraft as well as the pilot control input, such as pitch stick, roll stick, rudder pedals and throttle. The subject population was much more consistent than the MCL subject population since it involved 10 active duty USAF UAV pilots.

The third data set came from the NASA Langley Research Center Visual Motion Simulator Facility. The experimental data used in the study were obtained in the framework of investigation of the new delay compensation algorithms. The manual control task consisted of making a landing approach given different flight conditions. Recorded data included pilot activity and full aircraft state. The subject population consists of six pilots (both commercial and

military) including the VMS research pilot. Therefore, this subject set was somewhat diverse. While they were all pilots, their flying experiences were quite different.

The following sections of the chapter present the aforementioned experimental setups in detail.

4.2. Manual Control Lab software

The Manual Control Laboratory software was developed by the Engineering Solutions Inc, and represents a software package designed to model a variety of manual control tasks for educational and research purposes. The software provides the user with a graphic interface, which simulates a simple manual one or two degree-of-freedom (DOF) control task. The control tasks available are as follows: step response, compensatory tracking, and pursuit tracking. Data used in this study were obtained by running a set of experiments using the compensatory tracking task simulation. Figure 4.1 shows a screenshot of the MCL simulation interface. For a compensatory task the operator has control over the cursor, which is subject to an external disturbance input. The cursor moves horizontally across the screen and over the target area. This is a single degree of freedom (DOF) control task in which the operator has to force the cursor to stay within the limits of the target.
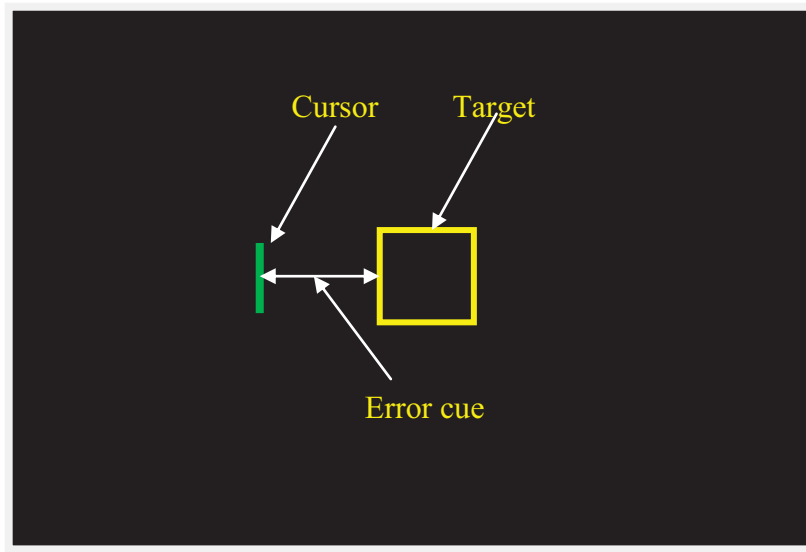
Figure 4.1. MCL simulation interface. One degree of freedom compensatory tracking task

The MCL software provides the user with the ability to change the reference input, plant dynamics, target size, time of simulation as well as allows introducing time delay into the man-machine system. The data acquired was sampled at 60 Hz. The external disturbance signal $RF(t)$ (Eq. 4.1) is represented by the sum of sinusoids of different amplitudes and frequencies (Table 4.1). The plant dynamics was chosen to be $\frac{1}{s}$. The duration of a single simulation is 35 seconds, which results in 2099 data points.

$$RF(t) = \sum_{i=1}^{n} A_i \sin(\omega_i t),$$
(4.1)

Table 4.1. Amplitudes and frequencies of sinusoids used in the reference signal during experiments with MCL

Sinusoid i	Amplitude A_i	Frequency $\omega_i, (rad/\text{sec})$
1	1.0	0.35
2	1.0	0.72
3	1.0	1.08
4	0.2	2.6
5	0.2	4.7
6	0.2	6.4
7	0.2	7.6
8	0.2	11.1
9	0.2	15.2

MCL records a full state of the systems: reference signal, tracking error, operator control activity, plant output. Moreover, upon completion of the simulation run MCL optionally prompts the user to graphically reproduce and save frequency response functions and power spectrum density of an operator, plant and/or plant plus operator. It automatically stores recorded data in

ASCII format. Figure 4.2 contains a sample time history of the reference signal, operator control activity and plant response signals.
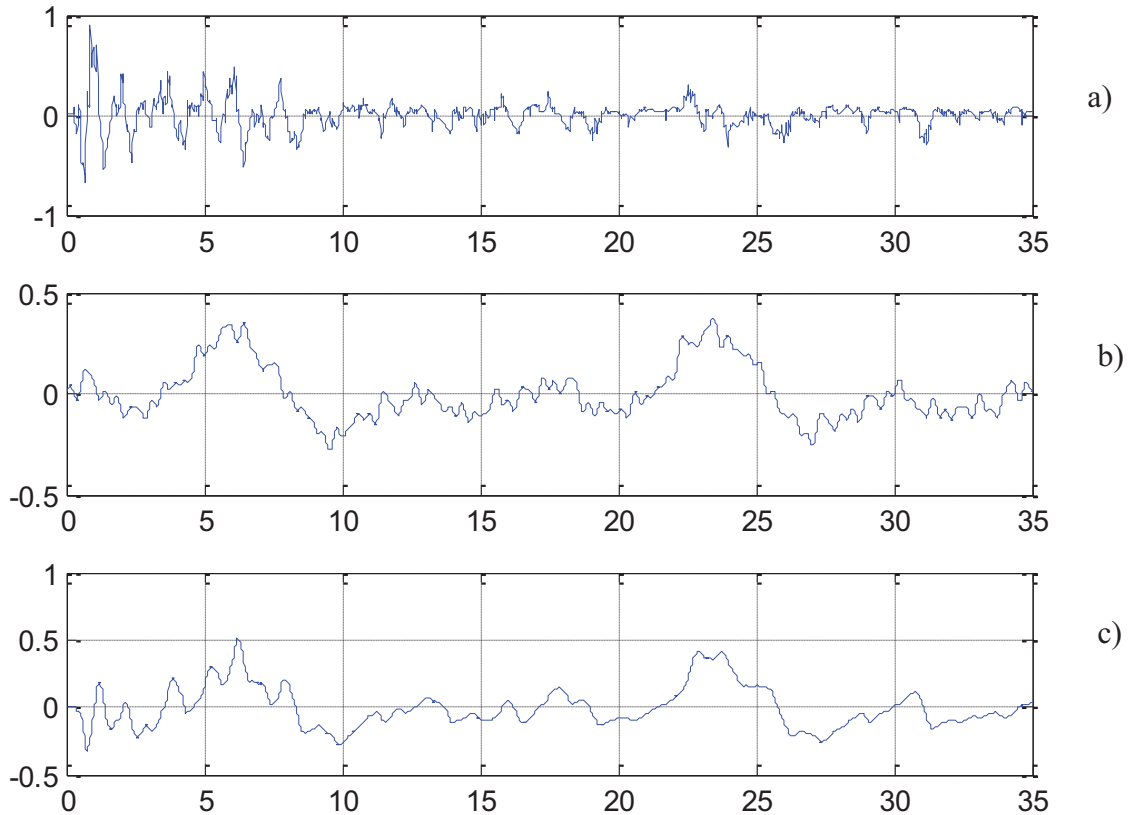
Figure 4.2. Sample time histories of signal obtained with the MCL software: a) actual human control activity; b) input reference signal; c) plant output

The experiment protocol included a verbal explanation of the experiments, instructor demonstration of the simulation and several pre-trial runs during which each subject had an opportunity to familiarize him/herself with the software as well as to practice in order to achieve an asymptote on the learning curve, i.e. when there is little or no improvement in performance observed (Figure 4.3). Total time spent within the limits of the target for each run, was chosen to be the measure of performance in these experiments.
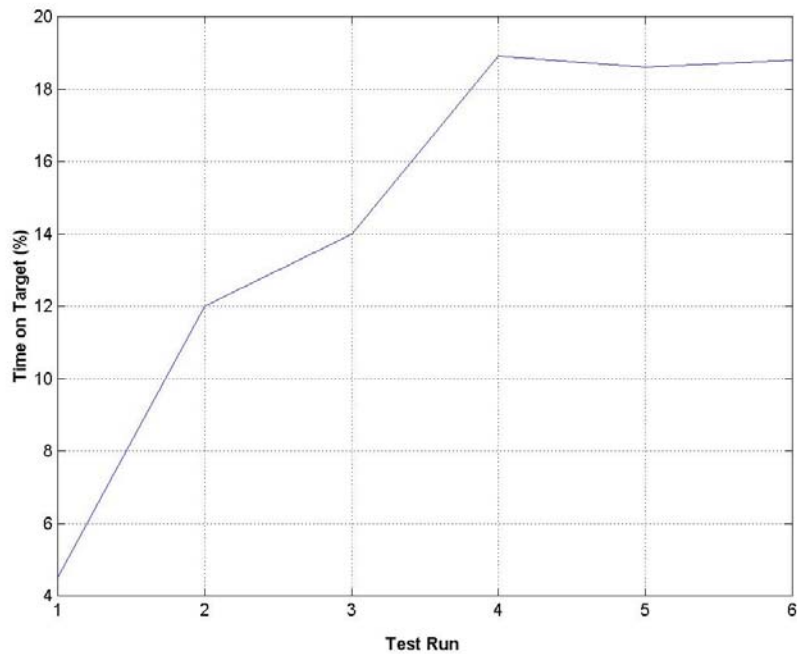
Figure 4.3. An example of the learning curve of a given subject. Adopted from George [14]

The available data set contains information for a total of 19 subjects. The subject population was very diverse, due to individual skill level. Subject population consisted of both novice operators as well as very experienced operators.

4.3. USAF UAV simulation data

The data set described in this section was obtained and provided by the United States Air Force using the Predator Synthetic Task Environment (STE), which is a fixed base flight dynamics simulator of the Predator RQ-1A System 4, Unmanned Aerial Vehicle (UAV) (Figure 4.4). Due to security concerns, information only on a single synthetic task was disclosed, namely the Basic Mid-air Maneuvering Task, where pilots had to reduce the airspeed at a constant rate while maintaining the heading, attitude and altitude of the aircraft.

Figure 4.4. USAF Predator RQ-1/ MQ-1/ MQ-9 Reaper Unmanned Aerial Vehicle (UAV) (photo available at: http://www.af.mil/photos/mediagallery.asp?galleryID=5541&page=5)

Figure 4.5 shows the UAV STE. According to Ball and Gluck [20], this simulator is a scaled down (hardware-wise) version of a Predator trainer, designed to be used by the research organizations around the country (USA), subject to ITAR restrictions against foreign disclosure. Hardware of the simulator includes the visual system, which is composed of two CRT monitors placed side by side, side-stick, throttle as well as rudder control inceptors. The left monitor (Figure 4.6) presents the image of the heads up display, which is usually superimposed over the camera view out of the nose of the UAV. In these experiments, the camera view was intentionally turned off to simulate instrument flying. The heads up display interface contains information on various flight parameters such as: angle of attack, airspeed, vertical speed, altitude, engine RPM. The cross in the middle of the screen corresponds to the vertical and lateral axis of the aircraft. The solid horizontal line crossing the entire screen is the artificial horizon, which moves up and down if there is change in pitch angle, and rotates around the center of the cross to simulate changes in the roll angle. The right screen (Figure 4.7) of the simulator produces the feedback information upon completion of the simulation run.

Figure 4.5. UAV STE: two monitors, side stick, throttle control, rudder control (not shown). (Courtesy of AFRL)
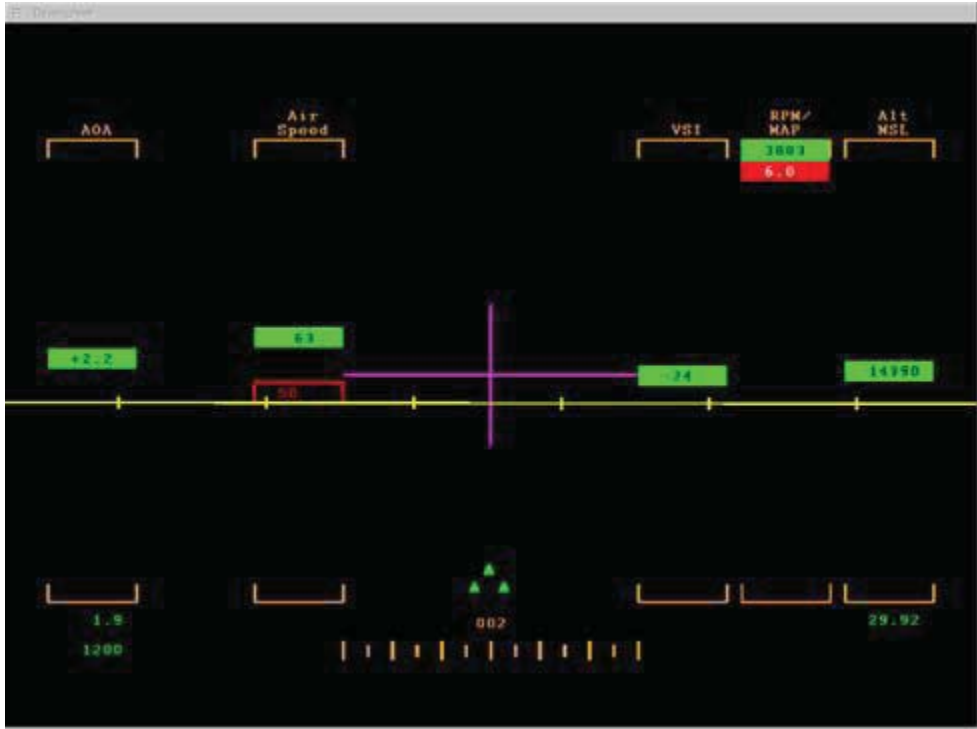
Figure 4.6. UAV STE: primary screen with simulated instruments. (Courtesy of AFRL)
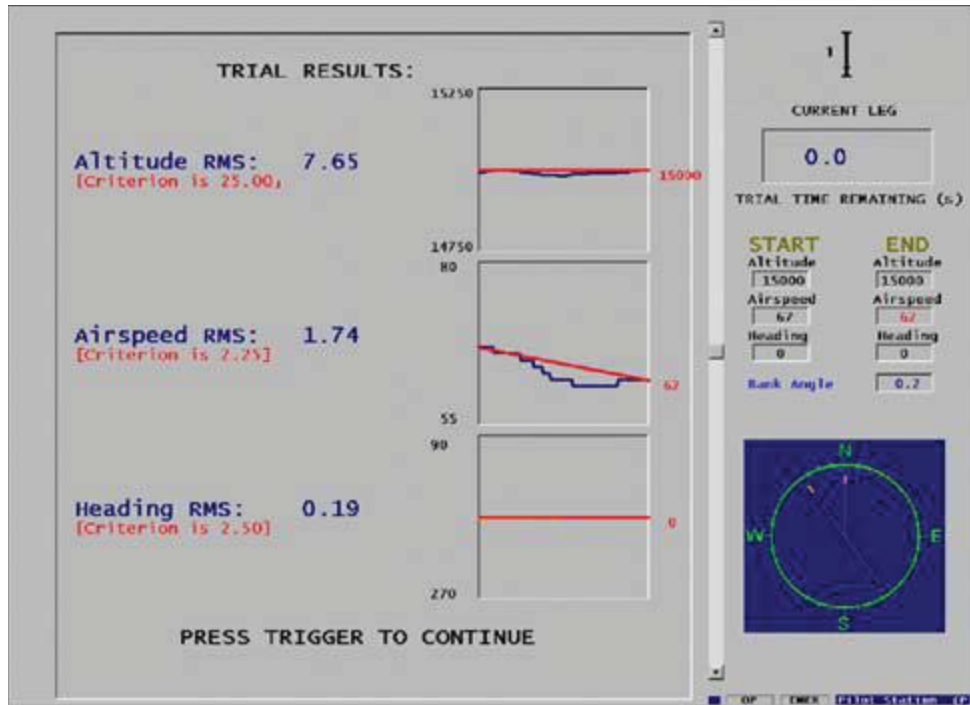
Figure 4.7. UAV STE: Secondary screen with feedback information. (Courtesy of AFRL)

The feedback data contains, but is not limited to altitude, airspeed, heading deviations plotted over the desired values. Numerical values correspond to root mean square data, which is a quantitative measure of the tracking performance of a pilot.

There are over 60 variables recorded during experiments. These include:

- pilot control inputs: roll stick, pitch stick, rudder pedal and throttle;

- aircraft state variables including accelerations, velocities and position;

- displayed pilot information from the heads up display such as airspeed, altitude and attitude;

- Other variables including subject number and trial run.

All data have been stored in ASCII format, which can be used in further analysis using mathematical platforms such as MATLAB. Figure 4.8 contains a sample time history of a pilot control activity.
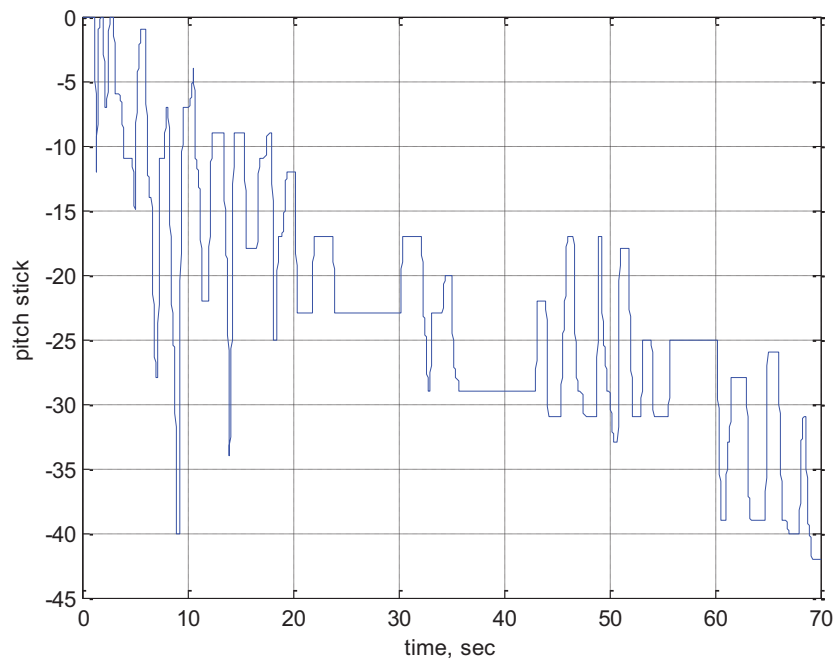
Figure 4.8. Time history of an actual control behavior of a UAV pilot

The nature of the control task in these experiments is pursuit tracking, rather than compensatory tracking. This conclusion was made based on the analysis of the graphical representation of the required change in airspeed. This has a direct implication on how such a manual control task is modeled. According to Hess [4], an additional feed forward path must be added to the structural model of the human operator to account for a pursuit nature of the control task. Figure 4.9 contains a block-diagram of the Hess structural model of the human operator with such additional feed forward path (dotted box) added. It feeds the delayed information of the reference signal derivative into the model before it is passed through the neuromuscular dynamics portion of the model. Other models of the human operator used in this study such as the descriptive model by Hosman and OCM can be modified in the similar fashion. Appropriate block diagrams are given in Appendix A of the manuscript.
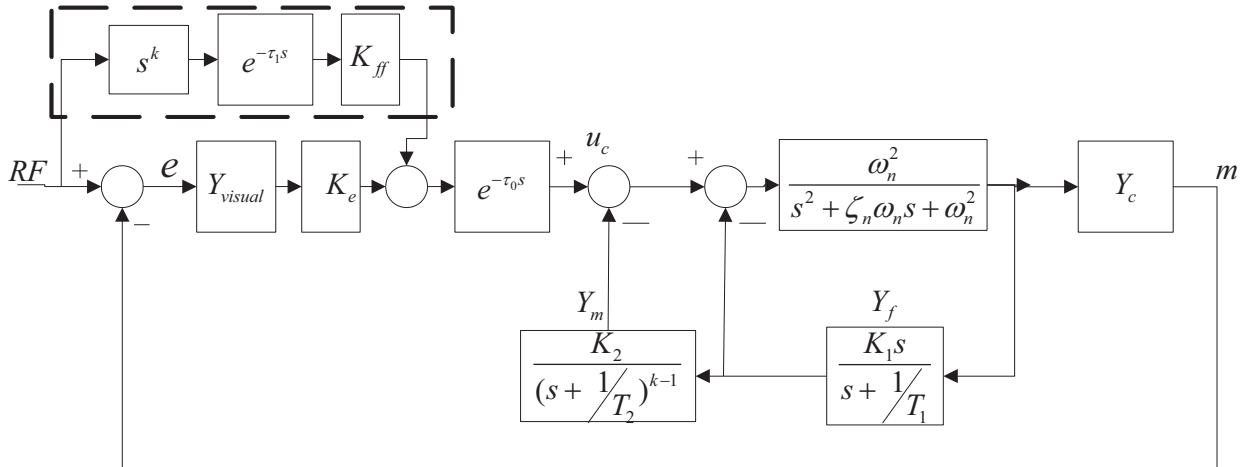
Figure 4.9. Hess structural model of the human operator with the feed forward path (dotted box) to account for the pursuit nature of the control task (Hess, [4])

4.4. NASA simulation data

Data used in Chapter 7 were obtained at the Visual Motion Simulator (VMS) facility at NASA Langley Research Center (Figure 4.10). The simulator features a six degree of freedom hexapod motion system, a two crew member cockpit with a state of the art Evans and Sutherland ESIG 3000 GT visual system, which provides the crew with the computer generated out the window imagery. The cockpit (Figure 4.11) is equipped with side-stick control inceptor, rudder pedals and throttle controls. Instruments are simulated in the form of analog gages as well as the heads down CRT displays, which simulate primary flight display, artificial horizon and a generic electronic engine display. The simulator motion system has an option to be driven by various motion cueing algorithms, which include classical adaptive algorithm, optimal, and non-linear optimal algorithms [21]. The control task chosen for the experiments involved landing approach under variable conditions.

Figure 4.10. NASA Langley VMS facility. (Courtesy of NASA Langley)
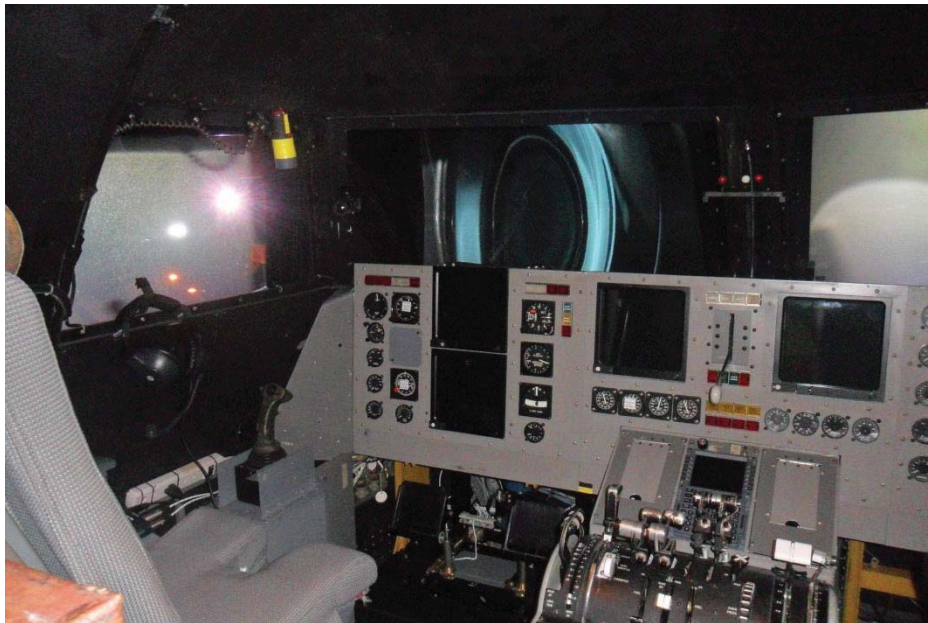
Figure 4.11. NASA Langley VMS cockpit view. (Courtesy of NASA Langley)

The simulator utilizes a large civil transport aircraft model in the landing approach configuration, gust and wind models, flight management and flight control computer systems. The simulated airport is Dallas Ft Worth (DFW) International Airport.

This research used results obtained only during the straight-in approach. During the straight-in approach the pilot makes a landing from a specified altitude and distance before the runway. A complete listing of the initial conditions can be found in Table 4.2. During the landing approach, the pilot uses several cues such as out-of-window view, glide slope error and localizer error. The latter two provide instrument representation of the longitudinal and lateral error relative to the ideal landing approach geometry. The task at hand, therefore, is purely compensatory tracking. During the straight-in approach, a 10 knots wind begins as a head wind, swings around to a 90 deg wind from the left in the mid-way of the approach, and continues to swing around to a tail wind as the aircraft crosses the threshold.

Table 4.2. Landing approach trim conditions

Altitude	1300 ft BARO, 697 ft AGL
Airspeed	135 kts
Heading angle	180 deg
Distance to runway	2 nautical miles
Flaps	Full, Gear down
EPR	1.19
Glide slope	ON
Localizer	ON

Over 60 variables are recorded and stored digitally during the experiments. These parameters include:

- The four pilot control input signals: roll stick, pitch stick, rudder pedal and the throttle;

- The accelerations, velocities and displacements in the 6-DOF earth fixed geodetic frame, accounting for 36 variables;

- Some variables of errors, such as glide slope error, localizer error, etc;

- Other variables, including variables in the motion system and the instrument readings.

The data were originally stored as text files. These files were then converted to MATLAB data files for further analysis. For a complete description of the experiments at NASA, please refer to the source by Guo [22].

4.5. Summary

It is important to mention the increasing complexity of the control task in the data sets used in this research. The MCL control task is the most basic of them all: a single degree of freedom compensatory tracking. The UAV data represent a much more complex simulation environment. Pursuit tracking of the airspeed assumed a two degree of freedom control, i.e. pilots were using both the pitch stick as well as the throttle. Consequently, the control task had to be split into two different channels of control. The research presented in this manuscript, is based on the pitch stick control only. The NASA LaRC VMS data were obtained in an even more complex environment, which included an active motion system. The simulated aircraft landing approach requires manual control in four different channels: pitch stick, roll stick, rudder pedals and throttle. The research presented in chapter 7 is based on the lateral aircraft control aspect of the landing approach. It was the responsibility of the pilot to null any roll of the aircraft due to side wind disturbance.

The other aspect of the used data is the diversity of the subject population. The MCL experiments, by far, used the most diverse group of subjects. The skill level of participants varied quite significantly. The most consistent subject population took part in the UAV experiments at AFRL. The NASA experiments involved a relatively diverse group of pilots with both civil and military background. The major differences between pilots were observed in the control strategies used to perform the same landing approach task. Since data used in this research is identical to that used by George [14], it is recommended to refer to the original document by

George [14] for a thorough analysis of the sample size and confidence limits of the data from each of the data sources.

5. Proposed enhancements to the selected models of the human operator

5.1. Introduction

The research community has accumulated substantial data throughout the years demonstrating a significant difference among individuals in terms of control behavior. On the other hand, there is a variety of widely used human operator models, which were built based on such diverse data. These models allow the prediction of the control behavior of a generic operator. However, they are less effective in modeling control behavior of a particular individual. The explanation here is such that most of the conventional operator models were designed and built based on the assumption, which originates in the pioneering work by Tustin [1], that human operator working in a closed loop man-machine system can be modeled as a linear system. Therefore, in the case of the structural models of the human operator, all subsystems are modeled as linear, time invariant functions. All individual-specific non-linear aberrations, observed during experiments, are usually accounted for by injecting a band-limited white noise (remnant), which has a limited ability to discriminate among different subjects. This study is aimed toward building a set of enhancements, which can be successfully incorporated into existing linear models of the human operator in order to identify and quantify the non-linear component of the control behavior of a given individual.

Zacharias and Levison [23] developed, implemented, and validated a compensatory tracking task for use in identifying changes in operator control strategy. Yoshihiko, et al. [24] developed a neuro controller based algorithm to determine the skill level of an operator performing an inverted pendulum stabilization control task. On the other hand, there has been virtually no research done to quantify the person-dependent, non-linear component of the control that would allow discriminating among different operators regardless of their skill level.

The first enhancement, which is referred to as *Testing Element of Control (TEC)*, is aimed at modeling the subcognitive adaptation mechanism of human behavior. It is hypothesized that such a mechanism is employed by the human operator in order to become familiarized with the system behavior, or in other words to adapt to the system response, in order to produce adequate control. Here, TEC is represented by a simple artificial neural network, which feeds off the tracking error and its derivative to produce a "personalized" augmentation of the linear

55

component of the control signal. It is very important to note that TEC does not completely account for all non-linearities in human control behavior. On the contrary, it is proposed to introduce TEC in addition (Figure 5.1) to the classical remnant into the man-machine system.
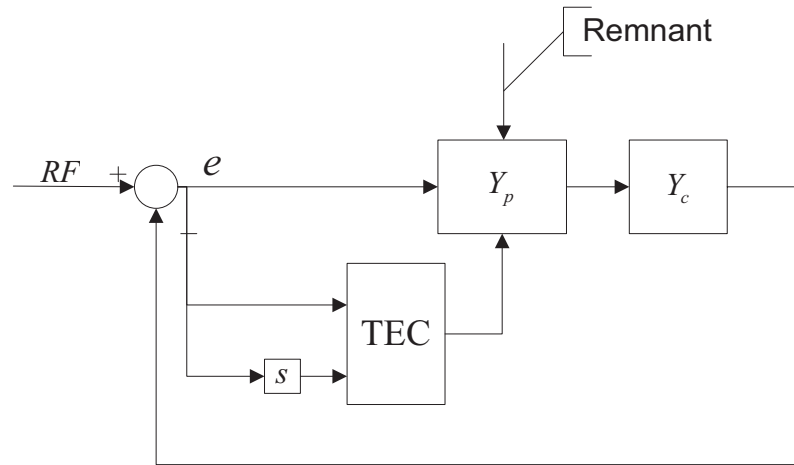
Figure 5.1. Block-diagram of a closed loop man-machine system with TEC and remnant added.

The development of this enhancement is inspired by the observation of "testing" inputs, which are introduced by an actual operator in order to learn the behavior of the system. The main hypothesis here is that different operators utilize this "system familiarization" technique differently, i.e. testing control inputs may be introduced at different frequencies, different rate and power by different operators.

The other enhancement is given in the form of an *equiripple* filter, which conditions the power spectrum of the cumulative control signal before it is fed into the controlled plant. The idea behind using such a filter is based on the observation of the actual control activities of different operators: there may be a significant variation in levels of power at any given frequency of the control signal depending on a given individual. The proposed enhancement allows shaping the simulated control signal power spectrum in order to match it with the spectrum profile of an actual control signal of a given individual.

This chapter describes in detail the theory behind these enhancements to the operator models as well as provides detail of implementation in the Matlab environment.

5.2. Testing Element of Control (TEC) algorithm

As has been pointed out earlier, remnant takes into account effects associated with nonlinearities present in the man-machine system. It can also account for the uncertainties in the system, which might not be associated with processing of the input signal. Remnant is an essential feature of any man-machine system, where a human operator may also periodically introduce some "testing" control signals for better, more accurate control of the system and/or to adjust his/ her control strategy.

It is a well-known fact that every individual can perform the same task in a manner different from the others. Such individual differences can be manifested in the amount of non-linear control operators generate. In other words, control behavior of different operators may have different power spectrum content (Figure 5.2), i.e. different operators would excite different frequencies. The observed differences can be attributed to different testing control inputs being introduced by different operators. The conventional implementation of the remnant in the form of a band-limited white noise does not allow discriminating between different testing control elements inherent to different subjects. This research, on the other hand, takes a different approach to modeling the non-linear element of control behavior of a human operator. It is proposed to distinguish TEC from other non-linearities. It is also proposed to model the TEC with the use of the soft-computing technique such as artificial neural network. In Chapter 3 it is indicated that one of the main features of ANN is its learning capability, which is directly used by the proposed methodology. The main hypothesis here is that one can design and train the artificial neural network to model the TEC of a particular individual.

One may argue that it would be more appropriate to use fuzzy inference systems (FIS) to serve the purpose, since it (FIS) carries on the reasoning mechanism, inherent to decision making process. Indeed, George [6] has demonstrated that FIS have great potential when modeling operator behavior, however, there is an assumption, which makes ANN more attractive than FIS for the current application. A human operator working in a closed loop with a plant while performing a high frequency control/tracking task is making his/her control movements in a more reactive/subcognitive mode, based on his/her training, experience and acquired reflexes, rather than by engaging in the decision making process. Therefore, it becomes quite problematic to extract the expert knowledge, which forms the basis for the if-then rules of any FIS. ANN, on

the other hand, inherits the human expertise by definition since it is trained based on the actual control activity data. The following subsections describe in detail the peculiarities of implementation of ANN.
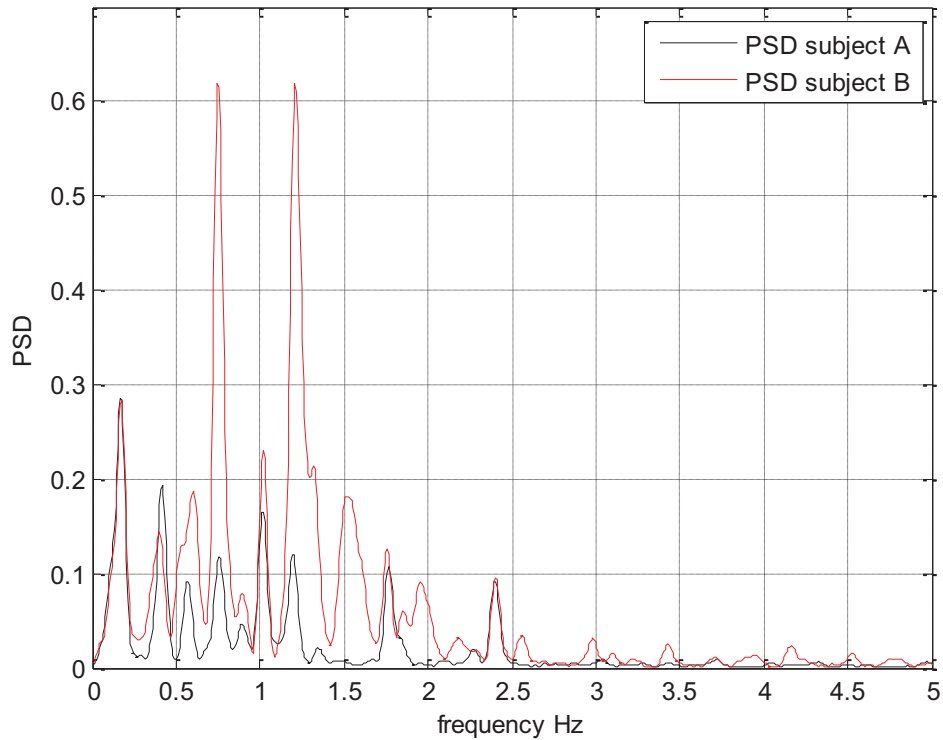
Figure 5.2. Actual control signal power spectrum of different operators

5.2.1. Neural network architecture

Chapter 3 provide some theoretical background on ANN. This section, however, illustrates how this theory can be applied to model the TEC behavior of a given operator working in a closed loop man-machine system.

Figure 5.3 presents a general diagram of the network that has been implemented in this study. There are three major layers of the network: input, hidden and output layers. The input layer is responsible for preconditioning the input data and distributing it among the nodes of the hidden layer. The hidden layer contains four nodes. Three nodes are neurons, whereas the fourth node is a constant and is often called the "bias" of the layer. More details on this are given later

in the text (5.2.3). The third layer consists of the output neuron and the post-processing block, which rescales the output signal. All connections inside the network have weights associated with them resulting in total of 13 weights. As will be shown in Chapter 6, these weights will be automatically tuned by the proposed automated parameter identification technique, in order to achieve optimum performance for each individual.

5.2.2. Input layer

There are two inputs used by the network. According to the general architecture of the man-machine system, the human operator adjusts his/her behavior based on the perceived tracking error. Therefore it was logical to use the tracking error signal $e(t)$ as a primary input to the ANN. George [14] demonstrated that the usage of the rate of change of the tracking error improves the accuracy of results. Therefore, since the task is similar, $\dot{e}(t)$ was included as an input.

Before the input signals are passed on to the hidden layer, they must undergo some preconditioning. The pre-processing blocks map the input signals onto the [0,1] interval. The system of Eq. 5.1 defines the mapping procedure. The parameters of such pre-conditioning: a_1, a_2, b_1, b_2 - are derived in order to ensure that the actual tracking error signal and its derivative, obtained for multiple subjects, are properly mapped onto the [0,1] interval.

$$\begin{cases} u_{11}(t) = a_1 \cdot e(t) + b_1 \\ u_{12}(t) = a_2 \cdot \dot{e}(t) + b_2 \end{cases},$$

(5.1)

Table 5.1 contains values of parameters a and b for different data sets used in this study.

5.2.3. Hidden layer

After the input signals have been rescaled, they are passed on and distributed among the nodes/neurons of the hidden layer. Each neuron performs two functions: summation and activation. In order to keep the number of unidentified parameters as low as possible it was decided to use a simple sigmoid activation function as opposed to Gaussian, or bell-shape functions. The shape of the sigmoid activation function and its mathematical expression were given in Chapter 3.
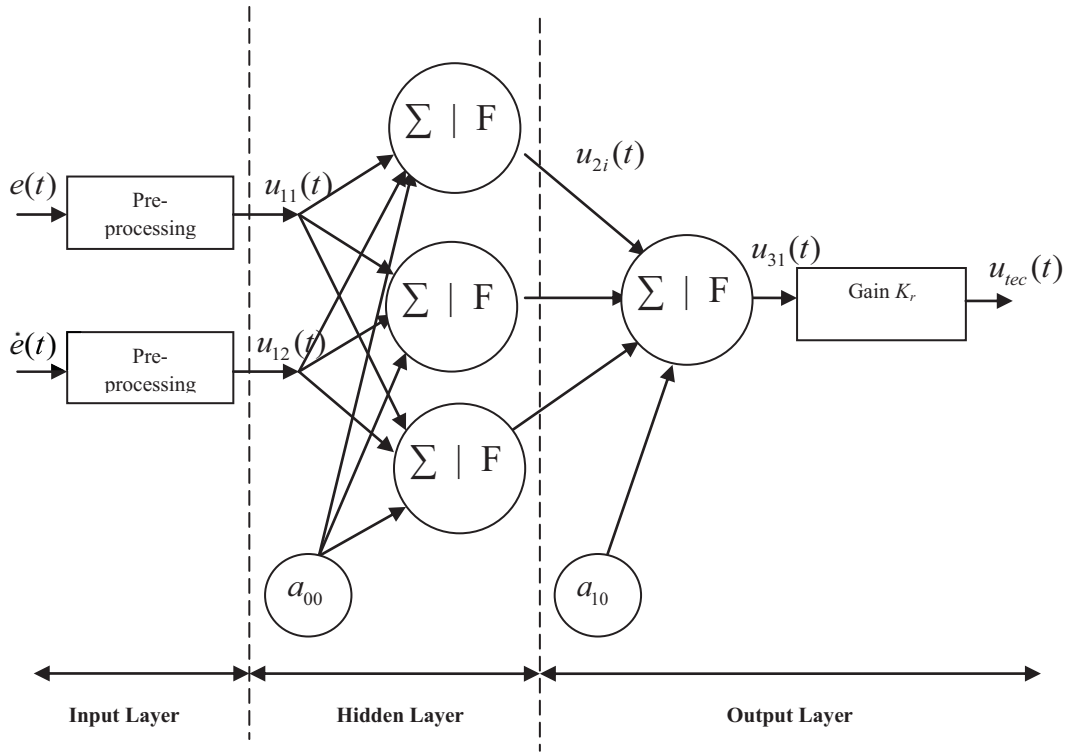
Figure 5.3. Architecture of the ANN used to model the control strategy element of the remnant

In order to make the ANN more flexible, i.e. the activation functions could slightly adjust their center relative to zero, an additional node is added to the layer. Such a node is referred to as a *bias* node. The value of the bias node is kept constant in the proposed architecture of the network and is equal to one. When this node is multiplied by the associated weight of the corresponding layer w_{ji0}, it provides a bias to each sigmoid activation function in the layer. The bias node models the tendency of a natural neuron to be either excitatory or inhibitory in nature.

The mathematical expression of the output signal $u_{2i}(t)$ for the *i-th* neuron in the hidden layer is given by the system of Eq. 5.2. The first expression performs summation of all incoming signals multiplied by the associated weighting coefficients. The second expression applies activation function.

$$\begin{cases} x_{1i}(t) = a_{00} \cdot w_{1i0} + u_{11}(t) \cdot w_{1i1} + u_{12}(t) \cdot w_{1i2} \\ u_{2i}(t) = \dfrac{1}{1+e^{-x_{1i}(t)}} \end{cases} , \tag{5.2}$$

Where a_{00} is the bias node of the hidden layer and w_{1ik} (with k varying between zero and two) are the corresponding weighting coefficients.

5.2.4. Output layer

The output layer contains only one neuron, which summarizes the output signals from the neurons of the hidden layer and passes them through its activation function (Eq. 5.3).

$$\begin{cases} x_{21}(t) = a_{10} \cdot w_{210} + \displaystyle\sum_{k=1}^{3} u_{2k}(t) \cdot w_{21k} \\ u_{31}(t) = \dfrac{1}{1+e^{-x_{21}(t)}} \end{cases} , \tag{5.3}$$

Where a_{10} is the bias node of the output layer and w_{21k} (with k varying between zero and three) are the corresponding weighting coefficients. The resulting output of the ANN $u'_{tec}(t)$ is then obtained by passing the signal u_{31} through a rescaling procedure (Eq. 5.4) similar to that preceding input layer, but in reverse order, i.e. it performs the post-processing rescaling of the signal from [0,1] interval onto the desired range of the control signal. The signal u'_{tec} is then multiplied by the gain K_r.

$$\begin{cases} u'_{tec}(t) = c \cdot u_{31}(t) + d \\ u_{tec}(t) = K_r \cdot u'_{tec}(t) \end{cases} , \tag{5.4}$$

Table 5.1 contains values of parameters c and d for different data sets used in this study.

Table 5.1. Values of parameters of Pre and Post processing for different sets of experimental data.

Parameters	MCL data set	UAV data set
$[a_1; b_1]$	$[1.6; 0.58]$	$[0.004; 0.5]$
$[a_2; b_2]$	$[0.3; 0.46]$	$[0.0022; 0.5]$
$[c; d]$	$[7.5; -3.75]$	$[300; -150]$

5.2.5. Training the network

In any type of application, the artificial neural network has to be properly trained. Improper training manifests itself in a network producing poor results, i.e. modeling of individual testing elements of control will be inefficient. Usually, training of the network is accomplished by running the network over a large set of data, and using a back-propagation algorithm to fine-tune the weighting coefficients of the network. In this research, however, training of the network in its conventional way is avoided completely. Since the ultimate goal of this research is to develop means by which one can model individual behavior of any given operator, it is logical to train the ANN to mimic control strategy of every individual separately. In other words, each operator has his/her unique set of weighting coefficients. In order to properly train the network using a conventional scheme, one would need a large data set for every individual. The available experimental data does not contain the required amount of information: single run per subject is available only. It will be shown, however, that using the proposed automated parameter identification technique (Chapter 6) permits the optimization of the ANN, so that it mimics individual differences in control behavior of operators without the necessity of training over a large number of runs. On the other hand, since the available experimental data is limited to one run per subject, it is difficult to determine whether the proposed automated parameter identification technique mitigates the risk of overtraining the network. Such analysis would require a large number of test runs for each individual and should be performed as an essential part of future research.

5.2.6. Implementation

The artificial neural network designed to model the testing element of the control behavior was implemented and used in the MATLAB SIMULINK environment. Figure 5.4 contains a set of block diagrams of the model. It can be seen that the SIMULINK environment allows building the model of the network in a comprehensive, easy to read manner. One can clearly see the architecture of the network and easily modify its parameters if necessary. The overall block-diagram (a) has the same architecture as in Figure 5.3. All essential components, such as preprocessing blocks, neurons of the hidden layer, bias nodes, neuron of the output layer and post-processing block are clearly visible. Block diagram (b) illustrates architecture of the first neuron of the hidden layer. One can see the weighting coefficients being applied to the incoming signals, which are then summarized and put through the activation function of that particular neuron. Part (c) contains the block diagram of the output layer neuron, which has a similar architecture to that of the neuron in the hidden layer.
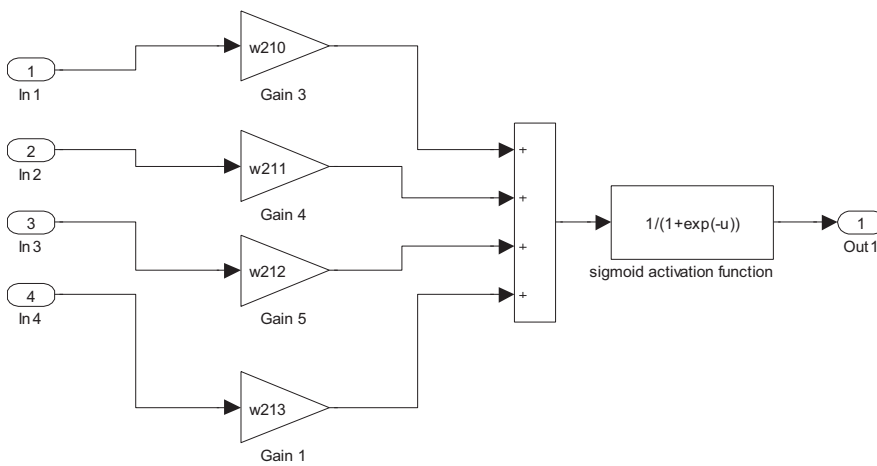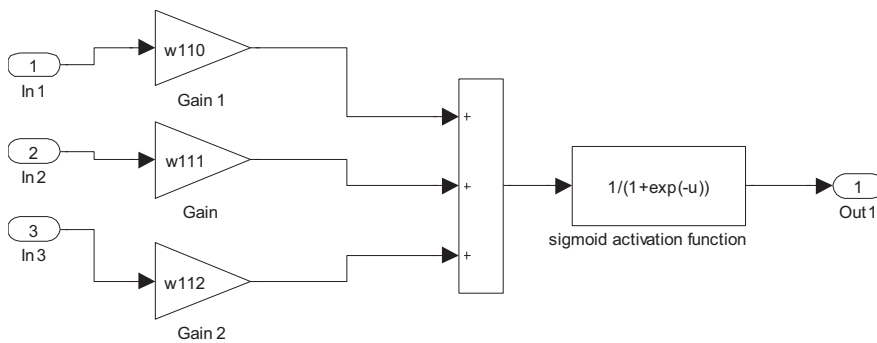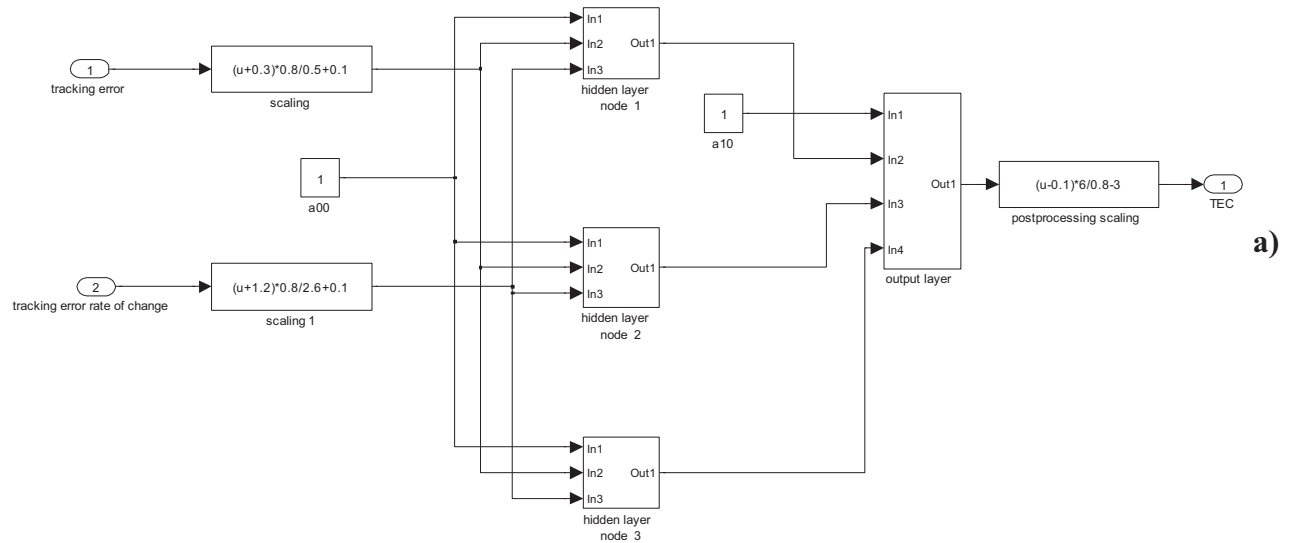
Figure 5.4. Block diagrams of the MATLAB SIMULINK implementation of the ANN used to model the testing element of the control behavior: a) overall block-diagram; b) hidden layer neuron structure; c) output layer neuron structure

64

5.3. Filtering

This section of the chapter contains the description of the filtering algorithm, which can be parameterized and further optimized to improve the fit of an individual's control data. The main hypothesis here is that every individual subconsciously conditions the control signal before it is passed through the control limb and into the plant (Figure 5.5). Such conditioning is manifested in different power spectra for each subject (Figure 5.1). Therefore, a customizable filter was introduced into the structural model of the human operator to shape the control signal so it matches the amplitude of the power spectrum of an actual control data.
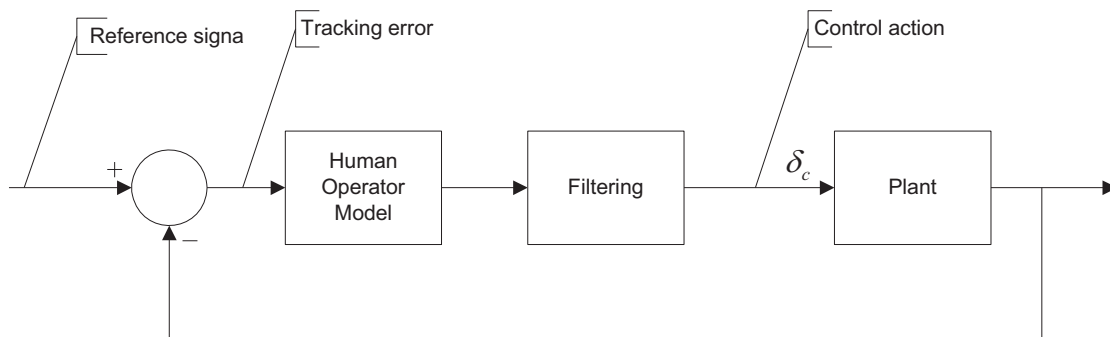
Figure 5.5. Man-machine system with the signal conditioning filtering block incorporated

The following is the mathematical description and implementation of the proposed filtering algorithm.

5.3.1. Mathematical background

Signal processing theory provides sufficient mathematical apparatus to build the required filter. The Parks-McClellan [25] algorithm is used to design linear phase equiripple filters, which were chosen to be used in the current research. This design method allows a finite impulse response (FIR) filter to be designed to a frequency response specification consisting of an arbitrary number of passbands and stopbands, in each of which a specified amount of ripple can be tolerated. This feature is especially important, since one might want the flexibility in adjusting only a certain section of the spectrum of the control signal, rather than boosting or attenuating the entire spectrum at once. The Parks-McClellan algorithm delivers such flexibility. The essence of the algorithm is in using the *Remez exchange routine* to solve the *Chebyshev approximation problem*. Remez routine [26] is an iterative algorithm, which looks for a polynomial to satisfy the *min-max optimization problem*. The latter can be formulated as follows: derive a set of

conditions for which it can be proved that the design solution for the linear phase finite impulse response (FIR) filter is optimal, i.e. the maximum approximation function is minimized (5.5)

$$\min_{over\ coeff.} \left\lfloor \max_{\omega \in S} |E(\omega)| \right\rfloor,$$
(5.5)

Where $E(\omega)$ is the approximation error function over the passband and stopband, and coefficients over which optimization occurs are the coefficients of the linear phase FIR filter. Thomas Parks and James McClellan [25] wrote a FORTRAN program, which implements the Remez algorithm. The Parks-McClellan algorithm is available in many computer based mathematical platforms including MATLAB. For more details on the min-max problem, please refer to the source [25].

5.3.2. Implementation

The main goal here is to be able to shape the power spectrum density (PSD) of the simulated control signal so it mimics the actual human operator control signal. Figure 5.6 contains a typical simulated control signal vs. actual control signal obtained during experiments using the MCL software. The simulated signal was obtained by running the Hess structural model using the known actual reference signal. It can be clearly seen that some of the control frequencies, especially in the higher frequency range are substantially underestimated. In order to compensate for such discrepancy and "boost" some of the frequencies a filter was introduced into the structural model as it is shown in Figure 5.7.
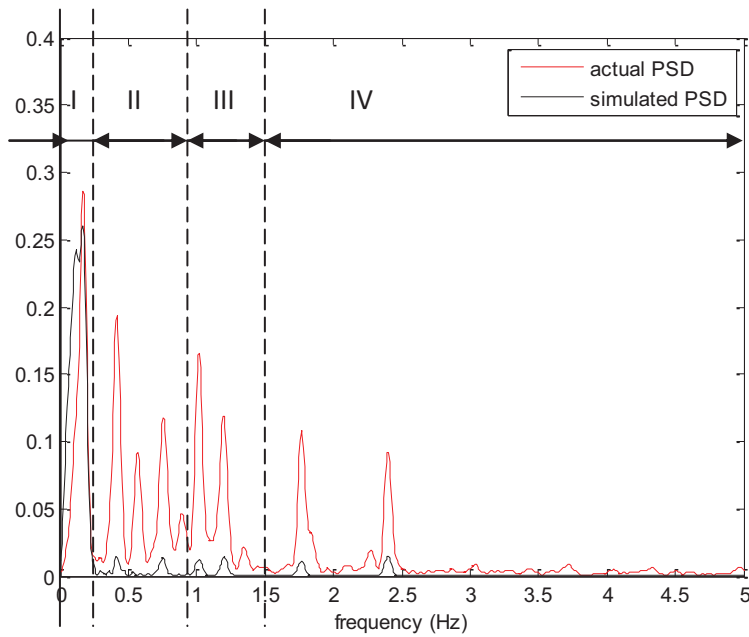
Figure 5.6. PSD of a typical actual control signal vs. simulated control signal produced by the Hess structural model.
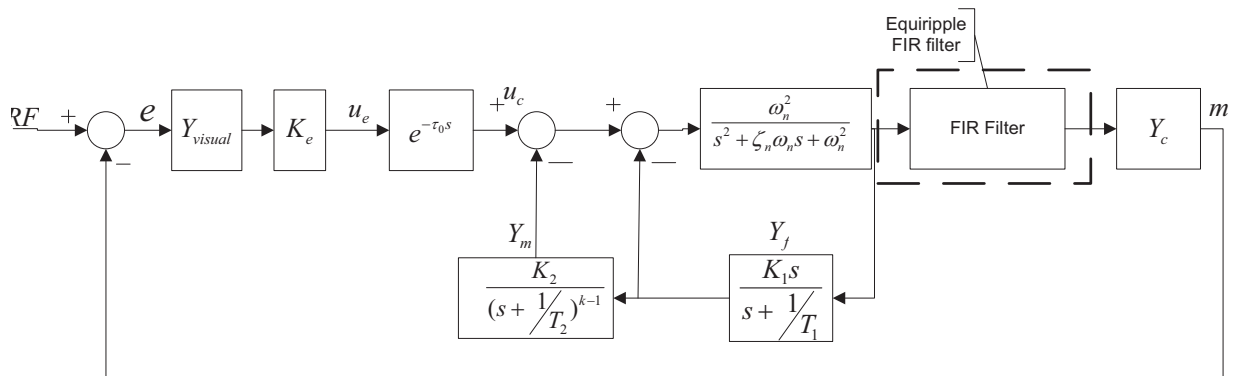
Figure 5.7. Simplified Hess structural model of the human operator with the equiripple FIR filter added

The filter itself is built by the MATLAB function ***firpm(n,f,a)***, which calls the Parks-McClellan algorithm. Before this function is called, one must specify an array f of normalized edge frequencies of the desired filter. For the MCL data sets such an array was composed of four sub-ranges, which were picked based on observation of the actual and simulated control signal frequencies. For example, the first sub-range [0 0.008] encompasses and isolates the first power bin from the entire spectrum, since it usually estimated quite accurate even by the original

67

version of the model, i.e. when no enhancements applied. Therefore, if the rest of the spectrum needs to be adjusted, one would be able to do this without affecting the spectrum in the first bin. The edge frequencies come in pairs: the starting and the ending frequency for every sub-range. The resulting array is given by (5.6):

$$f = \begin{bmatrix} 0 & 0.008 & 0.008 & 0.03 & 0.03 & 0.05 & 0.05 & 1 \end{bmatrix}, \qquad (5.6)$$

$$\underbrace{}_{\text{I}} \quad \underbrace{}_{\text{II}} \quad \underbrace{}_{\text{III}} \quad \underbrace{}_{\text{IV}}$$

Frequencies outside the specified sub-ranges are considered to be transition or "don't care" frequencies. Graphically, array f is shown on Figure 5.5 by vertical dashed lines. UAV data analysis and modeling utilizes an array with only one sub-range $f = [0\ 0.01]$. Unfortunately, in this case, it was not possible to include more sub-ranges, since the power spectrum of the control behavior in the UAV experiments is very narrow and located in the lower frequencies area (Figure 5.8). As a result, the sought filter boosts/attenuates the entire spectrum.
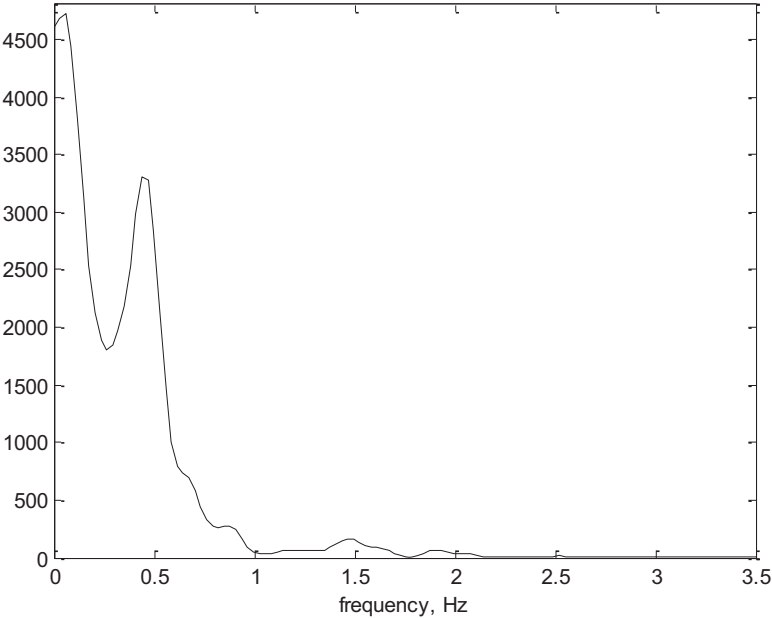
Figure 5.8. PSD of a typical actual control signal recorded during UAV experiments

Array a, then must contain the same number of values, which correspond to the desired values of the frequency response of the filter specified at the edge frequencies. In current

research, values of array *a* are subject to optimization, since they are considered to be subject dependent.

Once all parameters of MATLAB function ***firpm(n,f,a)*** are set, it returns an array of ***n+1*** coefficients of the filter, which is implemented in SIMULINK (Figure 5.9).
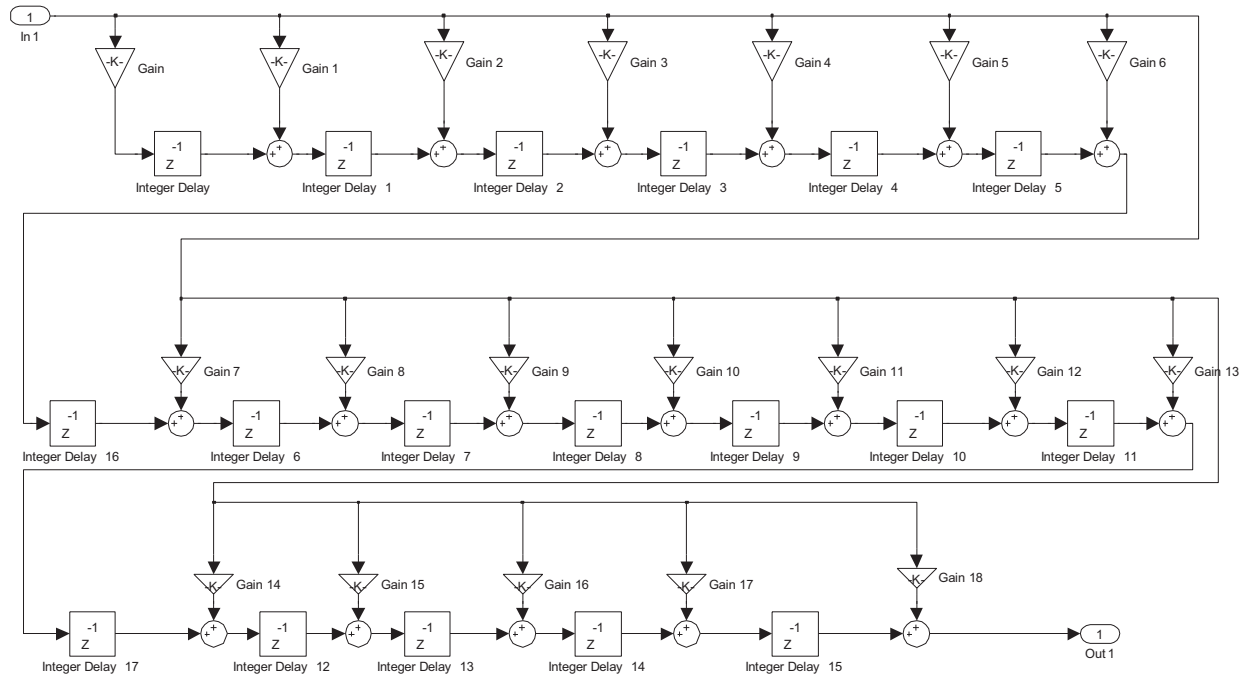
Figure 5.9. Block diagram of the FIR filter designed to shape the simulated control signal

As can be seen from the diagram, this is an 18th order FIR filter. During preliminary research it was determined that lower order filters produce less accurate results, whereas filters of the higher order may lead to instances when the filter does not converge. These observations are associated with the steepness of the slope of the filter frequency response at the edge frequencies f .

5.4.Integration of enhancements into selected models of the human operator

This section of the chapter discusses how the proposed enhancements are integrated into selected models of the human operator. Figure 5.10 is a block diagram of the Hess structural model with both enhancements in place (dotted boxes).
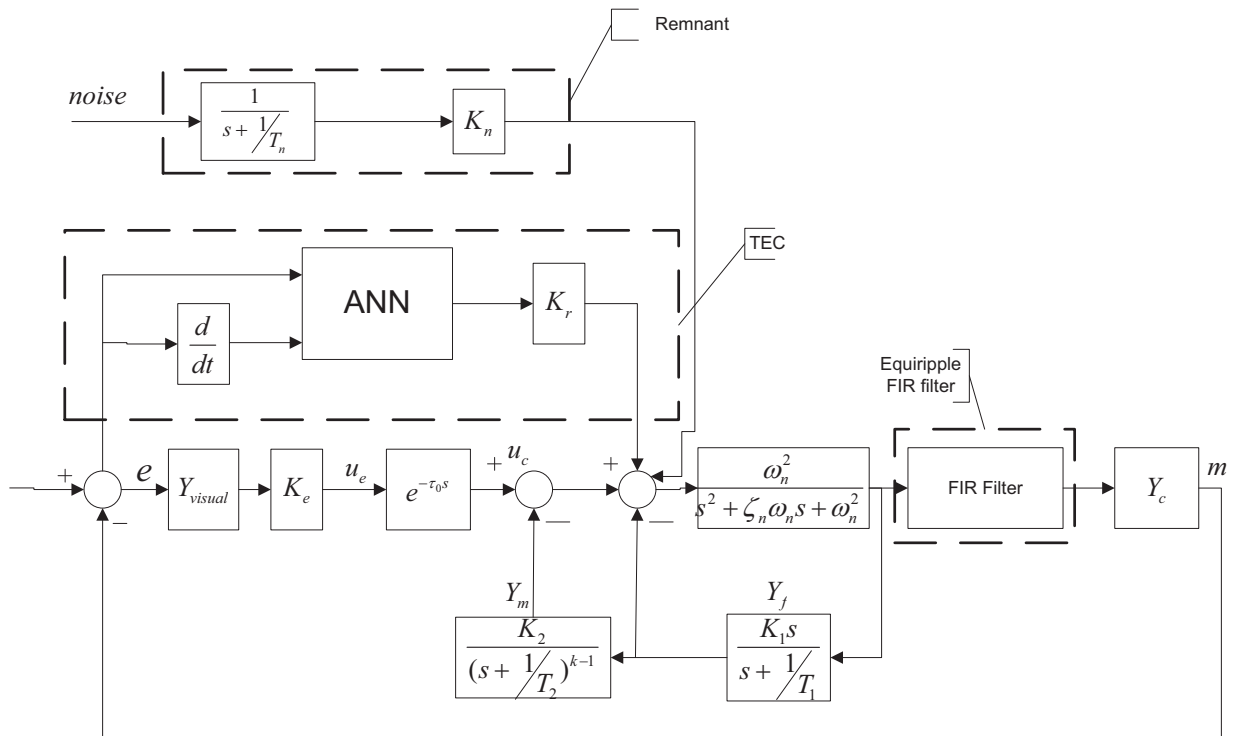
Figure 5.10. Hess structural model with TEC and Equiripple filter incorporated

Note that the testing element of control (TEC), which is modeled by the ANN is injected into the system before the cumulative signal is passed through the neuromuscular dynamics block. The filtering mechanism, however, is implemented right before the plant dynamics block. Following the same architecture, enhancements can be incorporated into the Hosman descriptive model (Figure 5.11) and optimal control model (Figure 5.12).
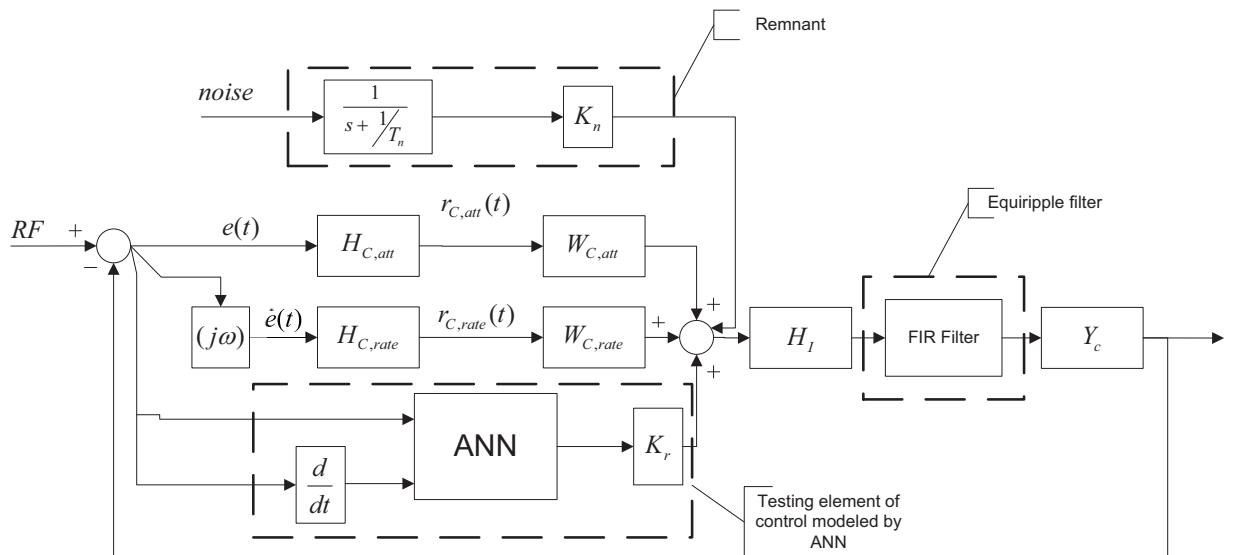
Figure 5.11. Hosman descriptive model with TEC and Equiripple filter incorporated
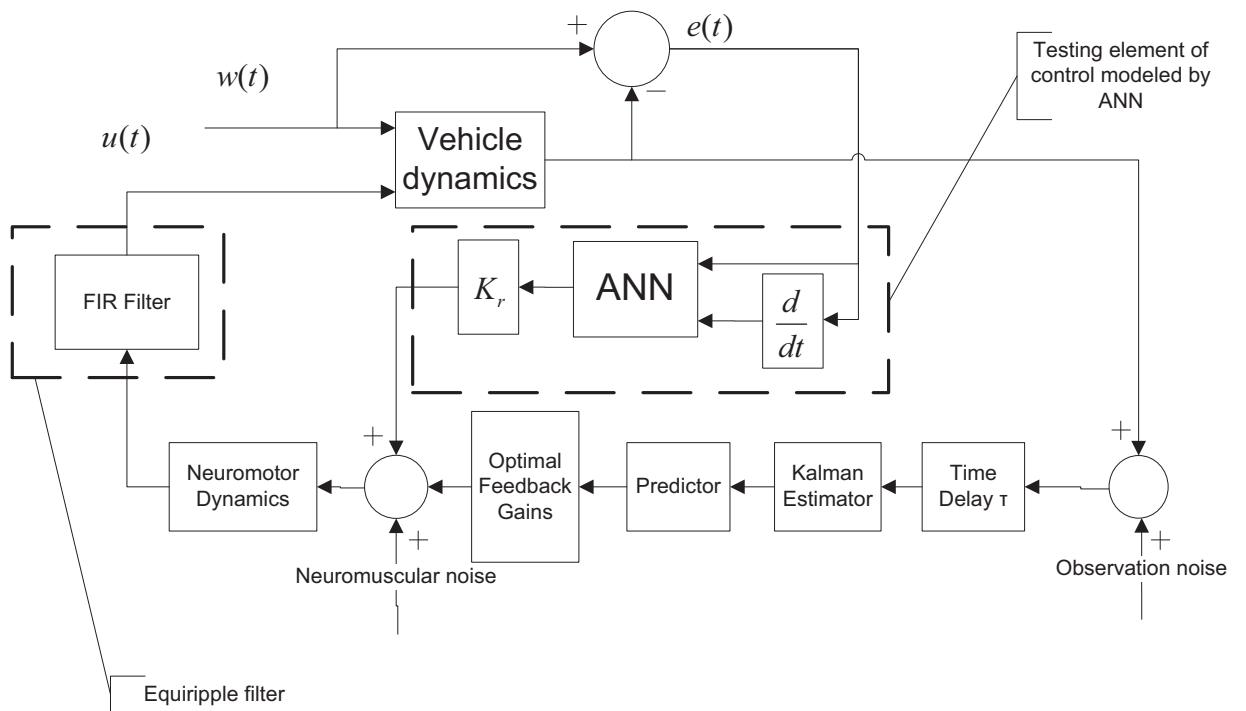
Figure 5.12. OCM with TEC and Equiripple filter incorporated

5.5.Summary

One of the goals of this research is to develop a set of tools, which would allow distinguishing between different operators by observing the individual's behavior. This study introduced two enhancements to existing models of the human operator which are designed to emphasize the individual differences in performance among operators. The first enhancement is built based on the hypothesis that different operators utilize individual-specific testing-type control inputs when familiarizing with, and performing any given control task. In order to model such control behavior it was proposed to use an artificial neural network, which is a physiologically inspired computational structure and capable of modeling the cognitive processing of an individual human operator. Another proposed enhancement is driven toward modeling an individual "fingerprint" of the power spectrum profile of the control behavior of every human operator. This enhancement took the form of a customizable filter, which can be optimized to mimic the shape of the individual power spectrum profile of an actual human operator.

In the next chapter of this manuscript one will be able to find the quantitative analysis of the efficiency of the proposed enhancements as well as the description of the automated parameter tuning algorithm, which is designed to automatically tune parameters of the structural human operator model and its enhancements in order to closely model the individual control behavior of various human operators.

6. Automated Parameter Identification Technique: theory and application

The primary scope of the research presented in this manuscript is to learn how to discriminate among different operators. This chapter presents the automated parameter identification (APID) technique, which was developed and used to identify subject specific parameters of the selected human operator models, such as: the Hess structural model, the Hosman descriptive model, OCM, and the modifications thereof. In the beginning of the Chapter the reader will find details of theory and implementation of the genetic algorithm optimization engine of the proposed APID. The description is followed by details of application of the APID to identify parameters of the selected models of a human operator. Subsection 6.2 discusses several issues associated with identifying parameters of the Hess structural model. A simplified metric is introduced to evaluate the effectiveness of the proposed model enhancements. The chapter is then completed by presenting results of application of APID to the selected models and their configurations. Results are accompanied by analysis and discussions.

The proposed APID can be described as an automated optimization algorithm (Figure 6.1), which is searching for values of the identified parameters resulting in a maximum match (fitness) between the actual and modeled operator control signals. The APID uses a genetic algorithm based optimization engine. Such choice is dictated by several factors, which include: high rate of convergence; ability to deal with highly non-linear systems; ability to optimize a large number of parameters, which may or may not be related to each other.
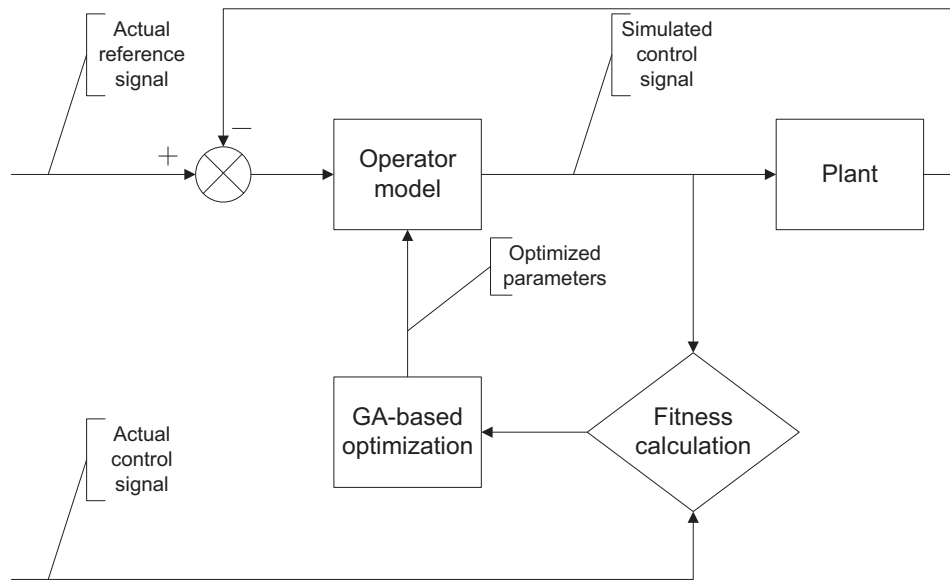
Figure 6.1. General architecture of the proposed APID

6.1. Bit-Climbing Genetic Algorithm

6.1.1. Architecture

Chapter 3 described basics of genetic programming using the simple genetic algorithm (SGA) as an example. This section describes in detail one of the implementations of a classical genetic algorithm, namely the bit-climbing algorithm (BCA), which was chosen to be used by APID. It was developed by Davis [19] and can be described as a modified hill-climbing algorithm with certain features adapted from the classical genetic algorithm. The BCA uses binary representation of the string of estimated parameters and/or variables similar to the classical GA. However, unlike classical genetic algorithms, it requires only a single chromosome for operation. The name "bit-climber" is inspired by the fashion in which the algorithm manipulates individual bits of the chromosome. Davis [19] discovered that BCA converges to a solution from 3 to 23 times faster than a traditional GA, while maintaining an acceptable accuracy. Since computational efficiency is crucial for this research it was decided to use the BCA instead of SGA or any other traditional GA.

The bit-climbing algorithm begins with constructing the initial chromosome. The BCA uses only a single chromosome, rather than a generation of chromosomes. On the other hand, the BCA chromosome is composed of identified parameters, put in a binary string, similar to the

74

classical GA. The number of identified parameters varies for each model. More details on this are presented in the following subsection. The initial chromosome is generated arbitrarily, i.e. there is no a-prior or "best guess" knowledge of the values of the identified parameters. Each identified parameter occupies 10 or 11 bits of the chromosome, depending on the desired accuracy. If, for example, the chromosome contains seven identified parameters and all parameters occupy 10 bits - it will consist of a total of 70 bits. Once the initial chromosome is generated the iterative process begins by "flipping" (changing values from zero to one and vise versa) bits of the chromosome in some arbitrary order. At each bit flip the fitness of the chromosome is calculated. Every time the new chromosome produces a "better" fitness, the old chromosome is replaced with the new one and the bit flipping continues. When all bits are tested, a new iteration proceeds with flipping bits. This iteration continues a pre-allotted number of times or until no improvement in fitness is observed. Finally, the iteration stops and the "best" chromosome is returned. Figure 6.2 contains the flowchart of the bit-climbing algorithm.

Each iteration of BCA optimization is followed by the post-processing binary to decimal conversion, which may involve division by a factor of a 100. Hence, if a given parameter occupies 10 bits in the chromosome, it can take on values between 0 and 10.23 with the precision of up to a second digit after the decimal point. In order to allow parameters to take on negative values, post-processing can include subtraction of a constant. The TEC model utilizes ANN, weighting coefficients of which can be negative. Figure 6.3 illustrates the post processing associated with identification of weighting coefficients of the TEC artificial neural network.
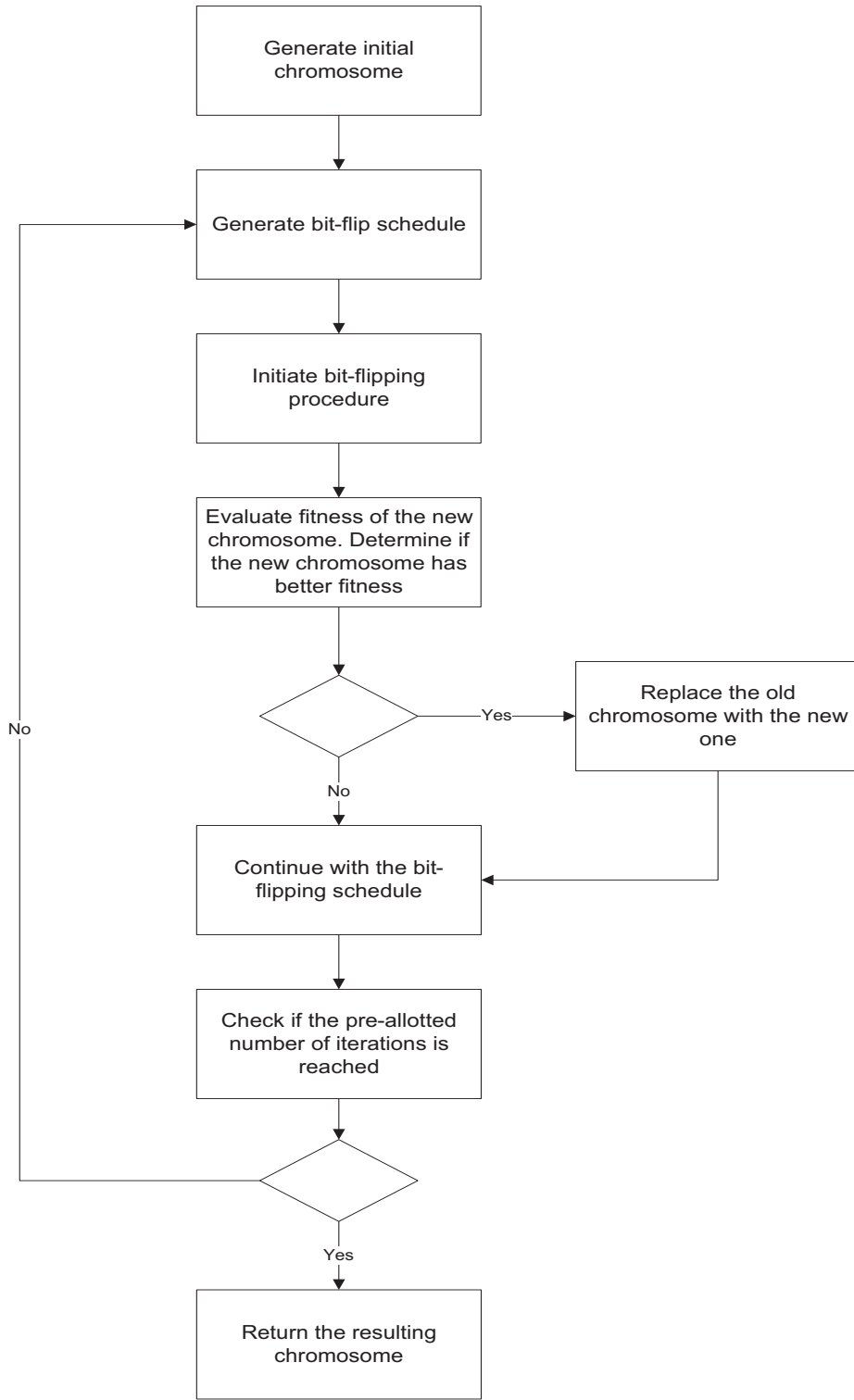
Figure 6.2. Bit-Climber Algorithm (BCA) flowchart
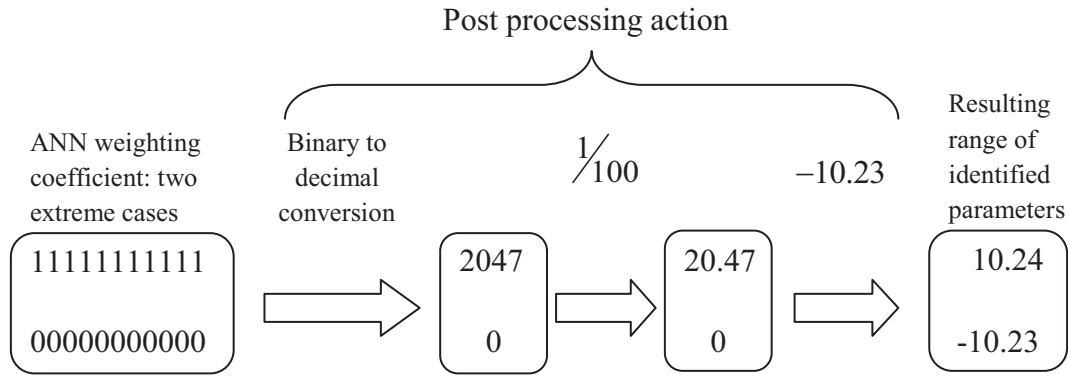
Figure 6.3. ANN weighting coefficients identification post-processing

Appendix B contains a complete list of identified parameters with the associated range over which identification occurs.

The BCA optimization routine (the outer loop of the BCA) is repeated for 10 iterations, thus ensuring the convergence of the algorithm to a solution. It was observed, however, that the BCA algorithm usually converges within first three iterations.

6.1.2. Fitness evaluation

This section discusses the theory and application underlining the metrics used to evaluate fitness of the chromosome generated by the BCA. In genetic programming, fitness score can be defined as an objective measure of how close the solution is to its maximum or minimum. The term solution used here means the optimum combination of identified parameters of a given model. Therefore, fitness of the chromosome is evaluated by comparing actual and simulated control signals in the power spectrum domain. The following paragraph discusses details of computing power spectral density of the available control signals.

Power Spectral Density (PSD) of a control signal was chosen as an evaluation space for the control behavior since it allows quantifying the operator control activity in terms of the frequencies at which an individual operates as well as how much energy is spent at each frequency. Figure 5.2 of chapter 5 clearly demonstrated that PSD is an appropriate tool to use in order to detect and identify control behavior of different operators.

The theory of signal processing stipulates, that it is possible to estimate the PSD of a finite length signal data set with the help of the Fast Fourier Transform (FFT). The aim of spectral estimation is to express the distribution (over the frequency range) of the power in a signal. The spectral density of a fixed random process x_n is related to the correlation sequence by the discrete Fourier transform and is given by:

$$S_x(\omega) = \sum_{x=-\infty}^{\infty} R_x(x)e^{-j\omega x} , \qquad (6.1)$$

Where R_{xx} is the autocorrelation sequence and ω is the specified frequency point. Eq. 6.1 can be rewritten as a function of the actual frequency f as follows:

$$S_x(f) = \sum_{x=-\infty}^{\infty} R_x(x)e^{\frac{-2\pi jfx}{f_s}} , \qquad (6.2)$$

Where f_s is the sampling frequency.

The PSD is then defined as:

$$P_x(f) = \frac{S_x(f)}{f_s} , \qquad (6.3)$$

Porat [27] offers one of the possible implementations for the routine to compute PSD.

In order to reduce the error in spectral estimates, the method of averaging of the estimates over multiple segments of data is used. Such method is also known as "windowing." The original time history of the control signal is divided into a series of overlapping segments. Each segment is then weighted by the type of window used. In this analysis the Hamming window was used. This choice was dictated by the fact that it is superior to a strict rectangular window due to lesser side-lobe leakage. The length of each windowed segment was chosen to contain 1024 data points. Overlapping regions, on the other hand, contained only 32 data points. The Fourier transforms are then calculated for every weighted segment of data, which is further averaged over the resulting ensemble of PSD estimates. The resulting "smooth" spectrum estimate is then defined as:

$$\hat{P}_x(f) = \left(\frac{1}{Un_x}\right)\sum_{k=1}^{n_x}\tilde{P}_x(f), \tag{6.4}$$

Where $\tilde{P}_x(f)$ is the power spectrum computed for each data segment and U is the correction factor associated with the energy loss and is equal to 0.612; n_x is the number of overlapping segments and is given by:

$$n_x = 1 + \left\lfloor\left|\frac{\left(T'_{rec}/T_{win}\right) - 1}{1 - x_{frac}}\right|\right\rfloor, \tag{6.5}$$

Where T_{win} - time duration of the spectral window; T'_{rec} - length of the extended time-history that had been filled with the trim values; x_{frac} - overlap fraction $[0;1]$ (the lower value corresponds to "no overlap" and the upper value corresponding to 100% overlap)

The fitness of a chromosome is computed by calculating the root mean square error (RMSE) between the two power spectrum estimates (6.6):

$$E(f) = \sqrt{\frac{\sum(\hat{P}_a(f) - \hat{P}_s(f))^2}{n}}, \tag{6.6}$$

Matlab implementation of the proposed APID algorithm as available in the dissertation by Zaychik [28].

6.2. Identified parameters

To demonstrate effectiveness of the APID, it was applied to the 13 different configurations of three different models of the human operator. Model configurations differ by the usage of the models of the TEC and EF, and, therefore, the number of identified parameters varied significantly throughout configurations. The Hess structural model alone contains seven different parameters including parameters of the proprioceptive feedback, neuromuscular dynamics, cognitive processing time delay, while the Hosman descriptive model and OCM have only two. In order to reduce the number of identified parameters while maintaining a certain level of performance accuracy, a sensitivity analysis has been performed. The main goal of this analysis was to determine to which parameters the Hess structural model performance is most sensitive.

The degree of sensitivity has been evaluated based on how close the Hess structural model matches the actual operator performance data, while several or all of its parameters are being varied. A more analytical approach involved analyzing the behavior of the poles of the characteristic equation of the overall transfer function of the Hess structural model.

It is considered that, in using the developed model to discriminate between operators, it is preferable to manipulate as few parameters as possible. Therefore, it is important to determine which parameters or combination of parameters results in the most variability among different subjects. This variability, which in this manuscript is referred to as Inter Subject Variation (ISV), of a particular parameter x can be evaluated as the standard deviation of that parameter σ_x expressed in percentage (6.7).

$$\Xi_x = \frac{\sigma_x}{\bar{x}} \cdot 100, \tag{6.7}$$

Where $\bar{x}$ is the mean of the parameter over a given subject population.

It is also very important to consider computational efficiency: the fewer the parameters the faster the identification algorithm converges.

The sensitivity of the Hess structural model was tested based on how close it can approximate the frequency response function obtained from an actual operator data set. Comparison was performed in a fashion similar to that used to calculate fitness score in the SGA-based PID algorithm, i.e. by calculating the root-mean square error between the actual and simulated operator control activities.

The sensitivity analysis involved testing parameters of the model individually and in groups (resembling certain structural components of the model) in an attempt to match individual control data sets obtained during MCL experiments. For a detailed description of these experiments refer to Chapter 4 of this manuscript. Table 6.1 contains values of the ISV along with the averaged values of the fitness score associated with the parameter(s) being varied.

When varied individually, best performance (lower fitness score and higher inter-subject variation) was obtained with parameters K_e, K_1 and K_2. When varied in groups, parameters of the proprioceptive feedback resulted in one of the lowest fitness scores as well as exhibited the largest ISV. One can also see that the case when all seven parameters were varied simultaneously

80

produced the lowest fitness score, along with the highest ISV values for each of the parameters. This observation, however, can be interpreted as follows. The average values of parameters T_1 and τ were determined to be quite small and equal to 0.001 and 0.2 respectively. Calculated ISV of these parameters was, on the other hand, very high: 316.2 and 114.4 respectively. These suggest that T_1 and τ have little to no effect on the overall performance of the model. Therefore it was decided to exclude them from the identification process and keep them constant at all times for all subjects. Parameters of the neuromuscular system ω_n and ζ when varied separately and in groups produced one of the highest fitness scores with the minimum inter subject variation. It may be concluded here that neuromuscular dynamics of the control inducing limb vary little among different subjects. It was proposed to keep them constant as well. This simple analysis suggests that the parameters K_e, K_1 and K_2 of the Hess structural model have the most influence on models performance as well as exhibit maximum variation among different control operators. Therefore, they can be used in the parameter identification study described in this manuscript.

In order to answer more rigorously the question what parameters of the Hess model have the most effect on its performance it was decided to perform the zero-pole analysis of the model. Based on the location and dynamics of poles the conclusion regarding what parameters of the Hess model have the most effect on stability and performance of the Hess model can be drawn.

Table 6.1. Standard deviation of identified parameters

Parameters varied	Standard deviation of identified parameters							Fitness score
	K_e	K_1	K_2	T_1	τ	ω_n	ζ	
K_e	18.63							**0.0385**
K_1		15.26						**0.0385**
K_2			18.28					**0.0385**
T_1				3.58				**0.0513**
τ					1.21			**0.0489**

ω_n						7.8		**0.0475**
ζ							1.27	**0.0513**
ω_n , ζ						84.87	181.1	**0.0451**
K_1 , K_2 , T_1		38.35	51.65	0				**0.0385**
K_e , τ	13.48				111.7			**0.0385**
K_e , K_1 , K_2 , T_1 , ω_n , ζ	81.48	60.57	26.26	316.2	114.4	41.01	48.45	**0.0244**

The overall open-loop transfer function (OLTF(s)) of the Hess model is computed and given by (6.7).

$$OLTF(s) = K \cdot \frac{K_e(s^2 - 6s + 12)\omega_n^2(s + T_1)}{s(s^2 + 6s + 12)\left[(s^2 + 2\zeta\omega_n s + \omega_n^2)(s + T_1) + K_1 s(K_2 + 1)\omega_n^2\right]} , \qquad (6.7)$$

While deriving this transfer function the cognitive processing delay was linearized by the 2nd order Pade approximation. Furthermore, the visual perception block was omitted from this analysis for the non-linearity simplification. Plant dynamics were modeled by the first order integrator. Figure 6.4 contains the root-locus diagram of the resulting $OLTF(s)$.
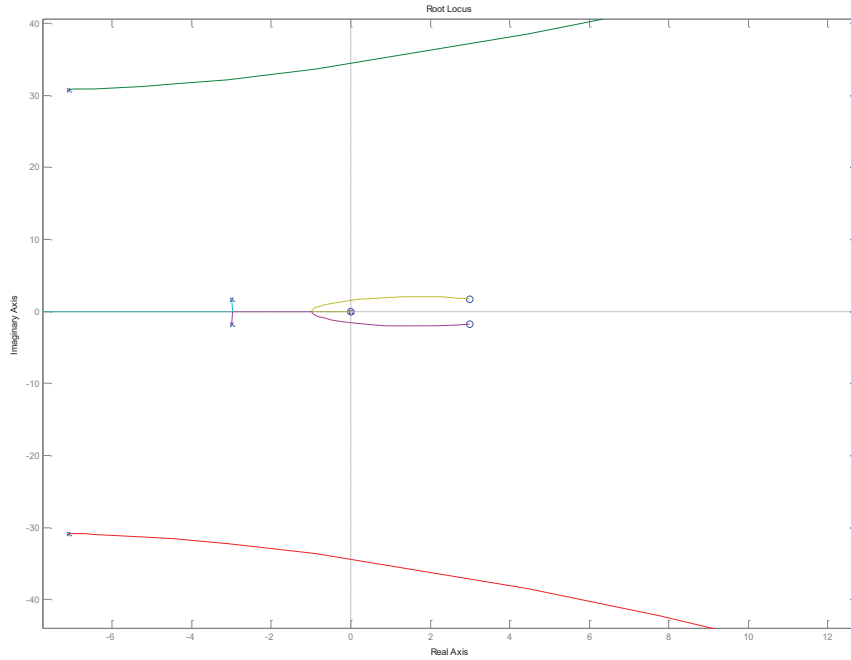
Figure 6.4. Root locus of the open loop transfer function

Inspection of the diagram reveals two dominant poles, which cross into the right hand side of the complex plane when the open loop gain $K = 1.54$. After close examining of this pair of complex conjugate poles, it was determined that they depend on K_e, K_1, K_2 and ω_n as well as terms of higher power. Such as $\zeta^3, K_1^{3/2}, T_1^3$. Since the average values for the damping ratio and the muscle spindles time constant are less than one, terms with higher powers of these parameters will have insignificant effect on the behavior of the dominant poles. It can be concluded here that only changes in K_e, K_1, K_2 and ω_n will seriously affect the stability of the system.

By taking into account both parts of the sensitivity analysis, it can be concluded that parameters K_e, K_1, K_2 have the most influence on the Hess structural model performance and behavior and, therefore, can be used in order to be able to distinguish between different operators. In other words, those parameters may vary substantially from subject to subject.

83

The Hosman descriptive model (Figure 6.5) has only two parameters to vary, namely w_{att} and w_{rate}. Note that there is no vestibular system path used in this model, since there has been no motion system involved in both MCL and UAV experiments.
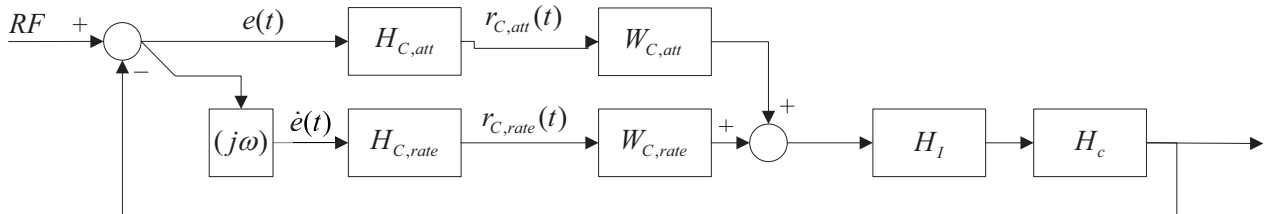
Figure 6.5. The Hosman descriptive model

In the optimal control model (Figure 6.6) there are two parameters being varied as well, namely the variances of the neuromuscular noise V_m and observation noise V_y.
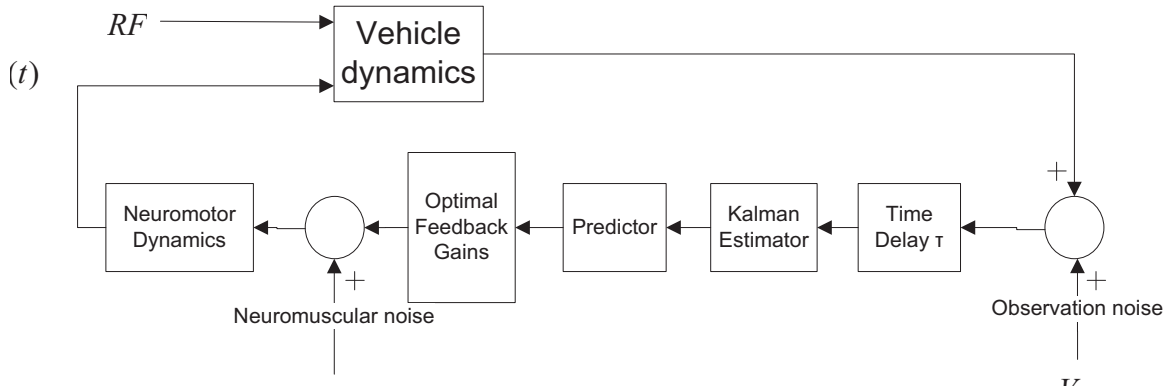
Figure 6.6. OCM

The models of the testing element of the control (TEC) and the equiripple filter (EF), described in Chapter 5, can be characterized by 14 and 4 parameters respectively. Table 6.2 summarizes configurations of the models tested for the MCL set of data. For the UAV data set, the configurations are essentially the same with one identified parameter added, namely the gain

of the feed forward path K_{ff}, which accounts for the pursuit nature of the control task (Figure 4.9)

Table 6.2. Identified parameters of the selected models and their configurations: MCL data

Hess structural model	Parameters of the Hess model			Parameters of the testing element of control model		Parameters of the equiripple filter				Parameters of the remnant	
	K_e	K_1	K_2	K_r	$w_{110} \ldots w_{213}$	lev_1	lev_2	lev_3	lev_4	T_n	K_n
Original Hess	X	X	X								
Hess with TEC	X	X	X	X	X					X	X
Hess with EF	X	X	X			X	X	X	X	X	X
Hess with TEC and EF	X	X	X	X	X	X	X	X	X	X	X

Hosman descriptive model	Parameters of the Hosman model		Parameters of the testing element of control model		Parameters of the equiripple filter				Parameters of the remnant	
	w_{att}	w_{rate}	K_r	$w_{110} \ldots w_{213}$	lev_1	lev_2	lev_3	lev_4	T_n	K_n
Original Hosman	X	X								
Hosman with TEC	X	X	X	X					X	X
Hosman with EF	X	X			X	X	X	X	X	X
Hosman with TEC and EF	X	X	X	X	X	X	X	X	X	X

OCM	Parameters of the OCM		Parameters of the testing element of control model		Parameters of the equiripple filter			
	V_m	V_y	K_r	$w_{110} \ldots w_{213}$	lev_1	lev_2	lev_3	lev_4
Original OCM	X	X						
OCM with TEC	X	X	X	X				
OCM with EF	X	X			X	X	X	X
OCM with TEC and EF	X	X	X	X	X	X	X	X

Table 6.3. Identified parameters of the selected models and their configurations: UAV data

Hess structural model	Parameters of the Hess model				Parameters of the testing element of control model		Parameters of the equiripple filter	Parameters of remnant	
	K_e	K_1	K_2	K_{ff}	K_r	$w_{110} \ldots w_{213}$	lev_1	T_n	K_n
Original Hess	X	X	X	X					
Hess with TEC	X	X	X	X	X	X		X	X
Hess with EF	X	X	X	X			X	X	X
Hess with TEC and EF	X	X	X	X	X	X	X	X	X

Hosman descriptive model	Parameters of the Hosman model			Parameters of the testing element of control model		Parameters of the equiripple filter	Parameters of remnant	
	w_{att}	w_{rate}	K_{ff}	K_r	$w_{110} \ldots w_{213}$	lev_1	T_n	K_n
Original Hosman	X	X	X					
Hosman with TEC	X	X	X	X	X		X	X
Hosman with EF	X	X	X			X	X	X
Hosman with TEC and EF	X	X	X	X	X	X	X	X

OCM	Parameters of the OCM			Parameters of the testing element of control model		Parameters of the equiripple filter
	V_m	V_y	K_{ff}	K_r	$w_{110} \ldots w_{213}$	lev_1
Original OCM	X	X	X			
OCM with TEC	X	X	X	X	X	
OCM with EF	X	X	X			X
OCM with TEC and EF	X	X	X	X	X	X

6.3. Metrics for evaluation

This section of the chapter discusses the issue of evaluating the performance of each model. It is clear that metrics are necessary in order to assess which model yields the most accurate approximation of the actual operator control activity. Researchers such as Hess, Hosman, Kleiman et al., have admitted that one of the major problems of operator modeling is how to judge the "similarity" of the simulated and actual data sets. The comparison of the results is sometimes performed qualitatively, rather than quantitatively. For example [29]:

> … the quality of the fit was determined by eye, i.e. no formal numerical criterion was employed.

A somewhat quantitative metric has been used by Hess [30] to evaluate the simulator fidelity by using the handling qualities sensitivity function (HQSF). The HQSF is derived as the magnitude of a cumulative transfer function of the Hess structural model of the human operator. Such an approach was employed when Hess used his structural model to predict the Cooper Harper handling quality ratings. The Cooper Harper handling qualities ratings scale (Figure 6.7) was developed by Robert Harper and George Cooper [31]. The scale divides the handling qualities space into 10 ratings: 1 being very good (the aircraft/simulator is controllable without the need for pilot compensation) to 10 being very bad (controlling the aircraft/simulator requires significant pilot compensation and control will be lost during some portion of required operation). These ratings are established based on the reports by individual pilots. Such an approach, even though it provides a quasi-quantitative metric, cannot be applied to evaluate the performance of the models for the current study for the following reasons: handling qualities are not among the primary objectives of the current research and the linearization process associated with computing HQSF is inapplicable when artificial neural networks are applied.

ADEQUACY FOR SELECTED TASK OR REQUIRED ACTION

AIRCRAFT CHARACTERISTICS	DEMANDS ON THE PILOT IN SELECTED TASK OR REQUIRED OPERATION	PILOT RATING
EXCELLENT HIGHLY DESIRABLE	PILOT COMPENSATION NOT A FACTOR FOR DESIRED PERFORMANCE	1
GOOD NEGLIGIBLE DEFICIENCIES	PILOT COMPENSATION NOT A FACTOR FOR DESIRED PERFORMANCE	2
FAIR – SOME MILDLY UNPLEASANT DEFICIENCIES	MINIMAL PILOT COMPENSATION REQUIRED FOR DESIRED PERFORMANCE	3
MINOR BUT ANNOYING DEFICIENCIES	DESIRED PERFORMANCE REQUIRES MODERATE PILOT COMPENSATION	4
MODERATELY OBJECTIONABLE DEFICIENCIES	ADEQUATE PERFORMANCE REQUIRES CONSIDERABLE PILOT COMPENSATION	5
VERY OBJECTIONABLE BUT TOLERABLE DEFICIENCIES	ADEQUATE PERFORMANCE REQUIRES EXTENSIVE PILOT COMPENSATION	6
MAJOR DEFICIENCIES	ADEQUATE PERFORMANCE NOT ATTAINABLE WITH MAXIMUM TOLERABLE PILOT COMPENSATION. CONTROLLABILITY NOT IN QUESTION	7
MAJOR DEFICIENCIES	CONSIDERABLE PILOT COMPENSATION IS REQUIRED FOR CONTROL	8
MAJOR DEFICIENCIES	INTENSE PILOT COMPENSATION IS REQUIRED TO RETAIN CONTROL	9
MAJOR DEFICIENCIES	CONTROL WILL BE LOST DURING SOME PORTION OF REQUIRED OPERATION	10

Flowchart decisions:

- IS IT SATISFACTORY WITHOUT IMPROVEMENT? — YES / NO → DEFICIENCIES WARRANT IMPROVEMENT
- IS ADEQUATE PERFORMANCE ATTAINABLE WITH A TOLERABLE PILOT WORKLOAD? — YES / NO → DEFICIENCIES REQUIRE IMPROVEMENT
- IS IT CONTROLLABLE — YES / NO → IMPROVEMENT MANDATORY

PILOT DECISIONS

Figure 6.7. Cooper-Harper Handling Qualities ratings scale. Adopted from Cooper [30].

Neusser [7] in his work on implementing a neurocontroller for lateral control of an automobile compared the performance of the neurocontroller augmented vehicle against the driver operated vehicle by calculating the error between the two and expressing it in terms of percentage.

Summarizing the above, one may conclude, that quantitative comparison of models is not a trivial task, which is worth exploring in the future. In this study, however, an attempt is made to move a step ahead toward building quantitative metrics for comparing human operator models. As has already been described previously, the proposed APID employs a selection process, which is based on the fitness score of a particular configuration of the model. The fitness score, in turn, is based on the differences between the power spectrum of the modeled operator behavior and the real operator behavior. In an attempt to quantify the fitness score space a

benchmark score is introduced. The benchmark score is produced by executing the precision model, which is an extension of the McRuer crossover model.

The benchmark will allow for a rough assessment of the model's data fitting capability: when normalized with respect to the precision model fitness score, models with fitness scores greater than the benchmark level will be discarded, models with fitness scores equal or lower than benchmark will be considered as competitive. Figure 6.8 illustrates this approach where in this illustration model A would be discarded.
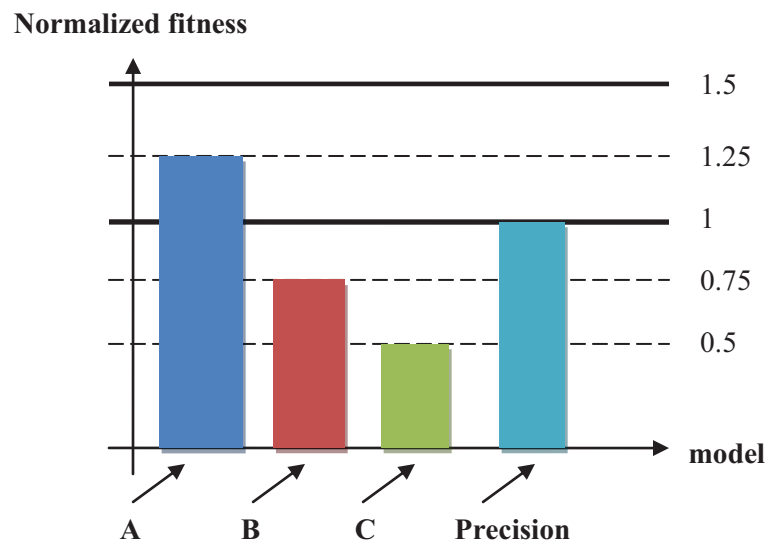
Figure 6.8. Sample diagram illustrating the benchmark fitness score at 1 produced by the precision model as compared to fitness scores of other models

6.4. Application results.

To achieve the goals of this research, an automatic parameter identification technique was developed along with two enhancements to the selected models of the human operator, which capture idiosyncrasies of individual control behavior. This section contains results, which were obtained by applying this methodology to two sets of data, namely the MCL data and the UAV data. These results illustrate for both data sets, which model, and/or configuration of the model yielded the closest approximation of the actual control behavior of an individual. Moreover, a cross-reference analysis is performed to determine which model, and/or configuration of the

model, has a higher potential to discriminate among different operators. The data set obtained during experiments at NASA is used in Chapter 7 to demonstrate the effectiveness of a simulator motion system in providing cues which produce appropriate pilot behavior.

6.4.1. Fitness analysis

6.4.1.1. *MCL data set*

This section describes the results of applying APID to the Hess Structural Model, the Hosman Descriptive Model and the Optimal Control Model. Each model was considered with and without proposed enhancements, thus resulting in four different configurations for each model. Utilizing the metrics discussed earlier, each configuration was compared against the Precision Model. Figure 6.9 contains histograms for a sample group of subjects from the MCL data set. The full set of histograms for the MCL data set is available in Appendix C.

The first and the most obvious observation here is that original OCM demonstrated the poorest results. It produced fitness scores higher than the Precision Model for all subjects in the sample. Addition of EF and TEC resulted in a substantial improvement of the performance, driving the fitness scores below the precision model benchmark, thus making the enhanced OCM more suitable for this task than the original version of OCM.

c)
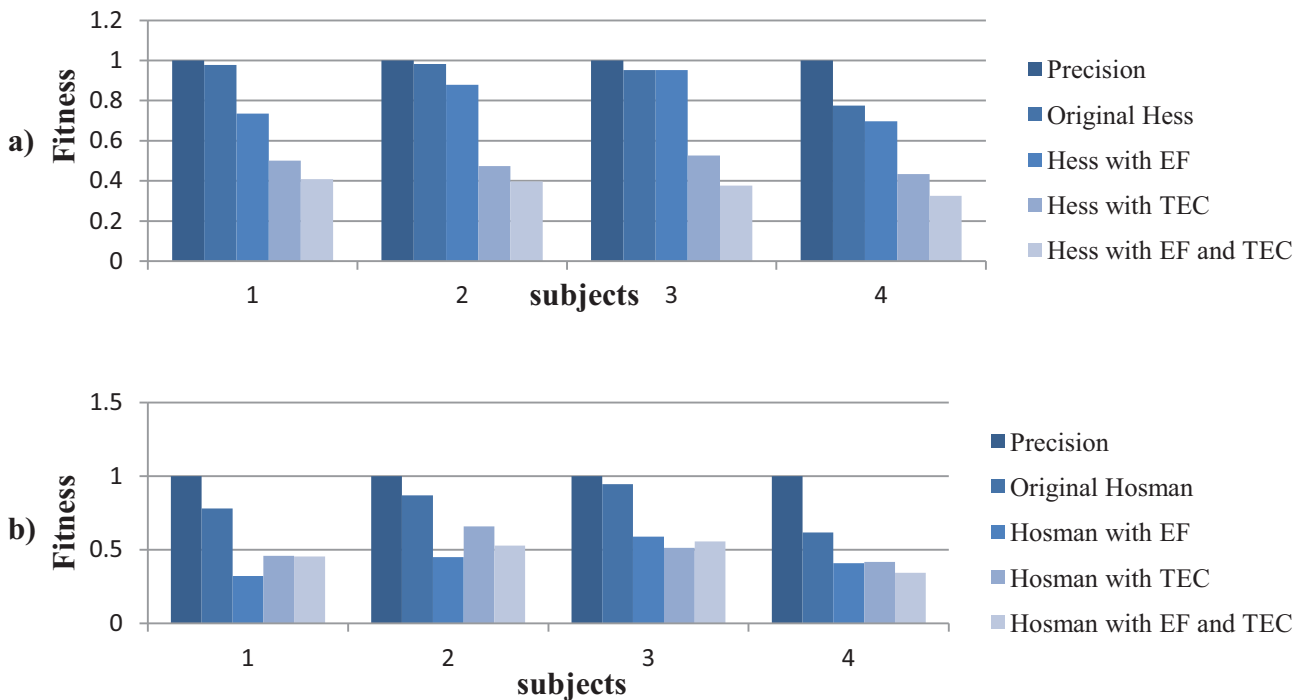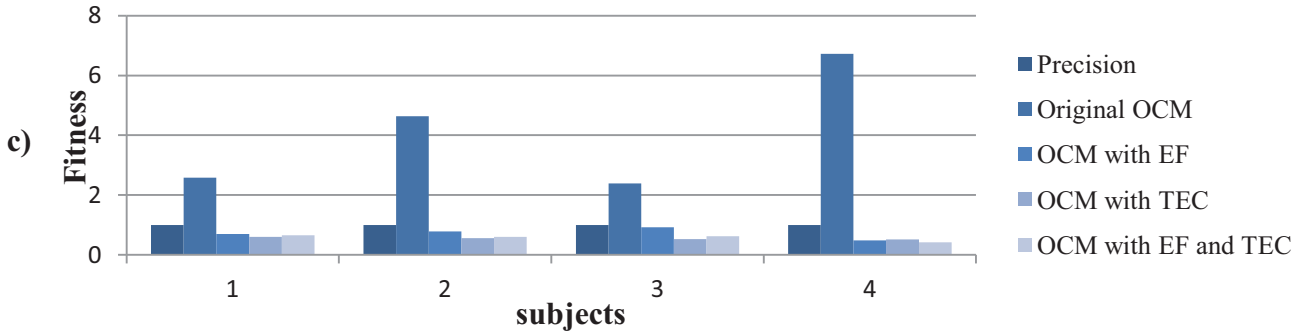
Figure 6.9. Fitness score comparison for a sample group of four subjects form the MCL data set: a) Hess structural model, b) Hosman descriptive model, c) OCM

It can also be seen that all three models exhibit a similar trend of improving (reducing) a fitness score with the addition of the equiripple filter (EF) and the testing element of control (TEC) algorithm. Figure 6.10 provides quantitative evidence for this statement. It illustrates exactly by how much the fitness score of a particular model was improved (decreased) with the addition of each of the enhancements, as compared to the fitness score produced by the original version of a given model.
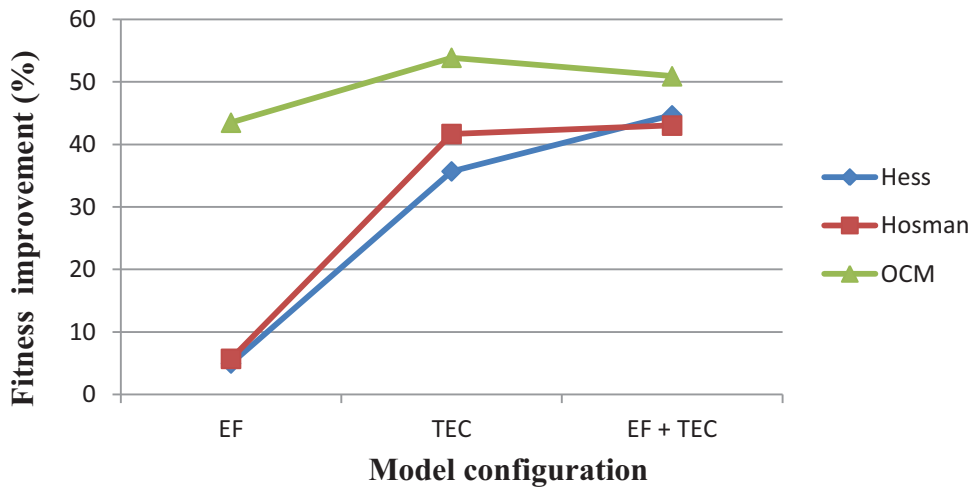
Figure 6.10. Improvement (percent) of fitness score associated with the addition of an equiripple filter (EF) and/or model of testing element of control (TEC). MCL data set

A generalized conclusion drawn here is that there is an overall positive effect from the introduction of the model enhancements. The TEC and EF+TEC model configurations resulted in an average improvement of the fitness score by 42 %. According to the diagram above, introduction of the model enhancements had the most effect on the OCM model. Section 6.4.2 compares the fitness scores across the entire subject population thus answering the question which model had the best fitness scores for each data set (MCL and UAV).

Section 6.4.3 discusses statistical significance of the obtained results. The inter-subject variation is calculated for each of the identified parameters and is presented as a function of the model enhancements.

6.4.1.2. *UAV data set*

This subsection of the chapter discusses results obtained for the UAV data set. Figure 6.11 contains histograms for a sample group of subjects from the UAV data set. The general observation here is that for the majority of subjects, the original versions of the Hess structural model, Hosman descriptive model and OCM resulted in fitness scores higher than that by the precision model. Further addition of the EF and TEC resulted in general improvement of the fitness. More detail on this is presented in the next subsection of the chapter. The full set of histograms for the UAV data set is available in Appendix D.
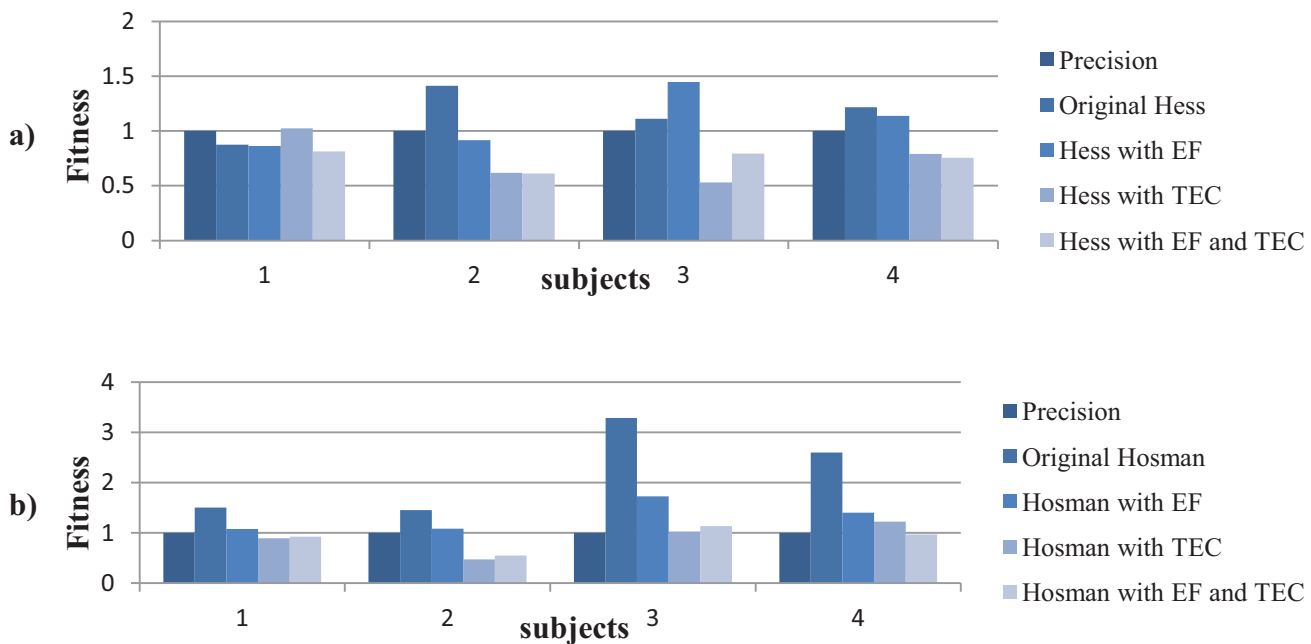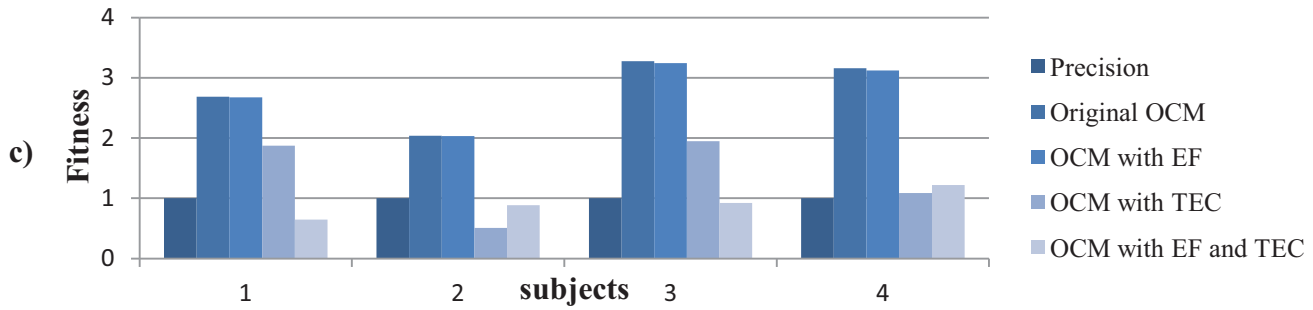
Figure 6.11. Fitness score comparison for a sample group of four subjects form the UAV data set: a) Hess structural model, b) Hosman descriptive model, c) OCM

The effect of introducing model enhancements is evaluated by computing the relative improvement in fitness of the selected models of the human operator. Figure 6.12 graphically illustrates the improvement effect expressed in terms of percentage relative to the original fitness score. This result was obtained by averaging over the entire population of the test subjects.

The main conclusion that can be drawn here is that there is an obvious positive effect from introduction of the model enhancements. However, equiripple filter alone had no effect on the OCM performance at all. In the case of the Hess and Hosman models, the fitness scores were improved on average by 10 % and 40 % respectively. The most impact on the performance of all models was obtained by the introduction of the testing element of control algorithm. The fitness score improvement averaged at least 36%.
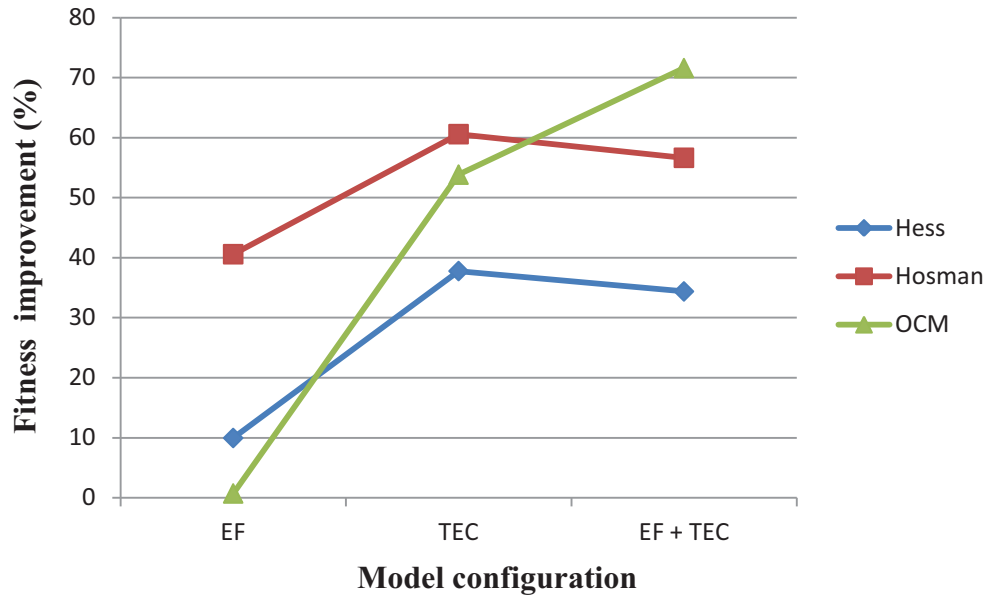
Figure 6.12. Improvement (percent) of fitness score associated with the addition of an equiripple filter (EF) and model of testing element of control (TEC). UAV data set

6.4.2. Cross-reference analysis

The goal of this subsection is to determine by statistical analysis, which model and/or the configuration of the model is best suited to achieve the following goals:

-   produce closest approximation of individual control activity data (lowest fitness scores);

-   result in maximum variation among subjects (ISV) expressed in terms of variation of identified parameters;

-   achieve the above two with the minimum number of identified parameters;

A comparison is made across the models: Hess vs. Hosman vs. OCM, as well as across their configurations for both MCL and UAV data sets. Figure 6.13 contains a histogram, which compares percentages of subject population for which a particular model configuration resulted in the lowest fitness score when analyzing the MCL data set. There are four categories compared: the original version of the model, original model with equiripple filter added (EF), original model with the testing element of control algorithm added (TEC), and, finally, with both

enhancements added (EF + TEC). It can be seen that in the first two categories, the Hosman descriptive model produced the lowest fitness score for the majority of subjects: 63 % and 64 % respectively. However, in categories TEC and EF+TEC, the obvious leadership is with the Hess structural model: 52 % and 68 %. This observation makes Hess and Hosman models strong candidates to become the "best model" to be used for the MCL data analysis.
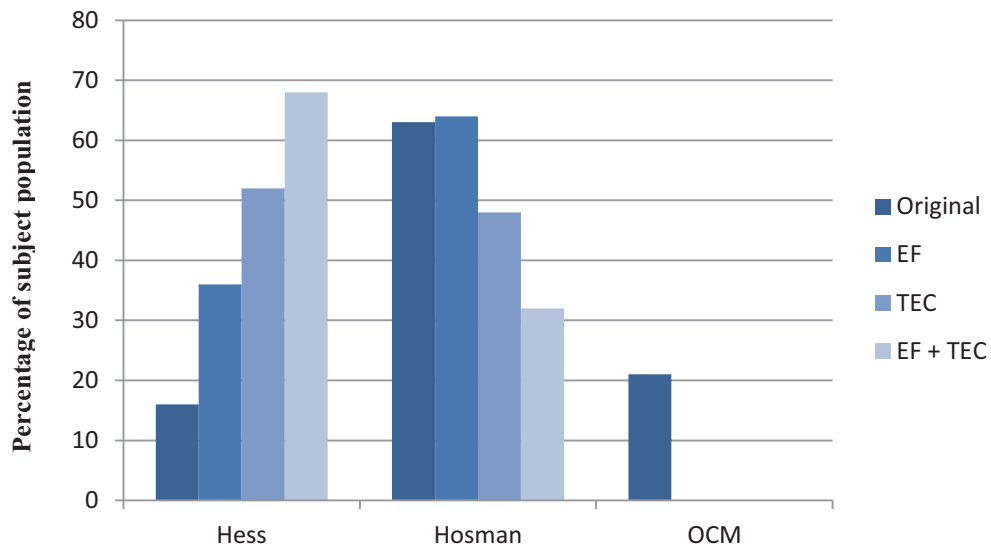
Figure 6.13. MCL data set: distribution of the model configurations, which resulted in the best fit of the actual control behavior

It can also be seen that only in the category of original versions of the models OCM could produce fitness scores lower than those produced by models by Hess and Hosman for only a few subjects.
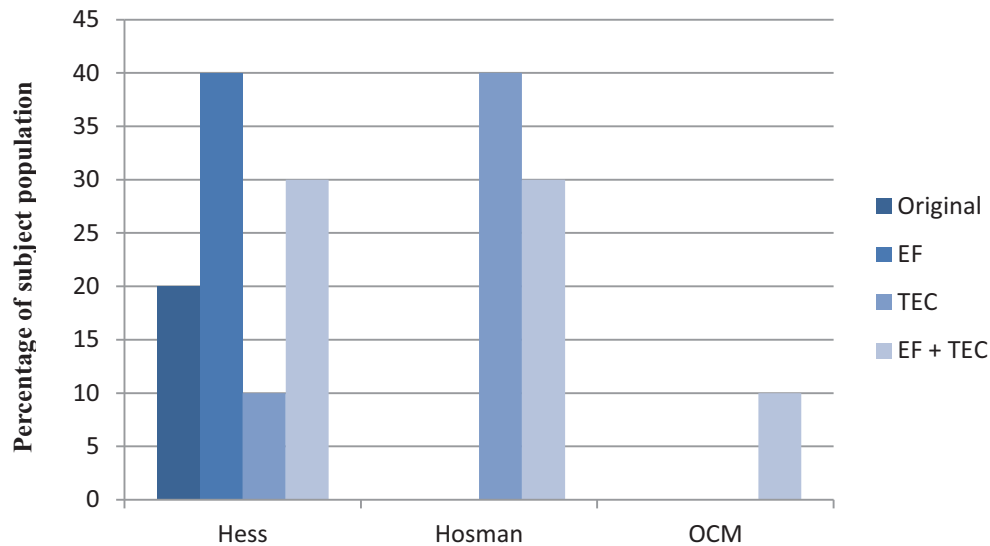
Figure 6.14. UAV data set: distribution of the model configurations, which resulted in the best fit of the actual control behavior

Similarly, Figure 6.14 compares results for the UAV data set. It can be seen that the Hess structural model dominated in the first two categories: original version of the model and with EF added. In the TEC category Hosman descriptive model demonstrated better results, whereas in the EF+TEC category models by Hosman and Hess performed equally. In the meanwhile, it can be seen that the OCM model was able to produce acceptable results only for 10% of the subject population and only when both enhancements were added. It may be concluded here that the OCM model is the least suitable to be applied when modeling the UAV pilot control behavior.

Appendix E contains a complete set of tables with the fitness score values obtained for both MCL and UAV data sets. It can be seen that for the MCL data set, the original configuration of the OCM model produced fitness scores in excess of the precision model for 58% of subject population. All other models and corresponding configurations resulted in fitness below the benchmark score set by the precision model. The UAV data set produced an interesting result. The original version of the precision model resulted in better approximation of the individual control data than any other model. With the addition of the EF and TEC, The situation started to shift in favor of the Hess structural model and Hosman descriptive model. One might make a conclusion here that according to both MCL and UAV data sets, the most suitable models to be

used here are the Hess structural and Hosman descriptive models. OCM has proved itself less efficient when modeling operator's control behavior.

6.4.3. Statistical Analysis

An attempt is made in this section to answer the question regarding which model and/or model configuration results in maximum inter-subject variation of identified parameter(s). Therefore, it was essential to look at some of the parameters of individually tuned models from the statistical point of view. Inter subject variation (ISV) was computed for each of the identified parameters of the selected operator models. Results are presented in the form of graphs, rather than error bars on histograms. The primary reason for that is to be able to demonstrate the dependence of ISV on the model configuration, i.e. the number of identified parameters.

Figure 6.15 illustrates the inter-subject variation (ISV) of identified parameters of the Hess structural model, the Hosman descriptive model and the OCM as a function of the configuration of a model obtained from the MCL data set.
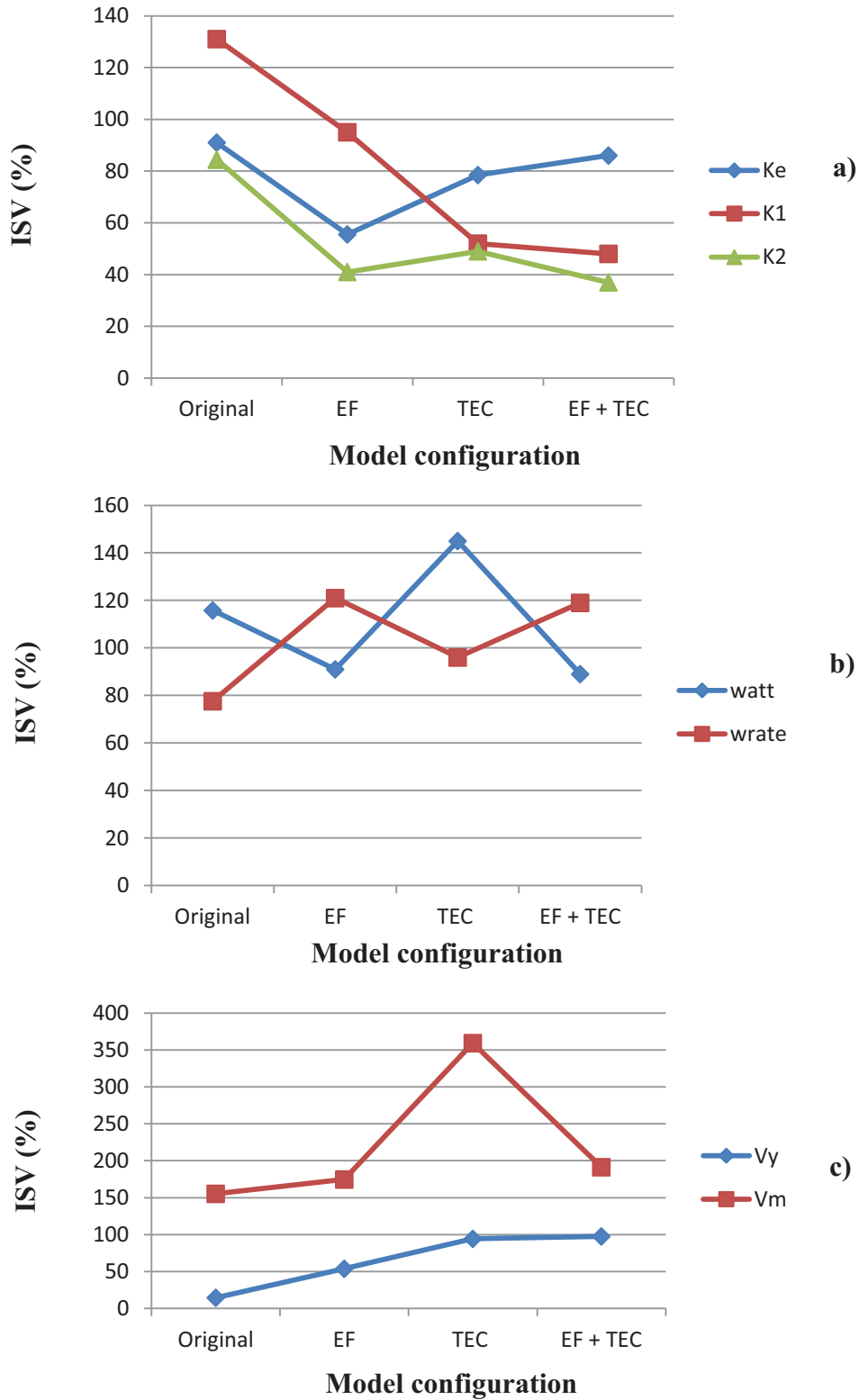
Figure 6.15. Inter-subject variation of selected parameters of the a) Hess structural model b) Hosman descriptive model c) OCM obtained for the MCL data set

The general observation that can be made here is that there is no universal answer whether the number of identified parameters seriously affects the inter-subject variation of those parameters. Parameters of the proprioceptive feedback K_1 and K_2 of the Hess structural model demonstrated steady decline in ISV with the increase of the number of identified parameters, whereas gain K_e varied the least with EF added, and varied the most in the original as well as with TEC and EF+TEC configurations of the model. The parameters of the Hosman descriptive model: w_{att} and w_{rate} - did not reveal a unanimous tendency to increase or decrease ISV as a function of the model configuration. Observation and neuromuscular noise variations of the OCM exhibited a general trend to increase the ISV with the increase of the number of identified parameters.

Figure 6.16 contains plots of the ISV of various parameters of the selected model obtained for the UAV data set. Note, that for the UAV data set, there has been another parameter added, namely K_{ff}, the gain in the feed forward path, which accounts for the pursuit nature of the control task. It can be seen, that this parameter varies quite consistently in the Hess and OCM models. Its ISV averages around 60%. It also demonstrates the largest variation in case of the original Hosman model. The least amount of variation is registered in case of the Hosman model with the equiripple filter added. Parameter w_{att} demonstrated a consistent increase in ISV with the increase in the number of identified parameters. In the meantime, the other parameter of the model, w_{rate}, demonstrated no variation at all. As a matter of fact, the average identified value of that parameter for the UAV data set is equal to 0 for the original version of the model, 0.013 when EF and TEC were added, and 0.019 with EF and TEC functioning simultaneously. It is an interesting result, which can be interpreted as follows: in this particular tracking task, operators do not rely on the tracking error rate of change when developing a control action.

It is difficult to draw any conclusion regarding the dependency of other parameters on the number of identified parameters. More research is needed in this regard.
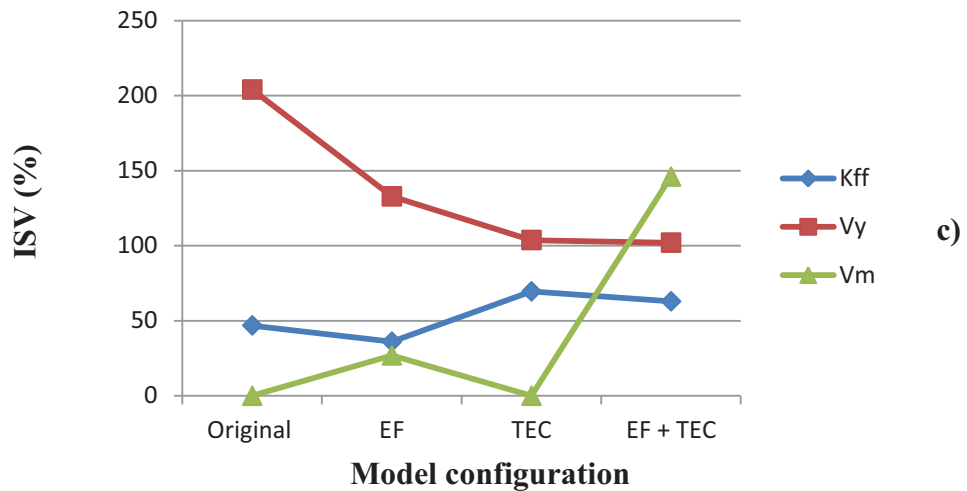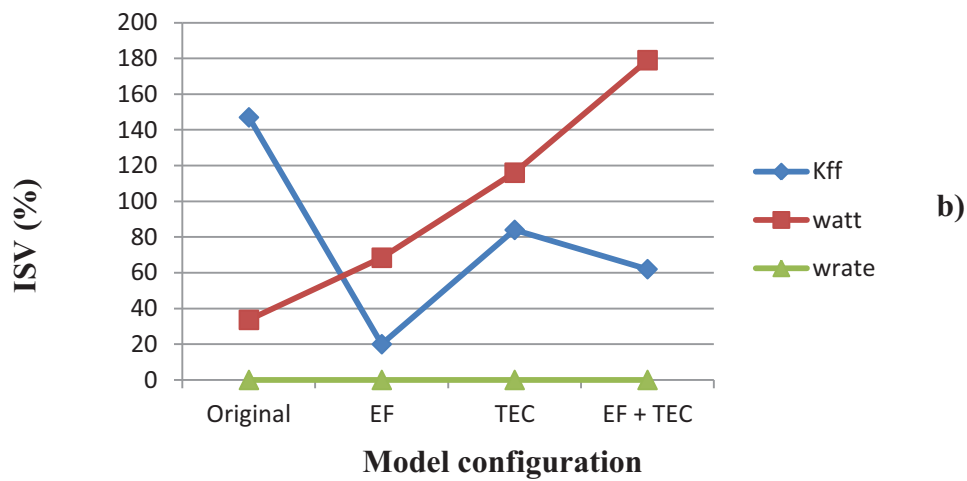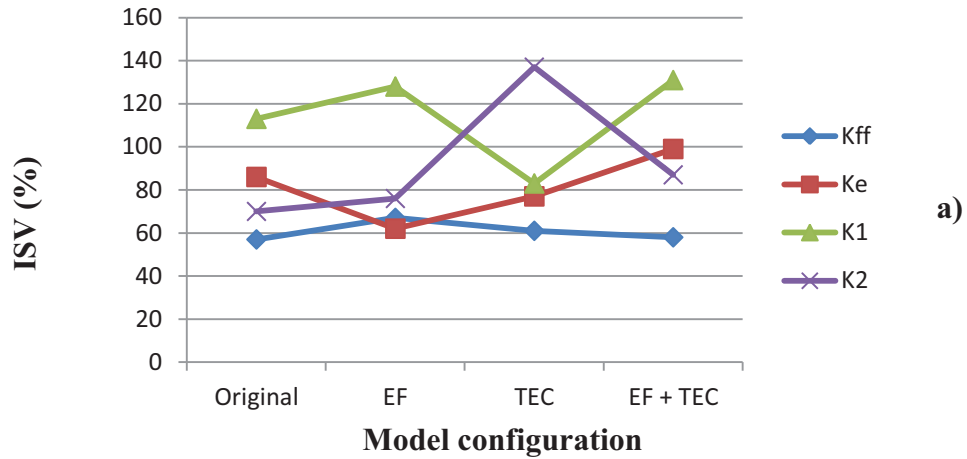
Figure 6.16. Inter-subject variation of selected parameters of the a) Hess structural model b) Hosman descriptive model c) OCM obtained for the UAV data set

6.4.4. Consistency of results

It is important to discuss briefly the consistency of the presented results. The bit-climbing algorithm, which lies at the heart of the automated parameter identification technique described in section 6.1, is a multi-iteration process, which is repeated a predetermined number of times. In order to evaluate the consistency of the results, the APID algorithms was repeated 25 times for each subject, followed by averaging and computing standard deviation of the fitness score. The following table 6.4 contains values of standard deviation of the fitness scores, expressed in terms of percentage.

Table 6.4. Standard deviation (%) of the fitness score as a function of the model configuration

		Original	EF	TEC	EF + TEC
MCL data	Hess	1.8	6.9	9.27	10
	Hosman	1.6	13.11	15	14.4
	OCM	0	0.49	6.44	2.05
UAV data	Hess	16.2	8.36	21.36	18.94
	Hosman	0.16	12.2	17.55	32.33
	OCM	0	0	26.67	19.9

One can see clearly the general tendency of the variation to increase with the increase in number of identified parameters. The OCM demonstrated the most consistent results: the original version of the model as well as with EF added produced little to no variation of the fitness scores. The other observation is that the results obtained for the MCL data set in general are more consistent than those for the UAV data. This is interesting and a somewhat unexpected result, since the UAV pilots are the most homogeneous group of subjects. All UAV pilots participated in the experiments are active duty pilots and, therefore, the skill level among subjects was not expected to vary significantly. The MCL group of operators was extremely diverse and included both novice operators as well as highly experienced ones. On the other

hand, the UAV control task is much more complex as compared to the MCL, since it requires control in multiple degrees of freedom, whereas during the MCL experiments, subjects were using only single control inceptor.

6.5. Summary

It has been demonstrated that genetic programming can be successfully used to identify parameters of the existing models of the human operator. The proposed automated parameter identification technique was able to successfully identify a variety of parameters, thus making it possible to closely model control behavior of an individual.

Also this chapter has demonstrated that the proposed enhancements to the existing models can be successfully implemented in real applications. The effectiveness of the testing element of control algorithm as well as the equiripple filter was evaluated based on the MCL and UAV data sets. It was shown, that implementation of the TEC algorithm results in a minimum of 40% improvement of the fitness scores for the MCL data and 38% improvement for the UAV data set.

The comparison analysis demonstrated that the Hess structural model along with the Hosman descriptive model are more suited to model the control behavior of an actual operator in the described control tasks (MCL and UAV). These conclusions, however, should not discourage the reader from using the OCM in the future. The effectiveness of the OCM has been empirically previously demonstrated in the variety of applications. Augmenting the OCM by the proposed model enhancements has improved the performance of the model for both MCL and UAV data sets.

The inter-subject variation (ISV) of the identified parameters has also been examined. It was determined, that several parameters, such as K_e of the Hess structural model, w_{att} of the Hosman descriptive model and V_y of the OCM tend to increase the ISV with the increase of the number of identified parameters. Other parameters of the Hess structural model, such as parameters of the proprioceptive feedback K_1 and K_2 demonstrated the opposite behavior with the increased complexity of the identified model. It was also determined that the ISV of identified parameters may also vary with the control task: different results were obtained for the

MCL and UAV data sets. These observations call for more research in this direction in the future.

The issue of the consistency of the results has also been investigated. The general conclusion here is such that fitness scores tend to vary more with the increase in the number of identified parameters. Results obtained for the MCL data set were, in general, more consistent (maximum variation was found to be 14.4%) than those for the UAV data set (maximum variation is 32.33%). Even though the observed variation in the results did not exceed 33 %, this observation calls for more research in the future.

7. Motion cueing and pilot modeling.

Recent research by Cardullo, et al. [5] significantly expanded the original Hess structural model by adding the vestibular paths as well as the models of the motion system and cueing algorithms. Figure 7.1 illustrates expanded Hess model for both rotational and translational channels.

Figure 7.1. Expanded Hess model [5] with motion feedback for a) rotational channel, b) translational channel

The highlighted boxes indicate the added motion feedback paths. Depending on which degree-of-freedom is being modeled, the expansion utilizes models of otoliths or semicircular canals (SCC), which model motion perception in the translational and angular channels respectively. The motion feedback paths are then complemented by the motion platform dynamics and motion cueing algorithm. Platform dynamics is modeled by a second order transfer function (7.1):

$$\frac{\omega_{mp}^2}{s^2 + 2\xi_{mp}\omega_{mp}s + \omega_{mp}^2} , \qquad (7.1)$$

Where the natural frequency $\omega_{mp} = 31.4 \left(\frac{\text{rad}}{\text{sec}} \right)$, and damping ratio $\zeta_{mp} = 0.7$. The washout algorithm is modeled by the classical high-pass filter (7.2):

$$\frac{s^2}{s^2 + 2\xi_{wo}\omega_{wo}s + \omega_{wo}^2} , \qquad (7.2)$$

With the natural frequency $\omega_{wo} = 1.02 \left(\frac{\text{rad}}{\text{sec}} \right)$, and damping ratio $\zeta_{wo} = 1.0$

The angular channel model utilizes the model of the SSC as proposed by Telban [21]:

$$\frac{\hat{\omega}}{\omega} = 5.73 \cdot \frac{80s}{(1+80s)(1+5.73s)} , \qquad (7.3)$$

where ω is the angular velocity and $\hat{\omega}$ is the perceived angular velocity, both in radians per second. The model for the otoliths, used in the translational channel, was also developed by Telban [21] and is given by:

$$\frac{F_P}{F} = \frac{(4s+.4)}{(.08s^2 + 5.016s + 1)} , \qquad (7.4)$$

where F_p is the perceived specific force and F is the actual specific force resulting from the translational motion.

This chapter illustrates the applicability of the proposed automated parameter identification technique (APID) to the problem of modeling operator control in the presence of motion feedback using the Hess structural model. In the first part of the Chapter a "generic" pilot is modeled based on applying the McRuer crossover model. It is demonstrated how the Hess structural model benefits from incorporating the motion system feedback by performing analysis based on modeling a generic pilot data. Then the Hess structural model is tuned to match the generic pilot control activity data. Subsequently, motion system feedback is included. Finally, resulting change in the simulated human operator control behavior is analyzed. In the second portion of the chapter, a similar approach is utilized while considering the actual pilot behavior, which was recorded during experiments at the NASA LaRC VMS Facility. Experiments at this facility included the use of a platform motion system. For the detailed description of the experiments, please refer to Chapter 4.

7.1. Generic pilot

7.1.1. Methodology

The analysis procedure employed in this chapter is based on comparing the performance of the Hess model with and without motion system feedback. The term performance used here can be described as the ability of the model to approximate the control behavior of a pilot. As stated above, the control behavior of a generic pilot is obtained by running the man-machine system with the McRuer crossover model of the human operator. The choice of the latter is justified by the fact that it has been empirically demonstrated that the pilot adjusts his/her behavior to compensate for the plant dynamics and can be modeled by the crossover model (Section 2.1) in the vicinity of the crossover frequency. The automated parameter identification technique is applied to the Hess structural model in order to match the performance of a generic pilot. The motion system feedback is then applied and pilot's performance is recorded. To evaluate the effectiveness of the motion system feedback, two models (with and without motion) are compared using power spectral density (PSD) analysis. The analysis in this section of the chapter is performed for two types of plant dynamics, namely $1/s$ and $1/s^2$. The proposed methodology can be summarized in the form of a step-by-step procedure.

1. Design the reference signal. For the first section of the chapter it is proposed to use the reference signal identical to that used during experiments with the MCL software. As stated previously the reference signal was composed of nine sinusoids of different frequencies and amplitudes (Table 4.1). Figure 7.2 illustrates time history of such a reference signal.
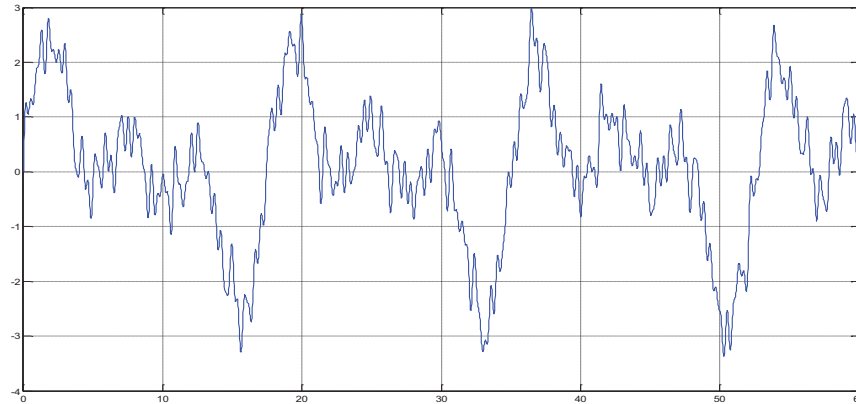
Figure 7.2. Reference signal in a form of a sum of sinusoids

2. Obtain the generic pilot control behavior by feeding the reference signal through the man-machine system (Figure 7.3) with the crossover model and recording generic pilot control signal u_c.
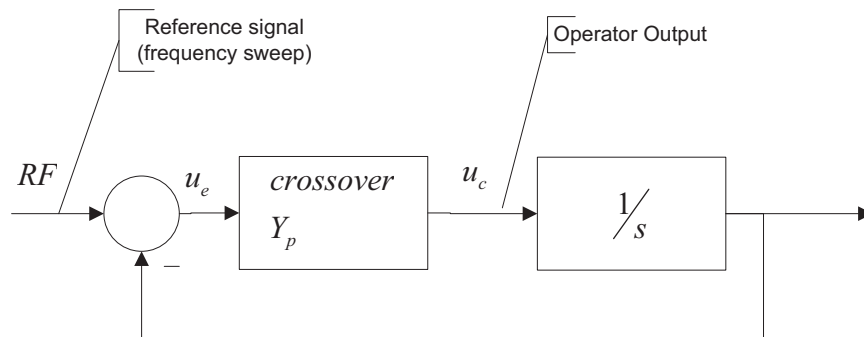
Figure 7.3. Man-machine system used to obtain a generic pilot control behavior ($1/s$ plant dynamics)

3. Apply APID to identify parameters of the Hess structural model (Figure 7.4), so it matches the operator control signal u_c recorded at the previous step. Note, that at this point no augmentations, such as filter and remnant are used with the model. It is assumed that a generic operator performs in a strictly linear fashion in the vicinity of the crossover frequency (crossover model) and there is no need to ascertain an individual control strategy or inject any type of noise in order to account for other sources of non-linearities in the system. Therefore, only the following parameters of the Hess model are tuned: K_e, K_1 and K_2.

4. Introduce models of the motion system and the motion cueing algorithm along with the vestibular system feedback path as shown in Figure 7.5. Generate the pilot control behavior signal u_{cm} using the reference signal from Step 1 and parameters identified in Step 3.

5. Compare signals u_c and u_{cm} obtained in steps 3 and 4 respectively. Perform comparison in the frequency domain. Draw conclusions regarding the effectiveness of the motion system/washout algorithm based on the observation of change in power spectrum of the simulated control behavior signal.
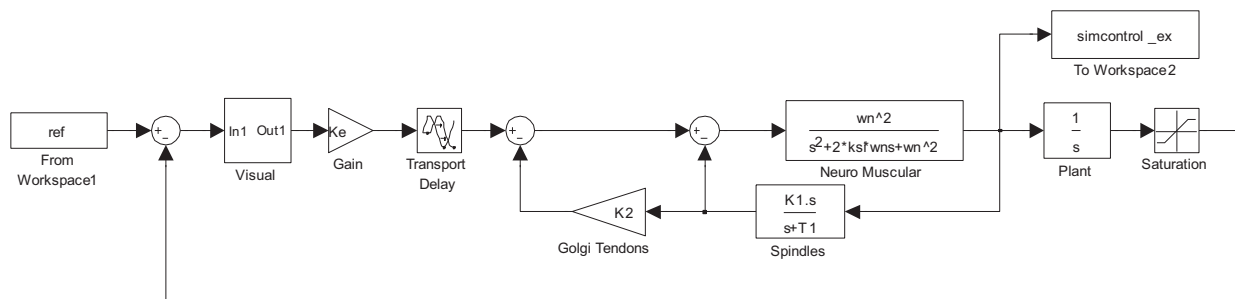
Figure 7.4. Hess structural model ($\dfrac{1}{s}$ plant dynamics). MATLAB SIMULINK block diagram
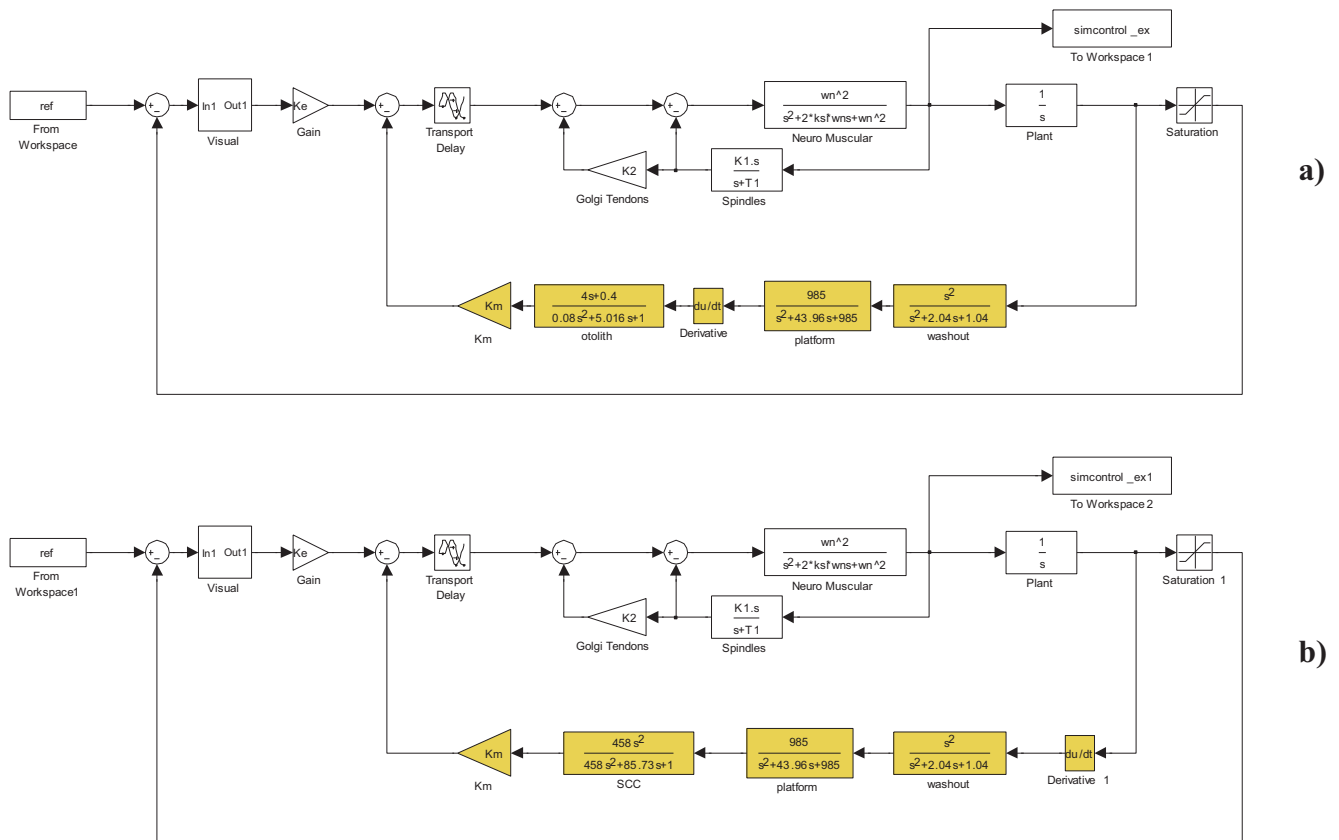
Figure 7.5. Hess structural model ($\frac{1}{s}$ plant dynamics) with vestibular system feedback path and motion system /washout algorithm models added: a) Translational channel; b) Rotational channel

MATLAB SIMULINK block diagrams

7.1.2. Results and discussions

According to step 2 of the proposed methodology it is necessary to obtain generic pilot control behavior by running the crossover model of the human operator. Figure 7.6 contains a representative portion of the human operator control signal time histories recorded for the reference signal used during experiments with the MCL software.
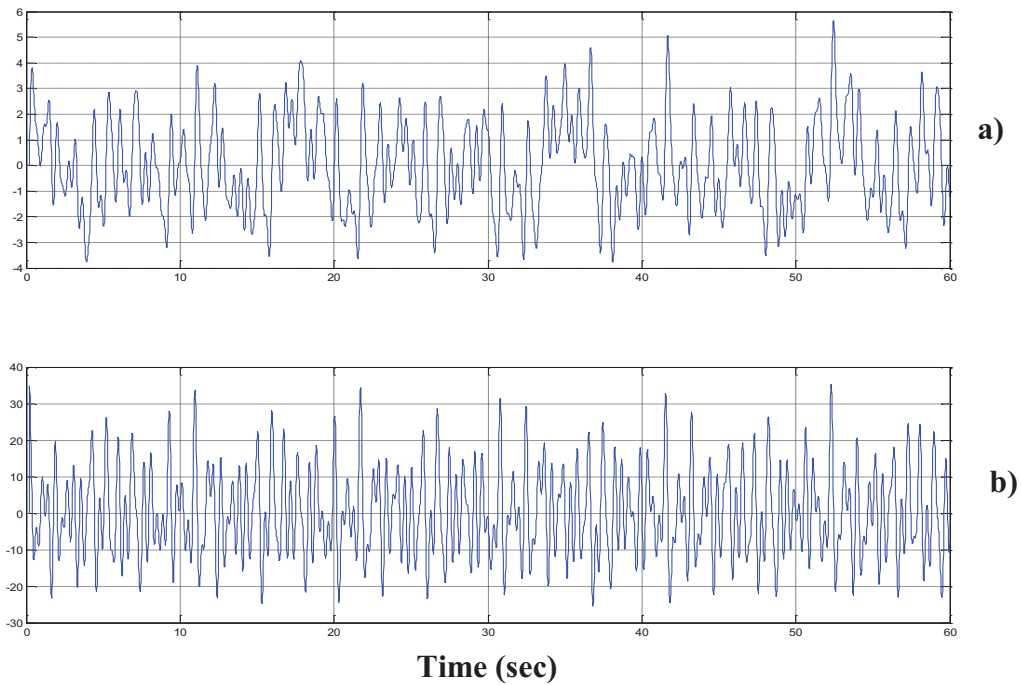
Figure 7.6. Time histories of the generic pilot control signal produced by the Crossover model for: a) $\frac{1}{s}$ plant dynamics; b) $\frac{1}{s^2}$ plant dynamics

It can be seen that the control signal obtained for the $\frac{1}{s^2}$ plant dynamics has higher frequency content as well as can be characterized by larger amplitude of oscillation.

The next step of the proposed methodology regulates application of the APID to the Hess structural model in order to match the control behavior of a generic operator. Once that is accomplished the motion system feedback is added (Figure 7.5) and the simulated control signal is recorded once again. The value of the gain K_m used in this section of the chapter is equal to 0.1 as it was originally proposed by Cardulo, et al. [5].

Figures (7.7 and 7.8) contain four sets of power spectral density graphs computed for three signals:

- The control behavior signal of the generic pilot produced by the crossover model
- The control behavior signal of the generic pilot produced by the Hess structural model after its parameters have been identified by the APID.

111

- The control behavior signal of the generic pilot produced by the Hess structural model with the motion system feedback added.

Close inspection of plots in Figure 7.7 yield an expected result: control signal produced by the Hess structural model (black dotted curve) lies practically on top of the generic pilot control behavior signal produced by the crossover model (blue solid curve). This observation supports the statement that the Hess structural model behaves similar to crossover model in the vicinity of the crossover frequency. Addition of the motion system feedback with the gain K_m being equal to 0.1 [14] results in suppression of power at higher frequencies. The first power bin, however, has been reproduced quite accurately.

Virtually the same observation is made for the case of lateral channel. Varying gain K_m does not improve the model fit. Moreover, further increase of the gain may result in overall system instability. Power spectral profile of the control signals (Figure 7.8) obtained for plant dynamics $1/s^2$ is quite different from that in Figure 7.7. The entire shape of the PSD profile has changed: the frequency content and power levels of the spectrum are much higher. This can be related to the observation, which was made earlier in the text regarding the increased amplitude and frequency of the generic pilot control signal. It is a well known fact that higher order dynamics are more difficult to control. It can also be seen that the original version of the Hess model (black dotted curve) no longer approximates the control signal by the crossover as closely as in the case of $1/s$ dynamics. While the highest frequency bin is approximated quite well, in the mid frequency range – the power levels are suppressed, and the power level of the first bin exceeds that of the control signal by the crossover model. Introduction of the motion system feedback does not seriously affect the performance of the model by Hess (red dashed curve).

The power level in all bins is lower than that of the crossover model except for the last one, where motion system feedback resulted in an increase of the power level. The same observations hold true for the lateral channel as well.

Table 7.1 summarizes the above discussion in a quantitative form. It contains numerical values of the identified parameters of the Hess structural model as well as values of the fitness

scores, which were computed to demonstrate the effect of introducing the motion system feedback into the Hess structural model.

a)

$$\text{Frequency } (^{rad}/_{sec})$$

b)

$$\text{Frequency } (^{rad}/_{sec})$$
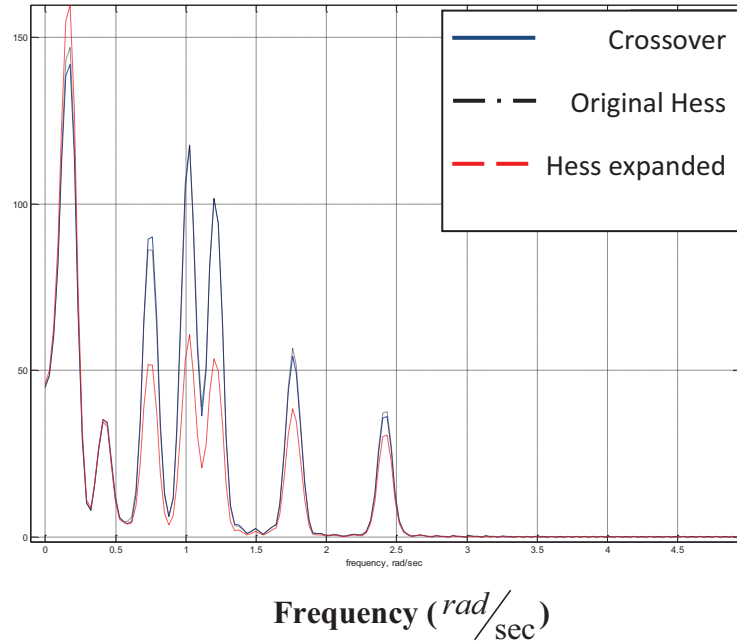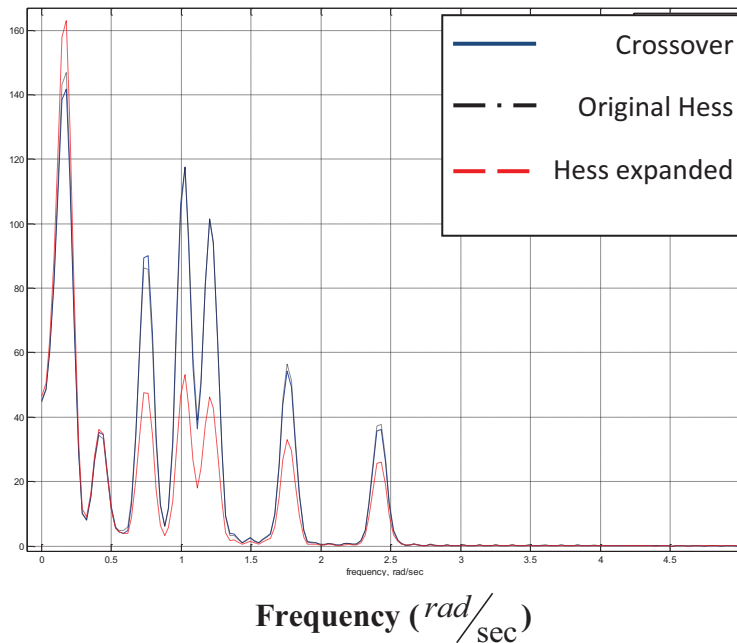
Figure 7.7. PSD of the control behavior signals of the generic human operator simulated by the Crossover Model, Hess Structural Model, Hess Structural Model with the motion system feedback. Graphs showed for a) longitudinal mode b) lateral mode. Plant dynamics $^1/_s$

a)

Frequency (rad/sec)

b)
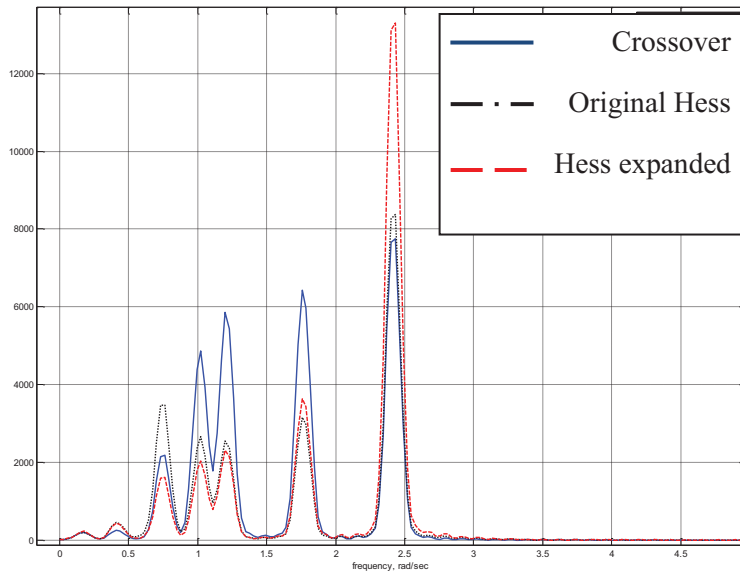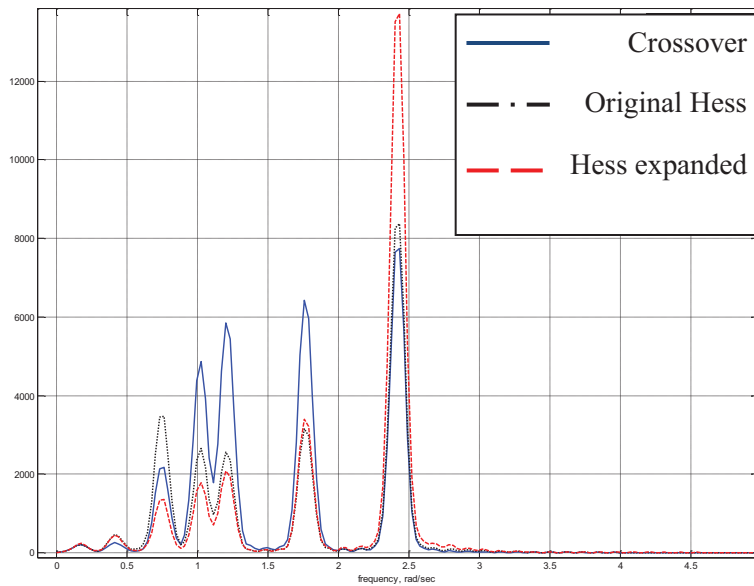
Frequency (rad/sec)

Figure 7.8. PSD of the control behavior signals of the generic human operator simulated by the Crossover Model, Hess Structural Model, Hess Structural Model with the motion system feedback. Graphs showed for a) longitudinal mode b) lateral mode, Plant dynamics $1/s^2$

Table 7.1. Fitness scores produced by the original Hess structural model with (Exp.) and without (Orig.) the motion system feedback for different degrees of freedom and different plant dynamics models.

Plant dynamics	Simulated DOF	Model	Identified parameters of the model				Fitness
			K_e	K_1	K_2	K_m	
$1/s$	Longitudinal	Orig.	102	5.43	5.26	**X**	0.444
		Exp.	102	5.43	5.26	0.1	4.89
	Lateral	Orig.	102	5.43	5.26	**X**	0.444
		Exp.	102	5.43	5.26	0.1	5.63
$1/s^2$	Longitudinal	Orig.	76.6	2.56	10.19	**X**	298.42
		Exp.	76.6	2.56	10.19	0.1	434.92
	Lateral	Orig.	76.6	2.56	10.19	**X**	298.42
		Exp.	76.6	2.56	10.19	0.1	469.84

It can be concluded here that there is no positive (improving) effect observed from introduction of the motion system feedback into the Hess structural model. This, however, can be explained by a simple fact, that the data on the generic pilot control behavior was obtained by running the off-line model of the human operator with no motion added. Therefore, addition of the motion system feedback is not useful. The following section of the chapter discusses the effects of motion system feedback when modeling the actual pilot behavior, which was recorded during experiments at the NASA LaRC VMS with motion system on.

7.2. Actual pilot

In this section of the chapter an attempt is made to evaluate the effectiveness of the motion system feedback using actual data obtained at the NASA Langley Research Center (LaRC) VMS

(Chapter 4). As opposed to the previous section of this chapter, the initial parameter identification of the Hess Structural Model occurs with respect to the actual control behavior of a pilot, which was recorded during experiments at NASA. Experiments that took place at the NASA Langley VMS Facility simulated the landing approach of a large civil transport aircraft under different control system delay conditions. In this study only the basic landing approach is considered, with no additional delay in the system. Table 7.2 contains trim conditions of the simulated aircraft.

Table 7.2. Landing approach trim conditions. NASA LaRC VMS.

Altitude	1300 ft BARO, 697 ft AGL
Airspeed	135 kts
Heading angle	180 deg
Distance to runway	2 nautical miles
Flaps	Full, Gear down
EPR	1.19
Glide slope	ON
Localizer	ON

The control task that's being investigated here can be described as compensatory tracking of the roll rate of the aircraft in the presence of a lateral wind disturbance. The pilot's task was to null the roll response of the aircraft due to the lateral wind. During experiments, the wind was simulated changing its direction clockwise as shown in Figure 7.9.a. As the wind moves to the side of the aircraft it induces a sideslip angle of the aircraft. The latter causes the aircraft to roll due to dihedral effect. The side wind exerting some lateral force on the vertical tail of the aircraft can contribute to the overall rolling motion of the aircraft (Figure 7.9.b.). The lateral component of the wind can be recorded and used as a disturbance signal, which acts upon the aircraft. The human operator in this case perceives the rolling rate of the aircraft and attempts to null the

effect of such a disturbance by controlling the aircraft and counteracting the wind induced rolling motion.
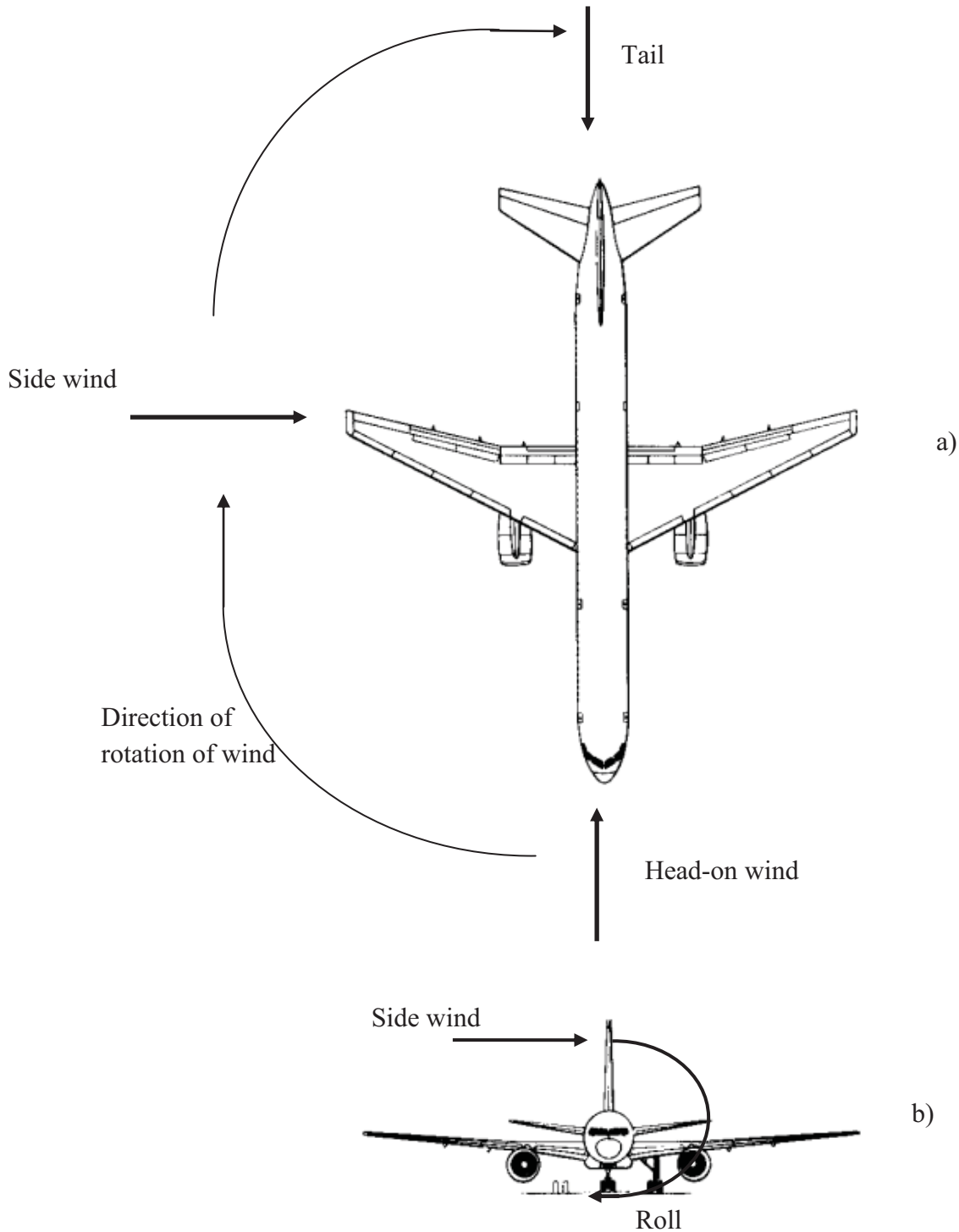
Figure 7.9. a) Graphical representation of the wind change pattern during the simulated landing approach; b) Side wind acting on the vertical tail and causing the aircraft to roll

Figure 7.10 contains the block-diagram of the resulting man-machine system.
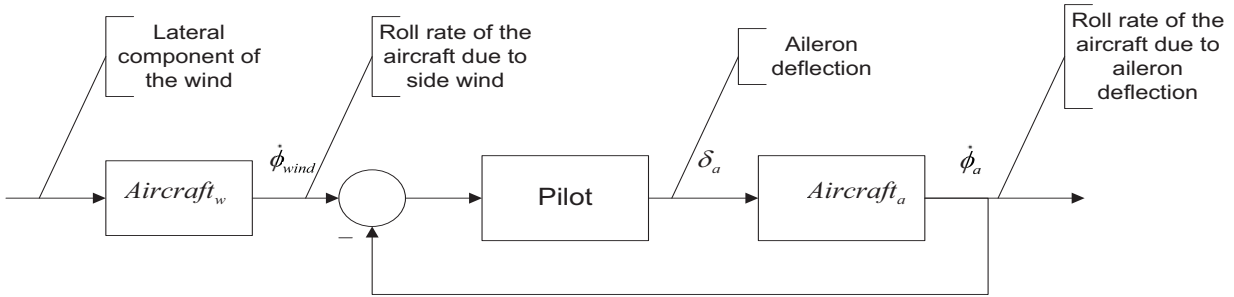
Figure 7.10. Block diagram of a pilot-aircraft closed loop control system used to model the stabilization task in the roll channel

7.2.1. Derivation of the aircraft model

In order to simulate the actual control behavior of a pilot during the lateral directional control of the aircraft it was decided to utilize a more sophisticated model of the aircraft, rather than a simple $\frac{1}{s}$ or $\frac{1}{s^2}$ dynamics. Roskam [32] offers a comprehensive description of the lateral directional dynamics of a wide fuselage jet aircraft. A complete transfer function relating aileron deflection δ_a to the roll angle ϕ is given by Eq. 7.5.

$$\frac{\phi}{\delta_a} = \frac{A_\phi s^2 + B_\phi s + C}{As^4 + Bs^3 + Cs^2 + Ds + E} \, , \tag{7.5}$$

Where coefficients of the numerator and denominator are the functions of the lateral-directional dimensional stability derivatives of an aircraft and are given by the systems of Eq. (7.6) and (7.7) respectively:

$$
\begin{cases}
A = U(1 - A_1 B_1) \\
B = -Y_\beta(1 - A_1 B_1) - U(L_p + N_r + A_1 N_p + B_1 L_r) \\
C = U(L_p N_r - L_r N_p) + Y_\beta(L_p + N_r + A_1 N_p + B_1 L_r) - \\
\qquad - Y_p(L_\beta + N_\beta A_1 + N_{T_\beta} A_1) + U(L_\beta B_1 + N_\beta + N_{T_\beta}) - \\
\qquad - Y_r(L_\beta B_1 + N_\beta + N_{T_\beta}) \\
D = -Y_\beta(L_p N_r - L_r N_p) - Y_p(L_\beta N_r - N_\beta L_r - N_{T_\beta} L_r) - \\
\qquad - g\cos(\theta)(L_\beta + N_\beta A_1 + N_{T_\beta} A) + (U - Y_r)(L_\beta N_p - N_\beta L_p - N_{T_\beta} L_p) \\
E = g\cos(\theta)(L_\beta N_r - N_\beta L_r - N_{T_\beta} L_r)
\end{cases}
, \qquad (7.6)
$$

$$
\begin{cases}
A_\phi = U(L_{\delta_a} + N_{\delta_a} A_1) \\
B_\phi = U(N_{\delta_a} L_r - L_{\delta_a} N_r) - Y_\beta(L_{\delta_a} + N_{\delta_a} A_1) + \\
\qquad + Y_{\delta_a}(L_\beta + N_\beta A_1 + N_{T_\beta} A_1) \\
C_\phi = -Y_\beta(N_{\delta_a} L_r - L_{\delta_a} N_r) + Y_{\delta_a}(L_r N_\beta + L_r N_{T_\beta} - N_r L_\beta) + \\
\qquad + (U - Y_r)(N_\beta L_{\delta_a} + N_{T_\beta} L_r - L_\beta N_{\delta_a})
\end{cases}
, \qquad (7.7)
$$

Where $A_1 = \dfrac{I_{xx}}{I_{zz}}$ and $B_1 = \dfrac{I_{xz}}{I_{zz}}$ respectively. Table 7.3 contains expressions for the

dimensional lateral-directional stability derivatives of an aircraft.

Table 7.3. Lateral-directional dimensional stability derivatives (Roskam, [32])

$Y_\beta = \dfrac{qS C_{y_\beta}}{m}, \quad (ft/\sec^2)$	$L_{\delta_a} = \dfrac{qS C_{l_{\delta_a}}}{I_{xx}}, \quad (1/\sec^2)$
$Y_p = \dfrac{qSb C_{y_p}}{2mU}, \quad (ft/\sec)$	$N_\beta = \dfrac{qSb C_{n_\beta}}{I_{zz}}, \quad (1/\sec^2)$
$Y_r = \dfrac{qSb C_{y_r}}{2mU}, \quad (ft/\sec)$	$N_p = \dfrac{qSb^2 C_{n_p}}{2 I_{zz} U}, \quad (1/\sec)$
$Y_{\delta_a} = \dfrac{qS C_{y_{\delta_a}}}{m}, \quad (ft/\sec^2)$	$N_r = \dfrac{qSb^2 C_{n_r}}{2 I_{zz} U}, \quad (1/\sec)$

$L_\beta = \dfrac{qSbC_{l_\beta}}{I_{xx}}, \quad (1/\sec^2)$	$N_{T_\beta} = \dfrac{qSbC_{n_{T_\beta}}}{I_{zz}}, \quad (1/\sec^2)$
$L_p = \dfrac{qSb^2C_{l_p}}{2I_{xx}U}, \quad (1/\sec)$	$N_{\delta_a} = \dfrac{qSbC_{n_{\delta_a}}}{I_{zz}}, \quad (1/\sec^2)$
$L_r = \dfrac{qSb^2C_{l_r}}{2I_{xx}U}, \quad (1/\sec)$	

Where the parameter q is the dynamic pressure and is equal to $q = \dfrac{1}{2}\rho V_p^2$

Table 7.4 contains values of the dimensionless lateral-directional stability derivatives as well as geometrical parameters of an aircraft and flight conditions.

Table 7.4. Lateral-directional dimensionless stability derivatives (Roskam, [32]) and parameters of the aircraft

Parameter	Value	Description (dimensions)
S	5500	Wing area (ft^2)
b	196	Wing span (ft)
U	227	Velocity ($ft/\sec$)
m	564000	Mass ($slug$)
ρ	0.002389	Air density ($slug/ft^3$)
I_{xx}	$13.7 \cdot 10^6$	Moments of inertia ($slug \cdot ft^2$)
I_{yy}	$30.5 \cdot 10^6$	

I_{zz}	$43.1 \cdot 10^6$	
I_{xz}	$0.83 \cdot 10^6$	
C_{y_β}	-1.08	
C_{y_p}	0	
C_{y_r}	0	
$C_{y_{\delta_a}}$	0	
C_{l_β}	-0.281	
C_{l_p}	-0.502	
C_{l_r}	0.195	Lateral-directional dimensionless stability derivatives
$C_{l_{\delta_a}}$	0.503	
C_{n_β}	0.184	
C_{n_p}	-0.222	
C_{n_r}	-0.36	
$C_{n_{T_\beta}}$	0	
$C_{n_{\delta_a}}$	0.0083	

For this study, however, the use of a reduced order aircraft transfer function relating aileron deflection δ_a to the resulting roll rate $\dot{\phi}$ was deemed to be sufficient (Eq. 7.8). Such a transfer

function can be obtained as a result of "rolling" approximation of the lateral directional dynamics of the aircraft. The transfer function is derived under the assumption that there is no other lateral motion modes, such as dutch roll or spiral mode, being excited.

$$\frac{\dot{\phi}}{\delta_a} = \frac{L_{\delta_a}}{s(s - L_p)}, \qquad (7.8)$$

Substituting parameters from tables 7.2 and 7.3, Eq. 7.8 can be rewritten as:

$$Aircraft_a = \frac{\dot{\phi}}{\delta_a} = \frac{0.0107}{s(s + 0.0046)}, \qquad (7.9)$$

According to the block diagram shown on Figure 7.10 another model of the aircraft ($Aircraft_w$), which would relate the roll rate of the aircraft to the side-wind, is required. Obtaining such a model involved using the interactive large civil transport aircraft model provided by NASA Langley. The interactive model has a simple GUI (Figure 7.11).
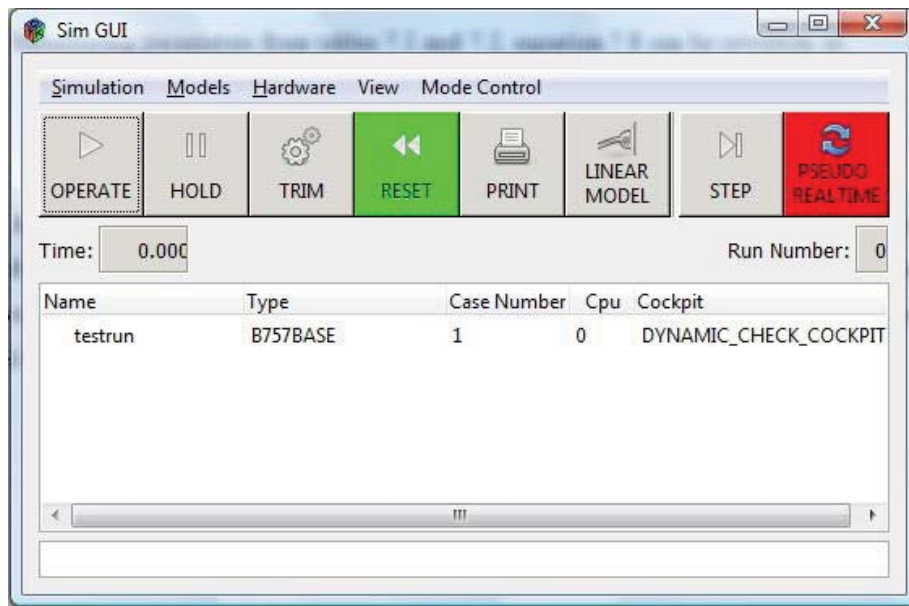
Figure 7.11. Large civil transport aircraft model GUI (courtesy of NASA Langley)

It allows simulating the behavior of the aircraft in response to various pilot inputs and/or external disturbances, such as turbulence. The interface of the model allows choosing from a

variety of predetermined control inputs, such as step, pulse doublet, sine wave etc. In addition to that, it is possible to feed any prerecorded, properly sampled external input as desired by the researcher. The modeled aircraft can be trimmed to virtually any flight conditions, including landing approach, cruise on low altitude, cruise on high altitude and so on. Recorded parameters match those recorded during actual simulation runs at the VMS research facility at NASA LaRC. The availability of this simulator allowed the derivation of the sought "side wind to roll rate" model by performing a standard parameter identification analysis based on the input-output data. The derivation process can be described as a four step process:

Step 1. Trim aircraft to the initial conditions corresponding to the landing approach conditions used during experiments at NASA.

Step 2. Feed the side wind external disturbance into the large civil transport aircraft model. Figure 7.12 graphically illustrates the side wind profile used during this derivation process. It is identical to that used during experiments at NASA.

Step 3. Record the roll rate response of the aircraft.

Step 4. Using Auto Regressive with eXternal (ARX) input model estimator, fit the available input/output data
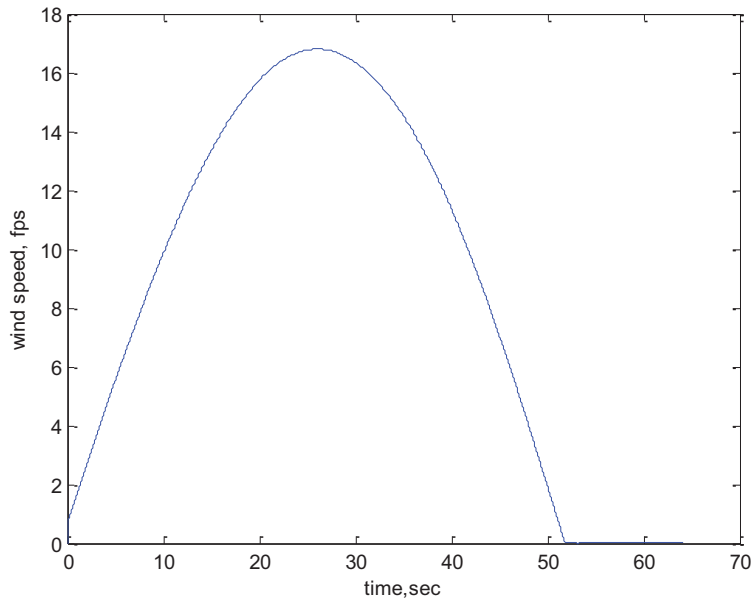
Figure 7.12. Lateral component of the wind acting upon the aircraft

With the procedure described above, it was possible to derive the following transfer function relating the lateral component of the wind acting upon the vertical tail of the aircraft to the roll rate of the aircraft (7.10):

$$Aircraft_w = \frac{\dot{\phi}}{V_{wind}} = \frac{0.2554s^3 - 14.4s^2 + 272.6s - 25.72}{s^4 + 84.37s^3 + 452.2s^2 + 1510s + 628.8}, \tag{7.10}$$

7.2.2. Methodology

The methodology used in this section to evaluate effectiveness of the motion system feedback is similar to that proposed in the previous section of the chapter where the analysis was based on the behavior of a generic pilot. First, APID is applied to identify parameters of the original version of the Hess model, in order to get as close as possible to the actual control behavior of a given pilot. In the second step the motion system is added. The resulting change in performance is evaluated by comparing PSD data of the actual and simulated control signals. During the third step of the proposed methodology, APID is applied to the expanded version of the Hess model, where gain K_m is identified along with other parameters of the Hess structural model. The performance of the optimized expanded version of the model is then evaluated again

124

by comparing the PSD data of the simulated control signal against that obtained in the previous step. Since here the parameter identification occurs with respect to the actual pilot data, it was also necessary to repeat the evaluation procedure with the Hess Structural Model enhanced by the TEC algorithm.

7.2.3. Results and discussions

Figure 7.13 contains PSD data of four signals: the blue solid line corresponds to the actual control activity of a pilot. The dotted black line represents the power spectral density of the pilot control behavior simulated by the original Hess structural model. Parameters of the model were optimized by the APID in an attempt to closely model the pilot control behavior. It can be seen, that the model performed quite poorly throughout the entire frequency range: the major power bin was underachieved substantially.
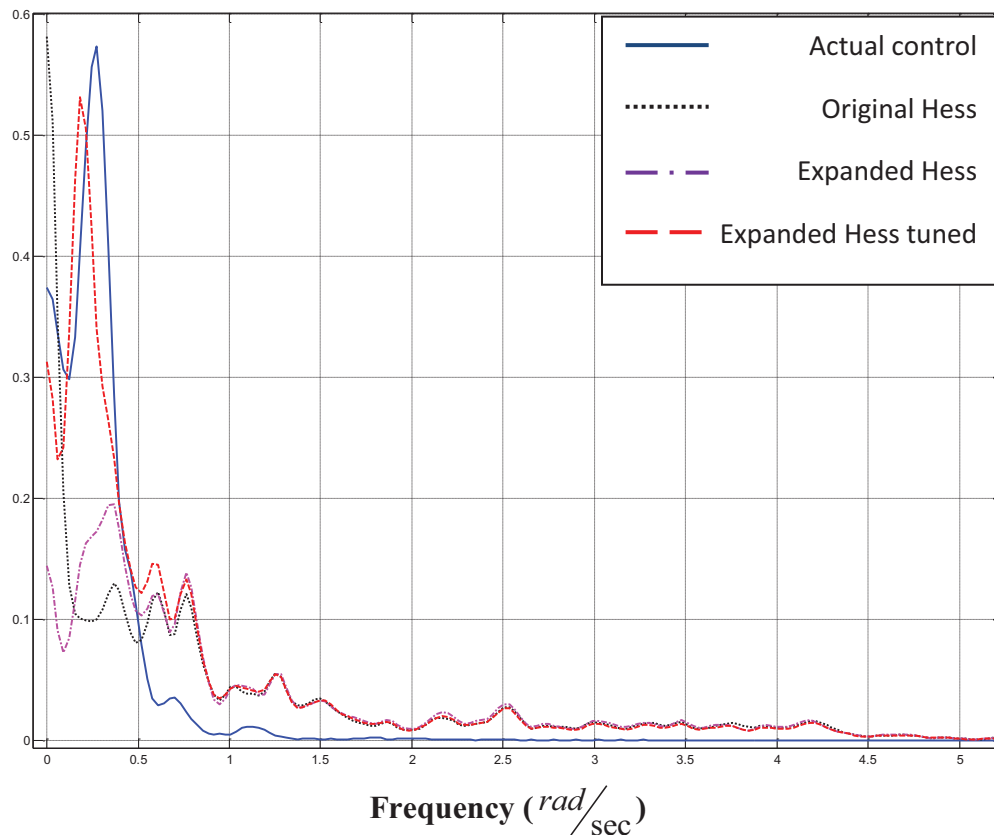
Figure 7.13. PSD of the actual control signal (blue solid) vs. simulated control signal by original Hess (black dotted), Expanded Hess (magenta dot-dashed) and Expanded Hess tuned by APID (red dashed). TEC is not present

125

Magenta colored dash-dotted line corresponds to performance of the Hess model with the motion feedback added into the system. Note, that the gain K_m used in the model is equal to 150, which is much greater than the original value proposed by George [14]. If the original value of 0.1 is used, then there is hardly any evidence of presence of the motion system feedback. At the initial stages of the investigation it has become clear that the gain K_m must be increased in order to achieve some effect on the performance of the model. As one can see from the graph, the increase in gain K_m resulted in a noticeable change of the power spectral profile of the control signal: the power level around the main power bin of the actual control signal started to elevate. In the mean time, there have been no significant alterations of the power profile in the remainder of the spectrum. This observation suggests that inclusion of gain K_m into a string of parameters identified by APID may improve the overall performance of the model. The fourth curve on the graph (red dashed curve), corresponds to the case when parameters of the Hess structural model were identified along with the gain of the motion system feedback. It is clear from the graph, that improvement was significant. The frequency (2.5 rad/sec) of the major bin of the actual pilot control signal was estimated very closely. Moreover, the power level was matched quite accurately as well. In the mean time, there has been no change in power spectral profile past 0.5 rad/sec – it remained slightly elevated compared to the actual control signal. Table 7.4 contains numerical values of identified parameters of the Hess model for three cases considered. One can see only a slight improvement of the fitness score when the motion system feedback was added. The major improvement of the fitness score followed after APID had been applied to re-identify parameters of the Hess model including K_m.

Since this section of the chapter concentrates on simulating the behavior of a given pilot, it was critical to repeat the evaluation procedure with the Hess structural model being enhanced by the TEC model. Figure 7.14 contains plots of PSD of the following signals:

- Solid blue – actual pilot control activity
- Black dotted – control behavior simulated by the Hess model enhanced by TEC.

- Magenta dash-dotted – control behavior simulated by the Hess model enhanced by TEC with the motion system feedback. Gain K_m in this case was not part of the identification process and was set equal to 150.
- Red dashed – control behavior by the Hess model enhanced by both TEC and motion system feedback, with K_m being identified by APID along with other parameters of the model
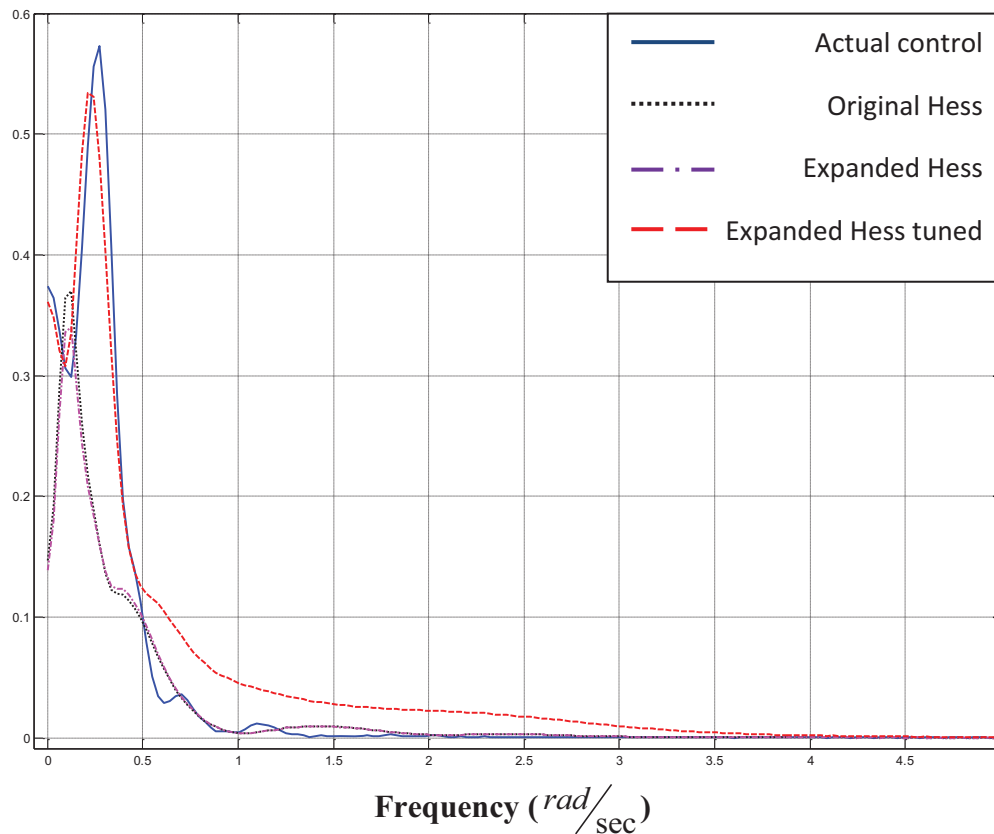

Figure 7.14. PSD of the actual control signal (blue solid) vs. simulated control signal by original Hess (black dotted), Expanded Hess (magenta dot-dashed) and Expanded Hess tuned by APID (red dashed). TEC is present

It is clear from the graph that the Hess structural model enhanced by both TEC and motion system feedback is capable of a very close approximation of actual pilot control activity. Table 7.4 contains numerical values of identified parameters of the model as well as the fitness scores.

The lowest fitness score was achieved by the "Hess + TEC + motion system feedback" configuration of the model, when K_m was identified by PID. The side by side comparison of the model configurations with and without TEC shows that the model with TEC performed better (fitness scores were lower) in all three cases. This observation supports the statement that addition of TEC allows closer approximation of the individual control behavior of a pilot.

Table 7.5. Fitness scores produced by the original Hess structural model with and without the TEC model with and without the motion system feedback.

Model of the TEC present	Model configuration	Identified parameters of the model				Fitness
		K_e	K_1	K_2	K_m	
NO	Orig.	16.2	8	2.08	X	0.0490
	Exp.	16.2	8	2.08	150	0.0483
	Exp.*	7	3.35	0.95	976	0.0263
YES	Orig.	0.41	1.92	2.56	X	0.0386
	Exp.	0.41	1.92	2.56	150	0.0389
	Exp.*	0	2.23	1.92	559	0.0157

Exp* - APID included K_m.

It is difficult not to notice that when APID was applied to identify parameters of the expanded version of the Hess structural model it had identified gain K_e to be equal to zero for this particular pilot. Technically, it means that the visual information path in the Hess structural model is nulled. This can be interpreted as if this particular pilot is not relying on the visual information at all while performing this (roll-rate stabilization) control task. The feedback information then consists of the proprioceptive and motion vestibular modalities. In an attempt to make any conclusion regarding such observation, APID was applied to control data from seven pilots, which had participated in experiments at NASA. Two model configurations were

considered: with TEC and without TEC. Table 7.5 contains values of identified parameters as well as fitness scores produced by the identified models.

Table 7.6. Identified parameters of the expanded (with motion system feedback) version of the Hess structural model with (X) and without (O) TEC.

Pilot #	TEC	Identified parameters				Fitness
		K_e	K_1	K_2	K_m	
1	O	7	3.35	0.095	976	**0.0263**
	X	0	2.23	1.92	559	**0.0157**
2	O	3.3	2.23	0.72	463	**0.0120**
	X	0.33	7.68	5.12	0	**0.0048**
3	O	2.9	0.95	0.69	316	**0.0325**
	X	0	2.54	0.18	225	**0.006**
4	O	3	0.84	1.76	416	**0.0191**
	X	0.89	8.13	2.56	64	**0.0135**
5	O	5	2.56	0.32	511	**0.0368**
	X	0.76	7.79	2.03	7	**0.0108**
6	O	3.7	1.28	2.56	879	**0.0258**
	X	1.29	9.59	2.16	0	**0.0118**
7	O	9.7	6.39	0.85	1020	**0.0125**
	X	0.29	5.19	2.63	255	**0.0054**

It is possible to make a few observations from this table:

1. Fitness scores of the human operator model with the TEC are at least 50% better (lower) that those with no TEC.

2. The visual system gain K_e dropped in value when TEC was introduced for all pilots. Two pilots were identified to have $K_e = 0$, suggesting that those pilots were not relying on visual information at all in this particular control task. This observation, however, comes in contradiction with the common knowledge that the visual information predominates among all sensory modalities of the human operator.

3. The motion system feedback gain K_m is lower for the case when TEC was in the system. Two pilots were identified to have $K_m = 0$, thus suggesting that they are not relying on the vestibular system feedback while performing a roll-rate stabilization task. This is true for the low frequency tasks. It is possible the pilot is relying mostly on vestibular sensation of the roll rate. The visual information has low gain in that case.

4. Considering the small size of subject population it is difficult to make any conclusion regarding the behavior of gains K_1 and K_2 as a function of TEC.

Based on these observations it is possible to conclude that a set of experiments should be devised to prove or disprove conclusions made regarding the use of visual system information as well as vestibular system when controlling the roll-rate of the aircraft.

7.3. Summary

In the first section of this chapter it was demonstrated that the use of the motion system feedback designed by Cardullo, et al. [5] does not necessarily have a positive effect on the models performance when simulating control task, which does not involve motion of course. This conclusion was drawn based on the results obtained when simulating the control behavior of a generic pilot without motion feedback. The latter was simulated by the Crossover Model. Two

plant dynamics were considered. In both cases, introduction of the motion system feedback resulted in overall decrease of the models performance.

The second section of the chapter concentrated on modeling control behavior of a certain individual. The actual data used during evaluation was obtained at the NASA LaRC VMS research facility. Experiments were conducted with the active motion system. It was demonstrated that the Hess Structural Model is capable of close approximation of the actual control activity when it is enhanced by the motion system feedback. Addition of the motion system feedback resulted on average in 50% increase in model performance.

Addition of the Testing Element of Control into the model resulted in even closer approximation of the actual control behavior of a pilot. Results obtained for several pilots suggest that some pilots may ignore the visual modality when performing a stabilization control task in the angular channel. Conversely, some pilots tend to ignore the vestibular modality when performing the same task. In order to prove these results further investigation is needed.

8. Conclusions and future research

8.1. Conclusions

A number of human operator models have been developed over more than 60 years of operator modeling history. Structural models such as the Crossover Model, the Hess structural model, and the Hosman descriptive model despite being quite successful in modeling an average (generic) pilot behavior, share the same drawback – they do not account for a non-linear behavior of an actual operator. The OCM model is a quasi-linear algorithmic model of the human operator which still lacks the behavioral component. The inter subject differences manifest themselves in the magnitude and frequency content of the non-linear component of the control behavior. Conventionally, the non-linear component of the control behavior in any man-machine system is accounted for by injecting remnant. Remnant, however, does not discriminate between the sources of the noise in the system. The primary goal of this study was to develop a set of algorithmic tools that would overcome this gap in simulating human behavior, and allow modeling of the control behavior of a given individual.

The most significant of all the novel aspects of this research is referred to as the testing element of control algorithm or simply TEC, which is capable of representing individual control strategy of different operators, which contributes to the overall non-linear element of control behavior. The TEC algorithm evolves from an artificial neural network, which is a biologically inspired computational tool capable of mathematical representation of human behavior. It was postulated in this study that every individual can be identified by his/her unique set of TEC parameters. Results presented in chapter 6 demonstrate a significant improvement in model's ability to model an actual operator control behavior with TEC incorporated into it.

Another model enhancement developed in this study can be applied to further improve the ability of a given model to simulate an individual control behavior of an operator. As differentiated from TEC it takes on the form of a filter, which can be customized according to the subject specific control data. The filter itself is an equiripple filter (EF) designed using the Parks McClellan algorithm. EF is intended to improve the shape of the power spectral density of the simulated control behavior so it matches that of an actual operator.

In addition to the model enhancements, this study utilized a novel automated parameter identification technique (APID), which was designed specifically to aid in identification of parameters of a given model of the human operator and its enhancements. APID identifies parameters of a given model of the human operator, which result in the closest approximation of actual operator control behavior. The uniqueness of the proposed APID is in using a genetic algorithm optimization engine to achieve this goal. The choice was dictated by the versatility and computational efficiency of genetic algorithms. There is also no obvious restriction on the number of identified parameters as well as there is no explicit requirement for them (parameters) to be related or influence each other.

Preliminary analysis was oriented toward determining to which parameters the Hess structural model are most sensitive in terms of performance. It turned out that gain coefficients of the proprioceptive feedback K_1 and K_2 as well as the visual signal processing gain K_e have the dominant effect on the performance of the model and, as a consequence, on the ability to represent individual behavior of different operators. The effectiveness of TEC and EF was demonstrated by applying them to the selected models of the human operator, such as: the Hess structural model, Hosman descriptive model and the optimal control model. Models enhanced by TEC and EF demonstrated an average improvement in performance of 42 % and 36 % respectively for the MCL and UAV data sets respectively. Results obtained for the MCL data set indicated that the Hosman descriptive model was able to closely model individual behavior of the majority (63%) of subjects while being applied "alone", i.e. with no enhancements. After the model enhancements are applied, the Hess structural model produced better results for 52% and 68% of subject population (TEC and TEC+EF cases respectively). In the case of the UAV data, the Hosman model outperformed other models with TEC and TEC+EF being applied: 40 % and 30% respectively. A consistency analysis of the results was performed to demonstrate the effectiveness of the proposed APID. The increase in variation of identified parameters associated with the increase in the number of identified parameters was documented. The maximum variation recorded is with the Hosman descriptive model applied to the UAV data set with both TEC and EF included and is equal to 32.33 %. That particular model configuration contains 17 parameters identified by APID. It was also determined, that results tend to vary more for the case of the UAV data. This, however, can be attributed to the fact, that the control task simulated by

the UAV test is far more complex than that modeled by the MCL. Moreover, original versions of the selected human operator models used in this study are capable of modeling only a single degree of freedom control task. Whereas the UAV airspeed control task involves control in at least two DOF: pitch stick and throttle. Analysis presented in this study concentrated only on the pitch stick control.

Chapter 7 used data from previous experiments conducted at NASA Langley and was aimed at evaluating the effectiveness of motion system's system feedback in the Hess structural model. The motion system feedback, developed by Cardullo, et al. [5], includes a model of the motion system itself, the washout algorithm and models of the human vestibular system. When the evaluation procedure was applied to control data of the generic pilot, obtained by running the Crossover Model, no improvement of the models performance was observed. Note, however, generic pilot control activity was obtained by running the crossover model of the man-machine system with no motion included. The second part of the analysis was performed based on experimental data obtained at the NASA Langley Visual Motion Simulator with the active motion system. The evaluation procedure involved applying APID to identify model parameters, which result in the closest approximation of the actual control behavior. It was demonstrated that after enhancing the Hess structural model with the motion system feedback and applying APID, the models performance was improved by 50%. The evaluation was repeated with the Hess structural model augmented by the TEC algorithm. In this case the fitness score of the model without the motion system feedback was improved by 21%. After the APID was re-applied, the fitness of the model was improved by 67 %. The results obtained during this research demonstrate that incorporating motion into simulation improves operator behavior as demonstrated by the models.

The observed results suggest that applying APID to the expanded (motion system feedback included) version of the Hess structural model can potentially answer the question whether the motion system is necessary for a particular simulation or not.

8.2.Future research

The research results presented in this study have demonstrated that the proposed enhancements to the existing models allow discrimination among different subjects. Proposed techniques bear great potential for future implementation in many areas of research & development and industry. However, there are still a lot of obstacles to overcome. In the following paragraphs, some of the directions for future research are discussed.

Computational efficiency is still a major issue. All programming in this study has been performed in MATLAB and the MATLAB SIMULINK environment. The computational efficiency expressed in terms of time it takes to complete a single iteration of APID is directly proportional to the number of identified parameters. In the case of the Hess structural model enhanced by both TEC and EF, the time it takes APID to complete a single iteration is on the order of one hour. Therefore, in order to be able to apply it in real time, it is considered to be one of the priorities to improve the computational efficiency of the APID. There are several possible solutions to this problem. First of all, it seems useful to depart from MATLAB and reprogram everything in C/C++ or Visual Basic.NET. This is especially important since one of the potential implementations of the proposed APID is to apply it in real-time systems. The ability to obtain information regarding the control behavior of an operator in real time has security and safety implications.

Further on, research should also concentrate on improving the model enhancements themselves. The neural network of the TEC has potential to be improved. Different types of activation functions can be used. The number of hidden layers and neurons can be varied as well. The proposed APID has the potential for improvement as well. The observed statistical decrease in consistency of identified parameters associated with the increase in the number of parameters to be identified should be addressed in future research.

The application investigation with the NASA data in chapter 7 has demonstrated that APID can be successfully applied in order to answer a very important question regarding the need for motion cueing systems in at least some applications. The results may provide more insight on what perception modalities are used by the pilot. To validate the results obtained in this research a set of experiments should be designed. These experiments should involve a properly designed control task, which should not be too complex so it does not require multi degree of freedom

control behavior. Experiments should also include motion/no-motion conditions as well as varying quality of the visual information. The latter is important to validate results regarding the usage of the visual information channel in the Hess structural model.

Appendix A. Human operator model block diagrams

Figure A. 1. Block diagram of the Hosman descriptive model adapted to the pursuit control task

Figure A. 2. Block diagram of the OCM adapted to the pursuit control task

This page intentionally left blank.

Appendix B. Full set of identified parameters

Table B. 1. Full set of identified parameters

Model	Identified parameters		
	Name	*Bits in the chromosome*	*Identification range*
Hess structural model	K_e	10	$[0 \; ; 10.23]$
	K_1	10	$[0 \; ; 10.23]$
	K_2	10	$[0 \; ; 10.23]$
Hosman descriptive model	w_{att}	10	$[0 \; ; 10.23]$
	w_{rate}	10	$[0 \; ; 10.23]$
OCM	V_y	10	$[0 \; ; 10.23]$
	V_m	10	$[0 \; ; 10.23]$
Equiripple filter	lev_1	10	$[0 \; ; 10.23]$
	$lev_2{}^*$	10	$[0 \; ; 10.23]$
	$lev_3{}^*$	10	$[0 \; ; 10.23]$
	$lev_4{}^*$	10	$[0 \; ; 10.23]$
Testing element of control	w_{110}	11	$[-10.23 \; ; 10.24]$
	w_{111}	11	$[-10.23 \; ; 10.24]$

	w_{112}	11	$[-10.23 \; ; 10.24]$
	w_{120}	11	$[-10.23 \; ; 10.24]$
	w_{121}	11	$[-10.23 \; ; 10.24]$
	w_{122}	11	$[-10.23 \; ; 10.24]$
	w_{130}	11	$[-10.23 \; ; 10.24]$
	w_{131}	11	$[-10.23 \; ; 10.24]$
	w_{132}	11	$[-10.23 \; ; 10.24]$
	w_{210}	11	$[-10.23 \; ; 10.24]$
	w_{211}	11	$[-10.23 \; ; 10.24]$
	w_{212}	11	$[-10.23 \; ; 10.24]$
	w_{213}	11	$[-10.23 \; ; 10.24]$
	K_r	10	$[0 \; ; 10.23]$
Remnant	K_n	10	$[0 \; ; 10.23]$
	T_n	10	$[0 \; ; 10.23]$
Pursuit tracking gain	K_{ff}	13	$[0 \; ; 8191]$

Parameters marked with the asterisk are available only for the MCL data.

Appendix C. Fitness score comparison histograms: MCL data set

Hess structural model

Hosman descriptive model

OCM
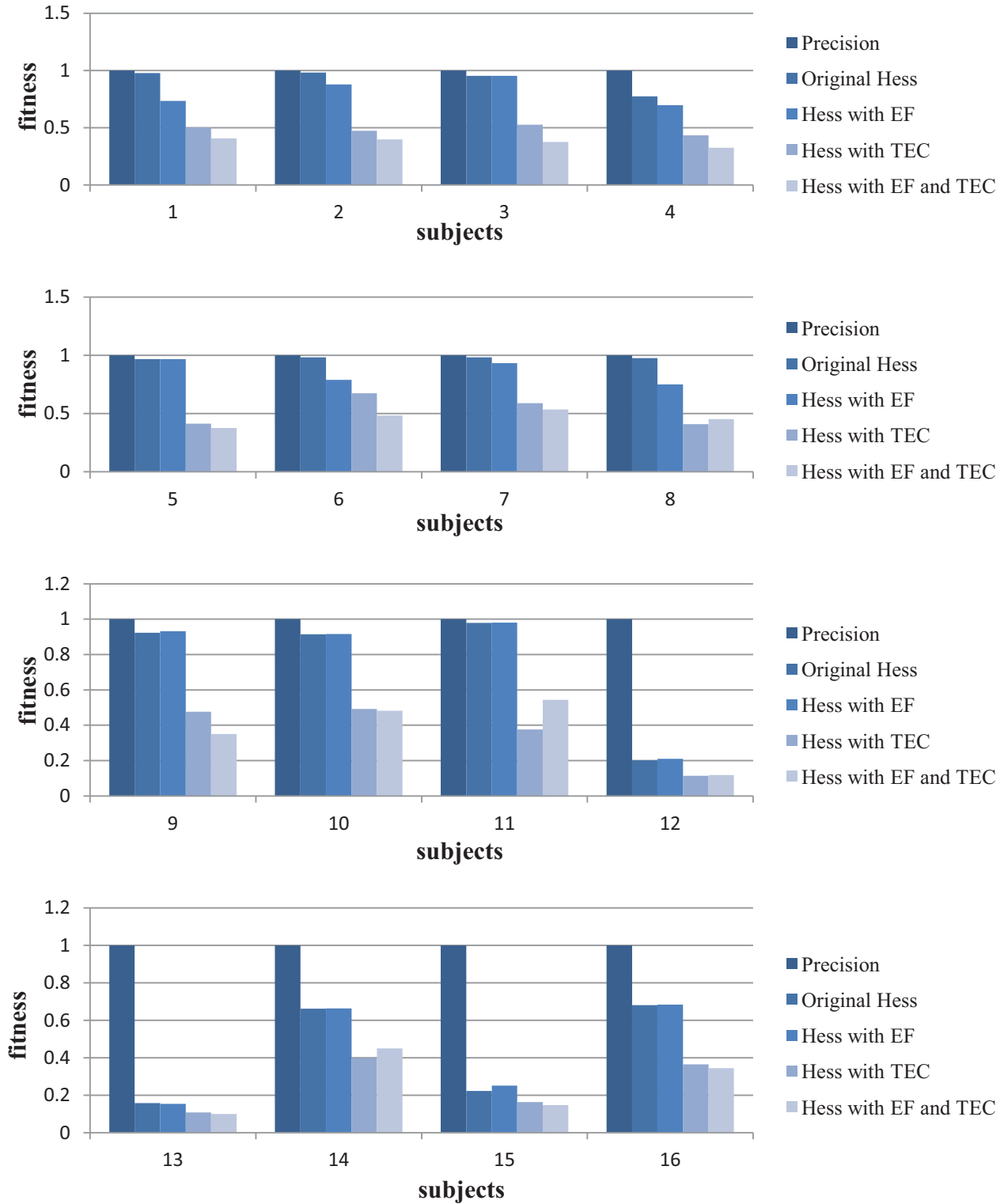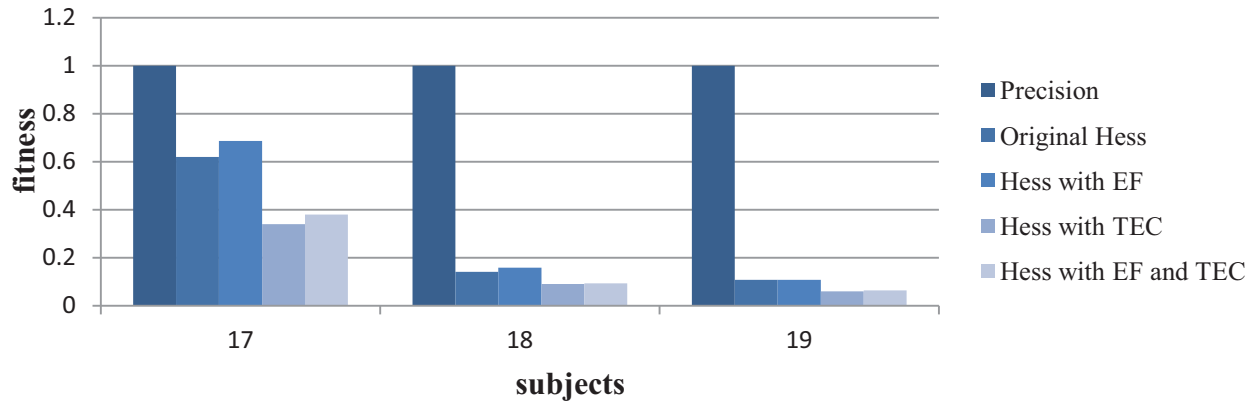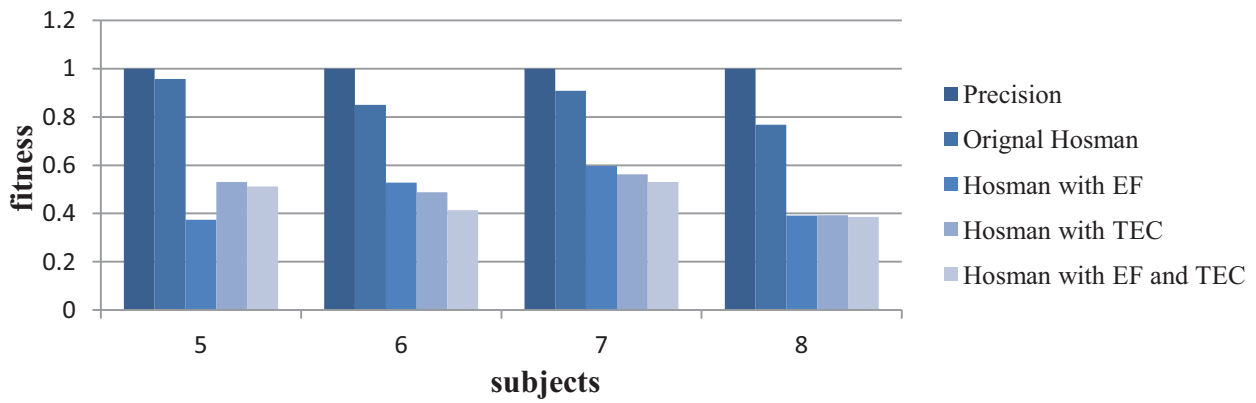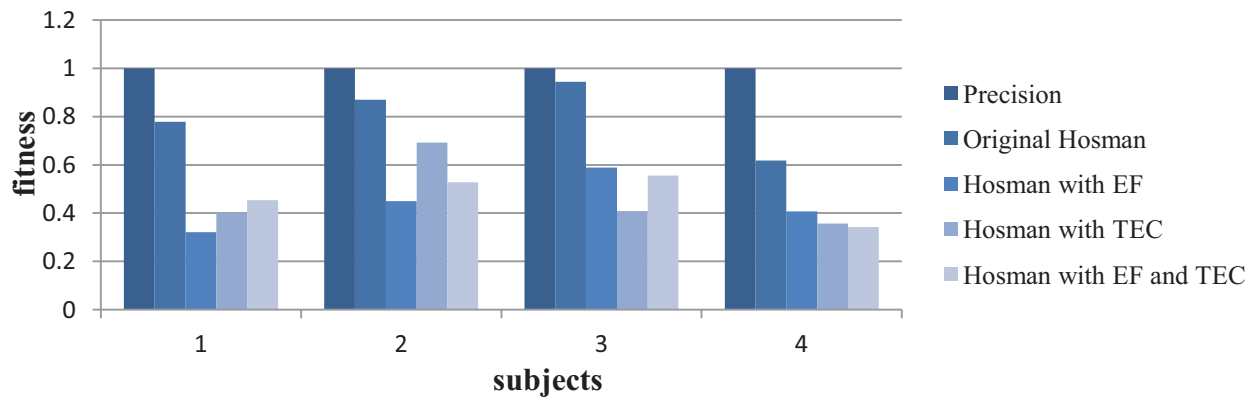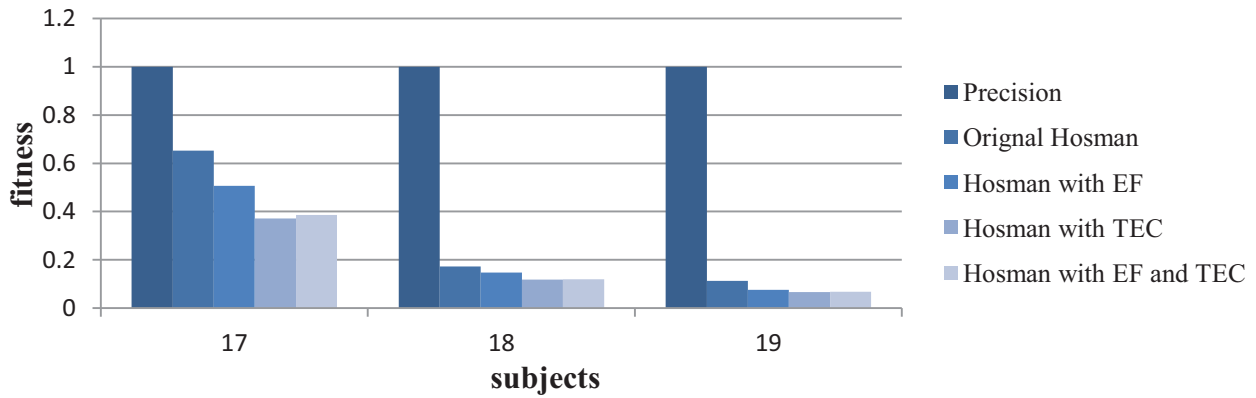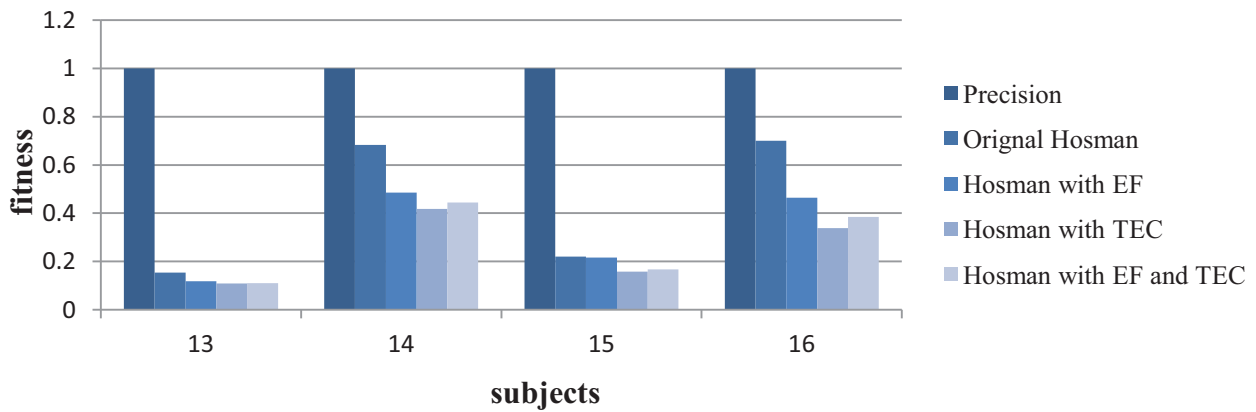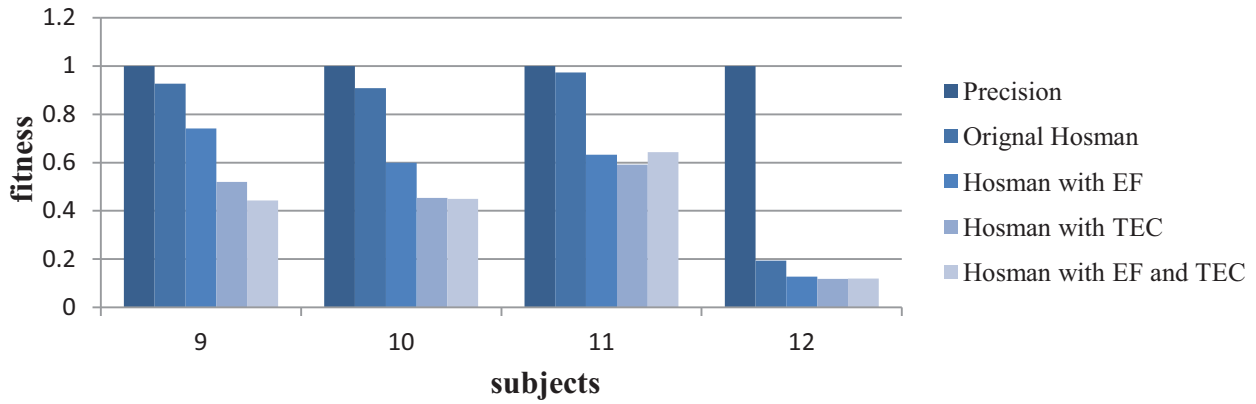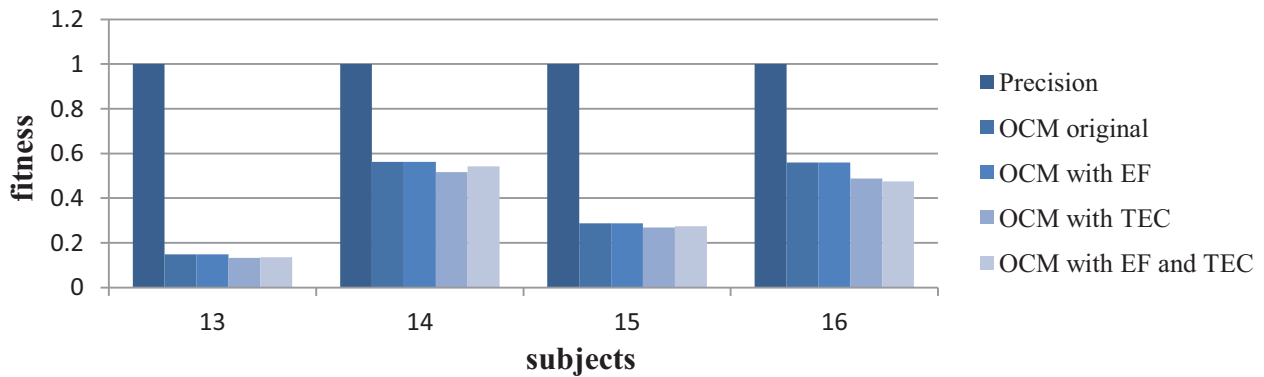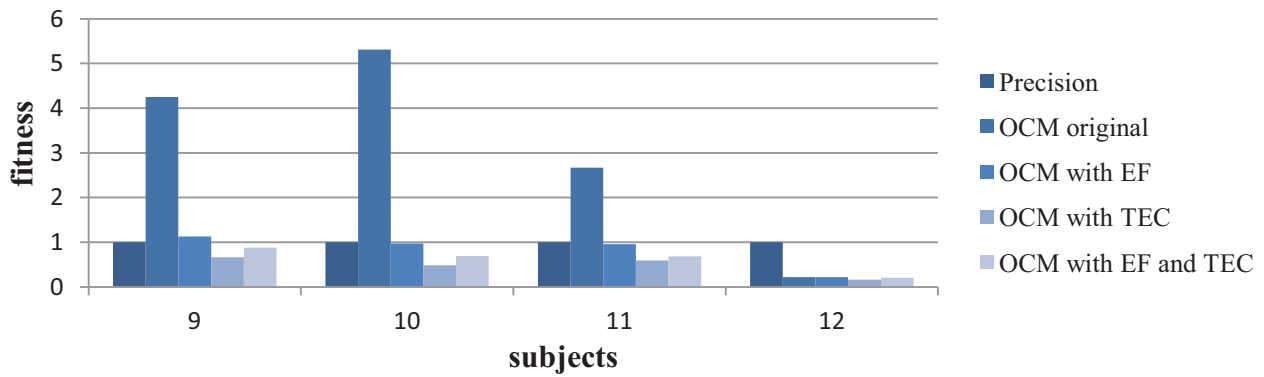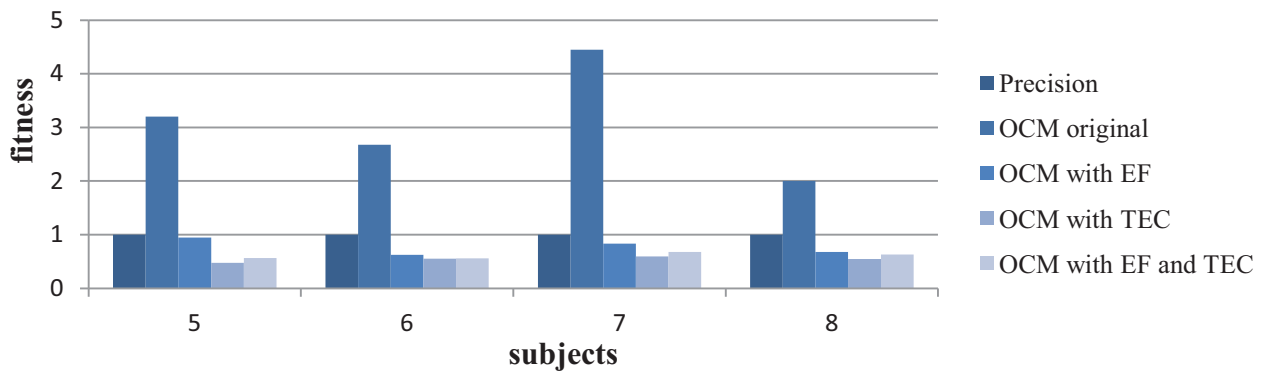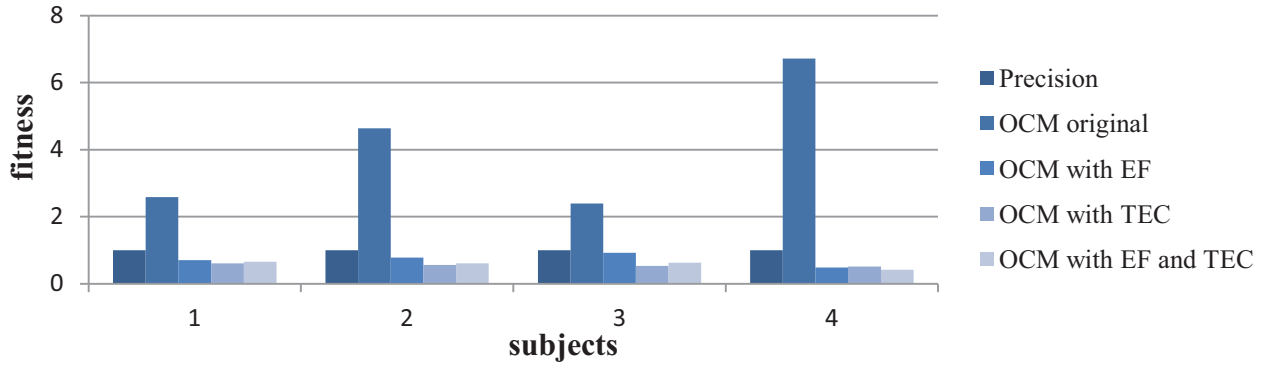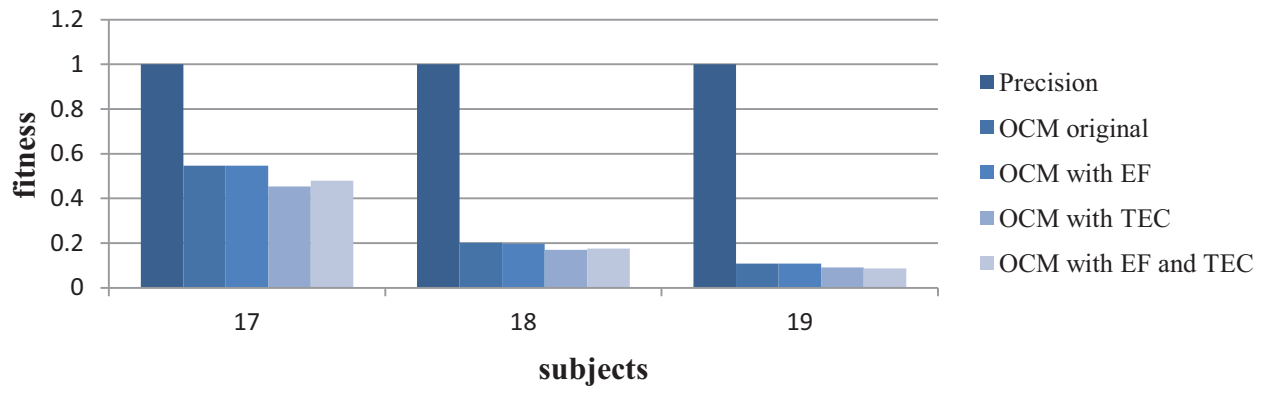
This page intentionally left blank.

Appendix D. Fitness score comparison histograms: UAV data set

Hess structural model

Hosman descriptive model

OCM
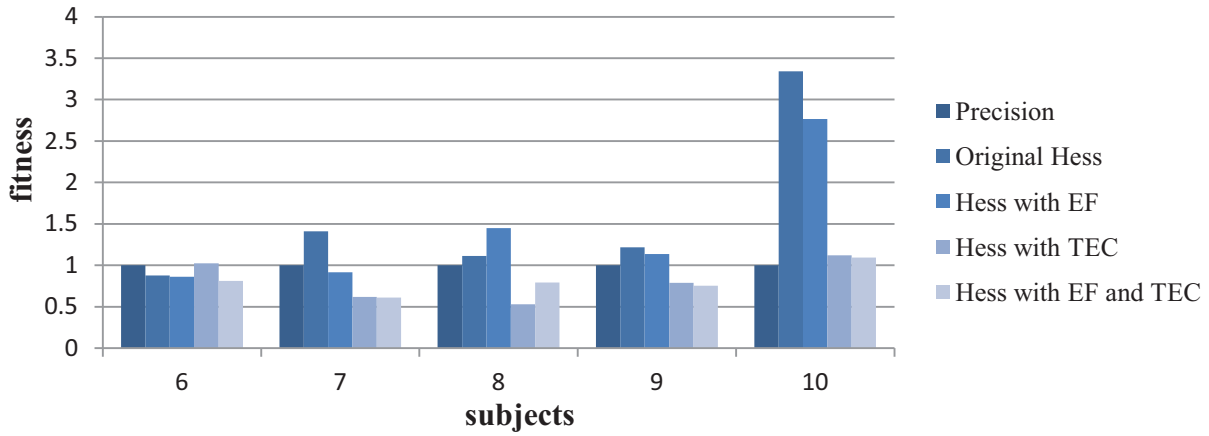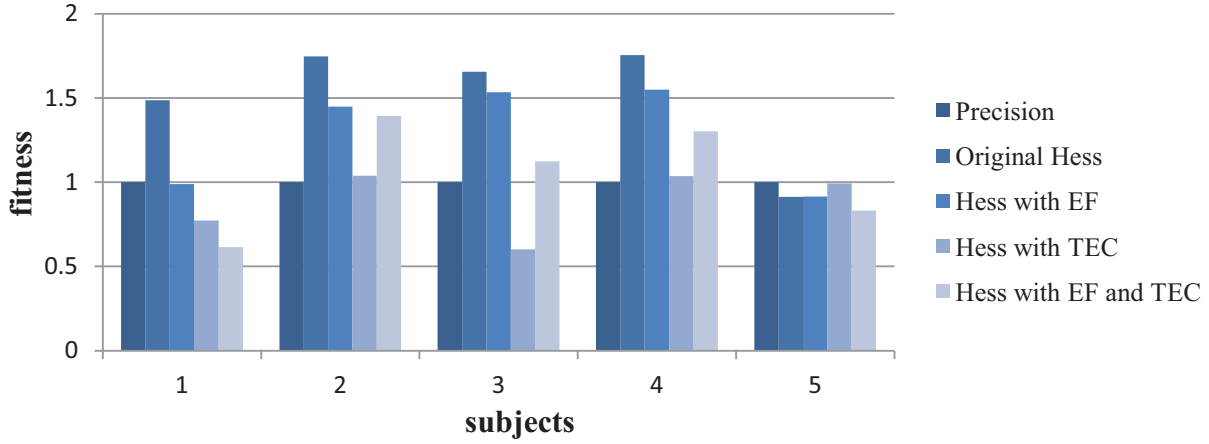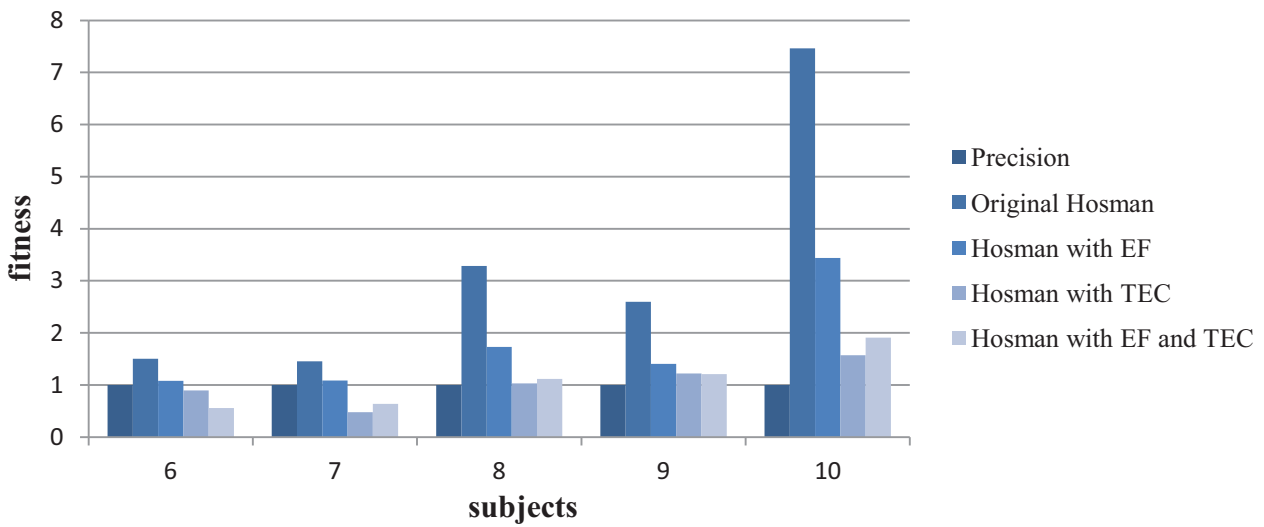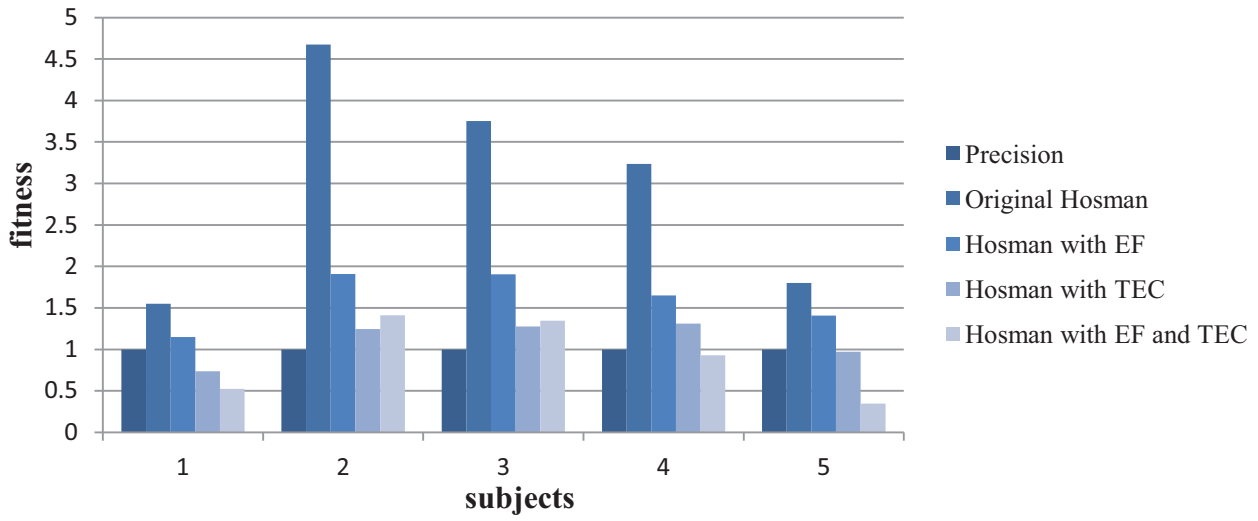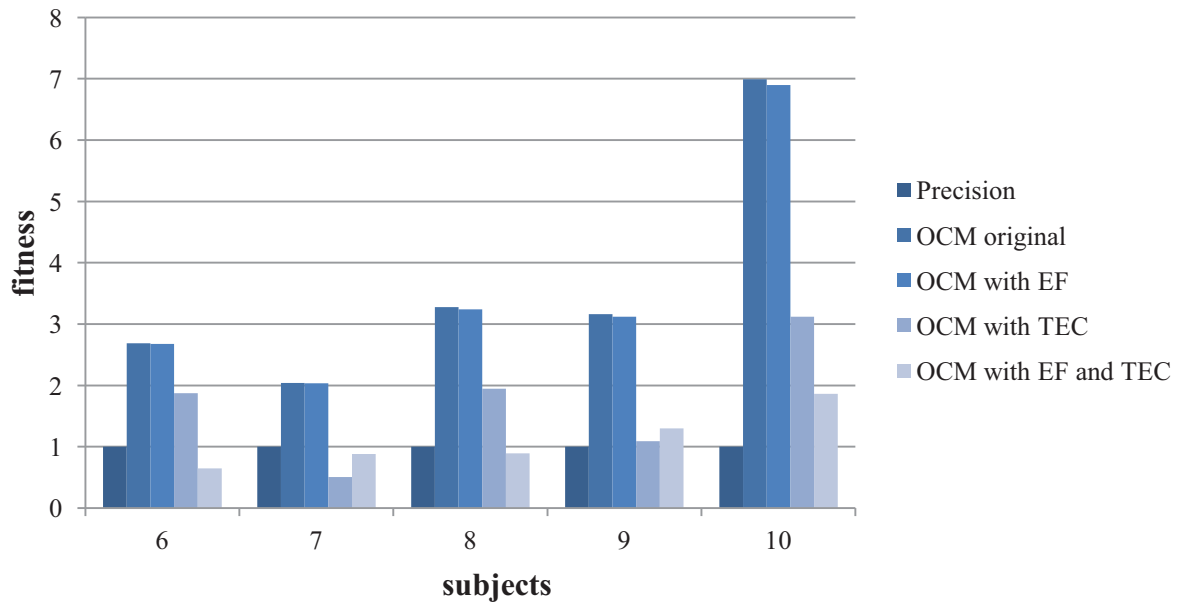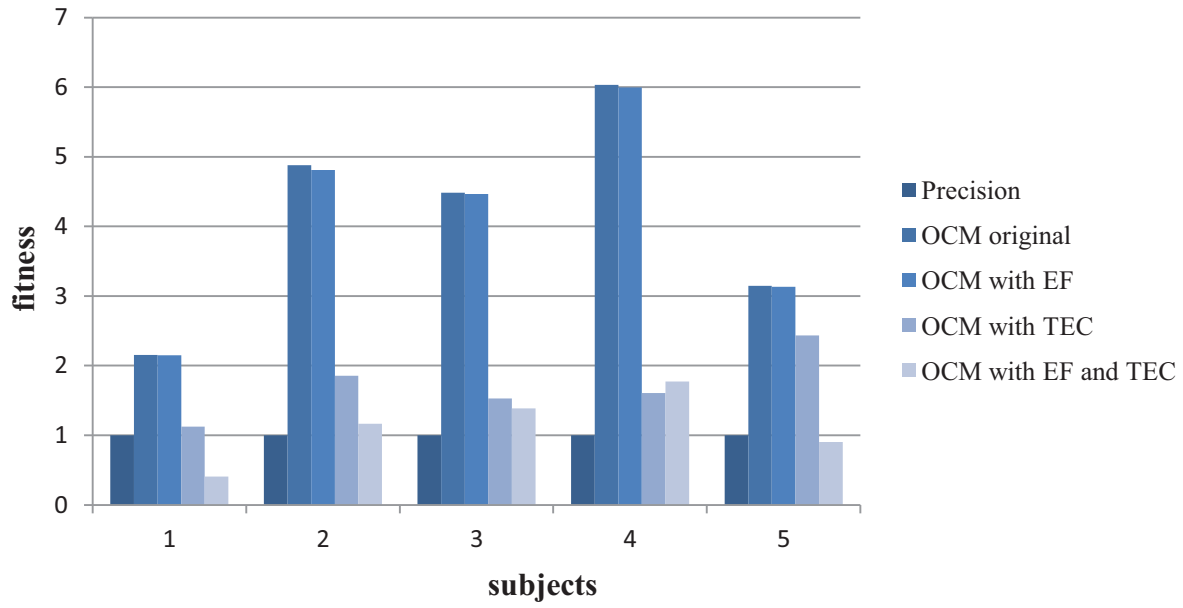
This page intentionally left blank.

Appendix E. Fitness scores.

Tables are using the following tri color markup scheme:

- Red color indicates that a particular fitness score exceeds that of the precision model and, according to the evaluation metrics discussed in section 6.3., the associated model configuration must be discarded.

- Green color indicates that the associated model configuration produced fitness score lower than that of the precision model.

- Yellow color marks up the lowest fitness score in a given model configuration category.

Fitness scores are normalized with respect to the fitness score produced by the Precision model of the human operator.

Table E. 1. MCL data set. No enhancements

Hess	Hosman	OCM
0.977048202	0.778719424	2.580545452
0.982048551	0.86889935	4.633296651
0.952501962	0.944344466	2.38875227
0.774639045	0.617672103	6.717458262
0.967333508	0.956396599	3.204276294
0.983284617	0.849695284	2.673371367
0.981586021	0.908153641	4.449504979
0.975455657	0.768062804	2.001423672
0.923157147	0.926524358	4.252436763
0.914218304	0.908505147	5.311488349
0.979005152	0.973386452	2.6683375
0.201040705	0.193642789	0.215605025
0.157274685	0.153955233	0.147764407
0.661554575	0.683249783	0.56187046
0.223232826	0.221060625	0.287189161
0.680590233	0.699451697	0.559392133
0.620298951	0.652494573	0.546546296
0.14095901	0.173264093	0.201611633
0.107873466	0.113021862	0.108900573

151

Table E. 2. MCL data set. Enhanced by EF

Hess + EF	Hosman + EF	OCM + EF
0.36870445	0.321458777	0.699715529
0.517101572	0.449989554	0.781311944
0.578181337	0.589228906	0.924039585
0.544991031	0.407225701	0.486857363
0.382457334	0.373860125	0.945073483
0.640110852	0.528022191	0.625650654
0.652226696	0.596806051	0.83221617
0.577886813	0.391280546	0.676295504
0.698746552	0.740498358	1.12924048
0.590324531	0.599184536	0.970492734
0.62120845	0.631823357	0.956400169
0.155638595	0.127219703	0.215605025
0.121568483	0.118865343	0.147764407
0.587169306	0.485704503	0.56187046
0.19946522	0.216329134	0.287189161
0.579979982	0.463859358	0.559392133
0.509494698	0.506513227	0.546547192
0.09640633	0.147164277	0.19717578
0.076003908	0.076713351	0.108900573

Table E. 3. MCL data set. Enhanced by TEC

Hess + TEC	Hosman + TEC	OCM + TEC
0.501441953	0.403613112	0.602932355
0.474329665	0.692664853	0.556252549
0.525775709	0.408592879	0.528054196
0.433321609	0.356621486	0.514574758
0.413695717	0.530483882	0.472885877
0.675050874	0.48771914	0.549403235
0.590445423	0.562408238	0.596335135
0.408576677	0.393001677	0.5447768
0.476454099	0.519227523	0.66450321
0.49132954	0.453163832	0.485833284
0.376059525	0.591950541	0.588115889
0.113235619	0.118393111	0.164078942
0.108430982	0.109803084	0.132649537
0.398698931	0.417582039	0.516324514
0.163920862	0.158589065	0.268006212
0.364718108	0.337991888	0.488347974
0.339822224	0.372058115	0.453675094
0.090609854	0.11883033	0.169515275
0.060245587	0.066357127	0.090642281

153

Table E. 4. MCL data set. Enhanced by TEC and EF

Hess + EF + TEC	Hosman + EF + TEC	OCM + EF + TEC
0.32743947	0.454153542	0.654178157
0.309497893	0.527705624	0.605741925
0.351822942	0.555878068	0.621289181
0.410047119	0.34209997	0.417743853
0.367694133	0.512499533	0.565009785
0.51484606	0.413293147	0.557709672
0.480430172	0.530156767	0.677699395
0.400883885	0.385723925	0.629168114
0.45889501	0.443660515	0.880923088
0.437049095	0.449694	0.694885187
0.535621498	0.643245716	0.686047735
0.124879945	0.119685677	0.20151044
0.090768405	0.110197347	0.135872096
0.373216337	0.444675332	0.541404801
0.199561364	0.167807026	0.274698281
0.321035576	0.384935451	0.474462812
0.317768585	0.386011236	0.479042471
0.080227087	0.119294945	0.176184061
0.065552807	0.06820905	0.08737615

Table E. 5. UAV data set. No enhancements.

Hess	Hosman	OCM
1.486703123	1.550655962	2.180604606
1.746890045	4.673013282	5.504399261
1.65559221	3.754214588	5.302134142
1.754150771	3.234688645	6.174770159
0.912374164	1.801224836	3.17744544
0.875647567	1.502079808	2.790787908
1.411627207	1.452627709	2.043619662
1.112479648	3.285779404	3.977398448
1.217207022	2.598383639	3.325132654
3.341000574	7.459604888	7.800785491

Table E. 6. UAV data set. Enhanced by EF.

Hess + EF	Hosman + EF	OCM + EF
0.987815606	1.148078831	2.175411243
1.449135194	1.90958304	5.426752575
1.533647337	1.904329011	5.280696158
1.548121189	1.651525533	6.135689252
0.915077312	1.408779165	3.165889123
0.862668416	1.078076199	2.78109885
0.916039664	1.086788559	2.038752544
1.447362093	1.727913558	3.937413328
1.13694022	1.403522656	3.284389771
2.767970058	3.439154877	7.69585647

Table E. 7. UAV data set. Enhanced by TEC

Hess + TEC	Hosman + TEC	OCM + TEC
0.772462126	0.736275202	1.140168162
1.03855594	1.246036572	2.091098131
0.601364644	1.275329286	1.807107397
1.036837436	1.309079344	1.647030234
0.991662894	0.971553024	2.459048264
1.023395613	0.893417062	1.94534656
0.61818819	0.474818047	0.508949505
0.529272035	1.027755172	2.365084427
0.789818183	1.223953056	1.145819481
1.121053918	1.571640195	3.482418536

Table E. 8. UAV data set. Enhanced by TEC and EF.

Hess + EF + TEC	Hosman + EF + TEC	OCM + EF + TEC
0.613697728	0.522595006	0.414044395
1.394127562	1.41199632	1.316479106
1.122686988	1.345787405	1.586223415
1.301669048	0.929118188	1.30396524
0.831668845	0.346108403	0.932565854
0.812559136	0.557167882	0.673480621
0.611524314	0.640016658	0.885110266
0.791828051	1.11581483	1.119632535
0.75349376	1.209789538	1.284213766
1.09344324	1.91059664	2.078630512

References

[1] Tustin, A., "*The Nature of the Operator's Response in Manual Control, and its Implications for Controller Design*", journal of the IEE, 94, Part IIA, No.2, 1947.

[2] McRuer, D., Weir, D. H., "*Theory of Manual Vehicluar Control*", Ergonomics, pp. 599-633, July 1969.

[3] Kleinman, D. L., Baron, S., Levison, W. H., "*An Optimal Control Model of Human Response. Part I: Theory and Validation*", Automatica, Vol. 6, pp. 357-369, Pergamon Press, 1970.

[4] Hess, R. A., "*A Model-Based Theory for Analyzing Human Control Behavior*", Advances in Man-Machine Systems Research, Volume 2, pp 129-175, 1985, ISBN: 0-89232-466-X

[5] Cardullo, F., George, G., Latham, R., "*Force Cueing Technology Integration and Feedback Metrics to Improve DMO Simulator Effectiveness*", Air Force Research Laboratory, Wright-Patterson AFB, OH 45433, 2006.

[6] George, G.R., Cardullo, F. M., "*Application of Neuro-Fuzzy Systems to Behavioral Representation in Computer Generated Forces*", Link Simulation and Training, 1996.

[7] Neusser, S., Nijhuls, J., Spaanenburg, L., Hoeffliner, B., Franke, U., Fritz, H., "*Neurocontroller for Lateral Vehicle Guidance*", IEEE Micro, February 1993.

[8] McRuer, D. T., Krendel, E., "*Mathematical Models of Human Pilot Behavior*", AGARDograph No.188, 1974.

[9] Jagacinski, R. J., Flach, J. M., "*Control Theory for Humans*", Lawrence Erlbaum Associates, Publishers, 2003.

[10] Hosman, R., "*Pilot's Perception and Control of Aircraft Motions*", Study, Delft University of Technology, The Netherlands, 1996.

[11] McRuer, D. T., "*Advances in Flying Qualities*", AGARD lecture series No. 157, May 1988.

[12] Magdaleno, R. E., McRuer, D. T., "*Experimental Validation and Analytical Elaboration for Models of the Pilot's Neuromuscular Subsystems in Tracking Tasks*" NASA Ames, 1971.

[13] Zadeh, L. A., "Fuzzy sets and systems". In: Fox J, editor. *System Theory*. Brooklyn, NY: Polytechnic Press, 1965: 29–39

[14] George, G., "*New Methods of Mathematical Modeling of Human Behavior in the Manual Tracking Task*", Study, State University of New York at Binghamton, 2008.

[15] Osowski, S., "*Sieci Neuronowe Do Przetwarzania Informacji*" Oficyan Wydawnicza Politechniki Warszawskiej, Warszawa, 2000

[16] Moody, J. E., "*The Effective Number of Parameters: An Analysis of Generalization and Regularization in Nonlinear Learning Systems*", Advances in Neural Information Processing Systems 4, 847-854, 1992.

[17] Holland, J. H., "*Adaptation in Natural and Artificial Systems*", University of Michigan Press, Ann Arbor, 1975

[18] Goldberg, D. E., "*Genetic Algorithms in Search, Optimization and Machine Learning*", Kluwer Academic Publishers, Boston, MA, 1989.

[19] Davis, L., "*Bit-Climbing, Representational Bias, and Test Suite Design. Proceedings of the Fourth International Conference on Genetic Algorithms*", University of California, San Diego, July 13-16, 1991.

[20] Ball, J. T., Gluck, K. A., "*Demo: the Predator UAV Synthetic Task Environment*", Air Force Research Laboratory, Warfighter Research Division, 6030 S. Kent St., Mesa ,AZ 85212-6061, USA

[21] Telban, R. J., Cardullo, F. M., "*Motion Cueing Algorithm Development: Human-Centered Linear and Nonlinear Approaches*", Langley Research Center, NASA/CR-2005-213747, 2005.

[22] Guo, L., "*Advanced Techniques for Mitigating the Effects of Temporal Distortions in Human in the Loop Control Systems*", Study, State University of New York at Binghamton, 2005.

[23] Zacharias, G. L., Levison, W. H., "*A Performance Analyzer for Identifying Changes in Human Operator Tracking Strategies*", Aerospace Medical Research Laboratory, Wright-Patterson Air Force Base, Ohio, 1979.

[24] Yoshihiko, K., Koichi, E., Jin, M., Sumio, O., Masashi, H., "*Acquisition of Human Operator's Skills and Dexterity using Neural Network: Automatic Generation of Neural Controller from Chaotic Time Series Data during*", Chino Shisutemu Shinpojiumu Shityo, Vol. 29, pp. 217-222, 2002

[25] Rabiner, L. R., McClellan, J. H., Parks, T. W., "*FIR digital Filter Design Techniques Using Weighted Chebyshev Approximations*", Proc. IEEE 63, 1975.

[26] Remez, E. Ya., "*Sur la détermination des polynômes d'approximation de degré donnée*", Comm. Soc. Math. Kharkov 10, 41, 1934.

[27] Porat, B., "*A Course in Digital Signal Processing*", Wiley, ISBN 0471149616, 1997.

[28] Zaychik.K., "Intelligent Systems Approach for Automated Identification of Individual Control Behavior of a Human Operator", Dissertation, State University of New York at Binghamton, 2009

[29] Hess, R. A., "*Structural Model of the Adaptive human Pilot*", Journal of Guidance and Control, Vol. 3, No. 5, September – October 1980.

[30] Hess, R. A., Siwakosit, W., "*Assessment of Flight Simulator Fidelity in Multiaxis Task Including Visual Cue Quality*", Journal of Aircraft, Vol. 38, No. 4, July-August 2001.

[31] Cooper G. E., Harper, R. P. Jr., "*The Use of Pilot Rating in the Evaluation of Aircraft Handling Qualities*", NASA TN D-5153, April, 1969

[32] Roskam, J., "*Airplane Flight Dynamics and Automatic Flight Controls*", Part I, Roskam Aviation and Engineering Corporation, 1979.

REPORT DOCUMENTATION PAGE

The public reporting burden for this collection of information is estimated to average 1 hour per response, including the time for reviewing instructions, searching existing data sources, gathering and maintaining the data needed, and completing and reviewing the collection of information. Send comments regarding this burden estimate or any other aspect of this collection of information, including suggestions for reducing this burden, to Department of Defense, Washington Headquarters Services, Directorate for Information Operations and Reports (0704-0188), 1215 Jefferson Davis Highway, Suite 1204, Arlington, VA 22202-4302. Respondents should be aware that notwithstanding any other provision of law, no person shall be subject to any penalty for failing to comply with a collection of information if it does not display a currently valid OMB control number.
PLEASE DO NOT RETURN YOUR FORM TO THE ABOVE ADDRESS.

1. REPORT DATE *(DD-MM-YYYY)*	2. REPORT TYPE	3. DATES COVERED *(From - To)*
01- 03 - 2012	Contractor Report	

4. TITLE AND SUBTITLE

Intelligent Systems Approach for Automated Identification of Individual Control Behavior of a Human Operator

5a. CONTRACT NUMBER

NNL06AA74T

5b. GRANT NUMBER

5c. PROGRAM ELEMENT NUMBER

6. AUTHOR(S)

Zaychik, Kirill B.; Cardullo, Frank M.

5d. PROJECT NUMBER

5e. TASK NUMBER

5f. WORK UNIT NUMBER

160961.01.01.01

7. PERFORMING ORGANIZATION NAME(S) AND ADDRESS(ES)

 NASA Langley Research Center
Hampton, Virginia 23681-2199

8. PERFORMING ORGANIZATION REPORT NUMBER

9. SPONSORING/MONITORING AGENCY NAME(S) AND ADDRESS(ES)

National Aeronautics and Space Administration
Washington, DC 20546-0001

10. SPONSOR/MONITOR'S ACRONYM(S)

NASA

11. SPONSOR/MONITOR'S REPORT NUMBER(S)

NASA/CR-2012-217555

12. DISTRIBUTION/AVAILABILITY STATEMENT
Unclassified - Unlimited
Subject Category 54
Availability: NASA CASI (443) 757-5802

13. SUPPLEMENTARY NOTES
 This report was prepared by State University of New York, Binghamton, NY, under NASA contract NNL06AA74T with UNISYS Corporation, Reston, VA.
Langley Technical Monitor: Jacob A. Houck

14. ABSTRACT

Results have been obtained using conventional techniques to model the generic human operator's control behavior, however little research has been done to identify an individual based on control behavior. The hypothesis investigated is that different operators exhibit different control behavior when performing a given control task. Two enhancements to existing human operator models, which allow personalization of the modeled control behavior, are presented. One enhancement accounts for "testing" control signals, which are introduced by an operator for more accurate control of the system and/or to adjust the control strategy. This uses the Artificial Neural Network which can be fine-tuned to model the "testing" control. Another enhancement takes the form of an equiripple filter which conditions the control system power spectrum . A novel automated parameter identification technique was developed to facilitate the identification process of the parameters of the selected models. This utilizes a Genetic Algorithm based optimization engine called the Bit-Climbing Algorithm. Enhancements were validated using experimental data obtained from three different sources: the Manual Control Laboratory software experiments, Unmanned Aerial Vehicle simulation, and NASA Langley Research Center Visual Motion Simulator studies. This manuscript also addresses applying human operator models to evaluate the effectiveness of motion feedback when simulating actual pilot control behavior in a flight simulator.

15. SUBJECT TERMS

Flight simulator; Human operator models; Intelligent systems; Motion systems; Simulator

16. SECURITY CLASSIFICATION OF:			17. LIMITATION OF ABSTRACT	18. NUMBER OF PAGES	19a. NAME OF RESPONSIBLE PERSON
a. REPORT	b. ABSTRACT	c. THIS PAGE			STI Help Desk (email: help@sti.nasa.gov)
U	U	U	UU	176	19b. TELEPHONE NUMBER *(Include area code)* (443) 757-5802